

Sorbonne Université

2021-2022

Stage de Master 2

Noé Bassel

Titre

Projet réalisé en collaboration avec le CERMICS
Ecole Nationale des Ponts et Chaussées
6 et 8 avenue Blaise Pascal
Cité Descartes - Champs sur Marne
77455 Marne la Vallée Cedex 2

Tuteur : Gabriel Stoltz

July 12, 2022

Contents

1	Introduction to molecular dynamics	4
1.1	The microscopic description of atomic systems	4
1.1.1	Classical phase space	4
1.1.2	Dynamical description	5
1.1.3	Reduced units	6
1.2	Statistical ensembles	7
1.2.1	Microcanonical ensemble	8
1.2.2	Canonical ensemble	9
1.2.3	From microscopic dynamics to macroscopic observables	10
1.2.4	Examples of instantaneous observables	10
1.2.5	Ergodic averages	11
2	Sampling equilibrium properties	12
2.1	Microcanonical averages	12
2.1.1	Elementary properties of Hamiltonian dynamics	12
2.1.2	Numerical schemes for Hamiltonian dynamics	14
2.2	Canonical averages	20
2.2.1	Langevin dynamics	20
2.2.2	Invariance of the canonical measure	21
2.2.3	Overdamped limit of Langevin dynamics	23
2.2.4	Convergence to equilibrium	24
2.2.5	Asymptotic variance for ergodic averages	25
2.2.6	Splitting schemes for the Langevin dynamics	26
2.2.7	Error analysis for splitting schemes	28
2.2.8	Unbiased sampling	30
2.2.9	Numerical illustrations	32
3	Study of the BAOA scheme	35
3.0.1	Definitions and notations	35
3.0.2	Relating invariant measures of discretization schemes	36
3.0.3	Error estimate on the phase space measure	37
3.0.4	Error estimates on the kinetic marginal distributions	38
3.0.5	Analysis of the second order error term for kinetic averages under $\mu_{\Delta t, P}$	39
3.0.6	Analysis of the discrepancy between the dominant error terms on the kinetic marginals.	41
3.1	Numerical results	43
3.1.1	Models	43
3.1.2	Equality of marginal configurational distributions	44
3.1.3	Comparison of marginal kinetic distributions	44
3.1.4	Verification of the first-order expansion	46
3.1.5	Example of first-order bias in a BAOA average	46
3.1.6	Effect of the friction parameter	46

4 Non-equilibrium Molecular Dynamics	50
4.1 Non-equilibrium molecular dynamics	50
4.1.1 General framework	50
4.1.2 Numerical implementation	52
4.1.3 Mobility	53
4.1.4 Shear viscosity	55
4.2 The Green-Kubo method	56
4.2.1 Numerical implementation	58
4.2.2 Mobility	59
4.2.3 Shear viscosity	64
5 Norton dynamics	67
5.1 Introduction	67
5.2 Mobility	67
5.2.1 The dynamics	67
5.2.2 Analytic calculations for the kinetic dynamics	68
5.2.3 Splitting schemes	70
5.2.4 Estimation of ρ_F	70
5.3 Shear viscosity	71
5.3.1 A Norton method	71
5.3.2 Numerical integration	73
5.3.3 Numerical results	73
5.4 Norton method- fixed	73
5.5 The dynamics	73
5.5.1 Fluctuation-dissipation part	75
5.5.2 Deterministic part	75
5.5.3 Application to shear viscosity	76
5.6 Numerical implementation	77
A Implementation details	79
B Notational conventions	80

Chapter 1

Introduction to molecular dynamics

1.1 The microscopic description of atomic systems

Molecular dynamics, and computational statistical physics at large, aim at simulating on the computer the behavior of physical systems. The hope is that one can infer quantities and properties of real-life interest from observing the results of numerical simulations, which may be relevant to understand the material properties of many-particle systems, or the nature of interactions in complex systems such as those found in biology. Computational simulations can thus act as surrogate experiments in cases where experimental setups are hard to achieve, or measurements are impossible. They can also be seen as surrogate tests of theoretical models, as they allow to test the validity of a mathematical description by comparing numerical predictions to experimental data. Molecular dynamics, in particular, is concerned with simulating atomic systems, most often (and as we shall systematically do) using a classical description.

1.1.1 Classical phase space

We consider a system of N particles evolving in d -dimensional space. The classical description contends that the *state* of a system is the datum of the positions and momenta of every particle in the system. We can interpret this as the statement that, given full knowledge of the positions and momenta at some initial time, and of the forces at play, one can deduce exactly the positions and momenta at any future time. It is often the case in computer simulations that we consider positions which are restricted to a bounded domain by the use of periodic boundary conditions. To that effect, let

$$\mathcal{D} = (LT)^{dN} \text{ or } \mathbb{R}^{dN},$$

where \mathbb{T} is the one-dimensional torus. We call \mathcal{D} the configuration space.

Definition 1 (Phase space). *We describe the positions and momenta of the atoms as vectors*

$$q = (q_{1,1}, \dots, q_{1,d}, \dots, q_{N,1}, \dots, q_{N,d})^\top \in \mathcal{D},$$

$$p = (p_{1,1}, \dots, p_{1,d}, \dots, p_{N,1}, \dots, p_{N,d})^\top \in \mathbb{R}^{dN},$$

where $q_i := (q_{i,1}, \dots, q_{i,d})^\top$ is the position vector of the i -th particle, and similarly for p . Let

$$\mathcal{E} := \mathcal{D} \times \mathbb{R}^{dN}.$$

Central objects in our study will be trajectories

$$(q_t, p_t)_{t \geq 0} \subset \mathcal{E},$$

which describe the time evolution of a physical system.

It is not clear *a priori* why we should choose momenta to describe the kinetic quality of the system, rather than velocities. However it is of no importance since we can change from one description to the other via the relation

$$v = M^{-1}p,$$

where $M \in \mathbb{R}^{dN \times dN}$ is a diagonal matrix recording the masses of each particle (d times per particle), and v is the velocity vector.

1.1.2 Dynamical description

In order to describe the evolution of the system's state, one must specify a dynamical law. This is done by giving a function $V : \mathcal{E} \rightarrow \mathbb{R}$ whose gradient in the i -th particle's coordinates

$$\nabla_{q_i} V := (\partial_{q_{i,d}}, \dots, \partial_{q_{i,d}})^\top$$

gives minus the force vector acting on the i -th particle. In our case we will always take the potential to be independent of the momentum, so that we can think of V as having domain \mathcal{D} . In the case where $\mathcal{D} = (L\mathbb{T})^{dN}$, it will be convenient to think of V as a function from \mathbb{R}^{dN} to \mathbb{R} which is C^1 and L -periodic in each direction. The function V is called the potential, and, as it encodes the dynamics of the system, it is of paramount importance. The time evolution of the system, then, is described by Newton's second law:

$$\frac{dp}{dt} = -\nabla V(q)$$

It will be convenient for our analysis to use of reformulation of Newton's equations, based on the Hamiltonian of a system.

Definition 2 (Hamiltonian). *The Hamiltonian of a classical system is its total energy, which is the sum of a kinetic energy term depending only on the momenta and a potential energy term depending only on the positions.*

$$(1.1) \quad H(q, p) = \frac{1}{2}p^\top M^{-1}p + V(q)$$

Using the Hamiltonian, we can rewrite the classical equations of motion as

$$(1.2) \quad \begin{cases} dq_t = M^{-1}p_t dt = \nabla_p H(q_t, p_t) dt \\ dp_t = -\nabla V(q_t) dt = -\nabla_q H(q_t, p_t) dt \end{cases},$$

The potential is the most important part of the microscopic description, and accordingly, the main problem in establishing a physical model of this kind is to determine potential functions which adequately capture the dynamic behavior of a given system. The choice of a classical description automatically implies a degree of approximation, since behavior arising from the laws of quantum mechanics, which may be relevant at a microscopic level, are described by Newton's law. Furthermore, if the aim is to simulate such systems numerically, computational constraints imply that some compromise has to be reached between theoretical accuracy and computational cost. If, for small systems, it may be possible to simulate all atomic interactions, for larger or more complex systems, it is often to use potential functions which are both cheap from a computational point of view and empirically shown to be accurate enough for the purpose of a simulation.

Our main numerical example will be the system given by the following potential, which is of this empirical form, and which is often used to describe the microscopic behavior of chemically inert fluids, such as Argon.

Example 1 (The Lennard-Jones fluid). We fix $L > 0$, $d = 3$, and N the number of particles. The Lennard-Jones fluid is the classical system given by the pair-interaction potential

$$(1.3) \quad V_{\text{LJ}}(q) = \sum_{1 \leq i < j \leq N} v(|q_i - q_j|),$$

where v is a radial function

$$v(r) = 4\varepsilon \left(\left(\frac{\sigma}{r}\right)^{12} - \left(\frac{\sigma}{r}\right)^6 \right).$$

The reference energy ε and length σ are shape parameters which respectively control the depth of the potential well of v and the equilibrium distance $2^{1/6}\sigma$. As seen on Figure 1.1, the potential combines two effects. At small interparticular distances, the dominant term is in r^{-12} , which translates into a strongly repulsive force between close pairs of particles, and makes individual particles essentially impenetrable. At long range, the dominant term is in $-r^6$, which translates into a weakly attractive force between distant particles. Contrary to the repulsive term, which is empirical, this scaling has a theoretical origin in the Van der Waals forces. From a computational standpoint, the fact that v is an even function of r allows one to compute the normalized force while sparing the expense of computing a square root, while the identity $r^{12} = (r^6)^2$ allows further economy. The shape parameters σ and ε must be chosen empirically to describe the behavior of a particular atomic species. For Argon, values of reference are: $\sigma =$, $\varepsilon =$.

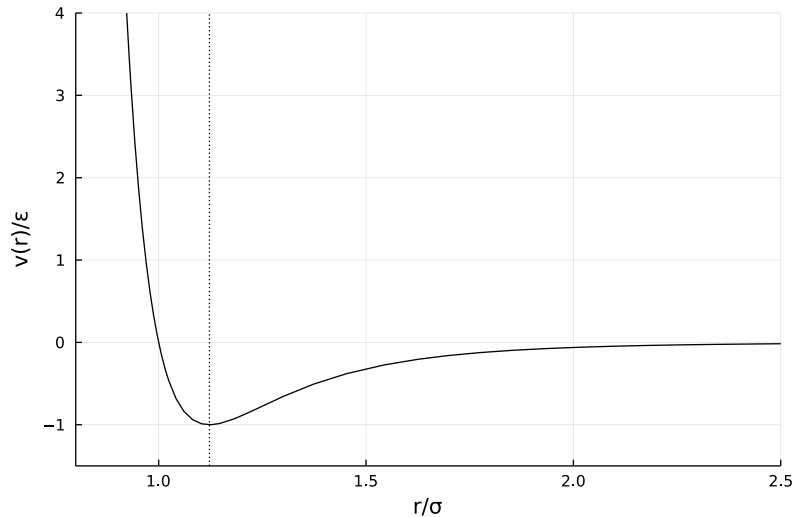


Figure 1.1: The pair potential v , with lengths and energy given in reduced units. The equilibrium interparticular distance is indicated by the vertical dotted line.

1.1.3 Reduced units

It is convenient, given an atomic system, to describe quantities therein within a system of units in which they are of order one. This has several advantages. Firstly, like any reasonable system of units, they make quantities easier and more intuitive to reason about. Secondly, from the computational point of view, numerical artifacts due to loss of precision at very large or very small scales and overflow errors can be avoided more often. Thirdly, they may help transfer knowledge about one system to another. For instance, in the Lennard-Jones system, expressing a

quantity in reduced units, and knowing the dependency of these units on the parameters (ε, σ, M) of the system, one can infer properties about a system with parameters $(\tilde{\varepsilon}, \tilde{\sigma}, \tilde{M})$ by applying the inverse transformation, thus effectively yielding equivalence of different systems under different conditions, and sparing the cost of running redundant simulations.

We describe a general procedure to construct a set of reduced units. Our choice, although not necessarily unique, is quite natural, especially when dealing with the Lennard-Jones system. Let us fix a reference mass m_* , a reference energy ε_* and a reference length σ_* . Then various reference quantities can be derived by natural conversions and dimensional analysis:

$$\begin{aligned} (\text{time}) \quad t_* &= \sqrt{\sigma_*^2 m_* \varepsilon_*^{-1}}, \\ (\text{temperature}) \quad T_* &= \varepsilon_* k_B^{-1}, \\ (\text{velocity}) \quad v_* &= \sigma_* t_*^{-1}, \\ (\text{volume}) \quad V_* &= \sigma_*^3, \\ (\text{area}) \quad A_* &= \sigma_*^2, \\ (\text{density}) \quad \rho_* &= V_*^{-1}, \\ (\text{force}) \quad F_* &= m_* \sigma_* t_*^{-2}, \\ (\text{pressure}) \quad P_* &= F_* A_*^{-1}, \end{aligned}$$

and one can of course go on. The point is that if X is a quantity, one can obtain its reduced value X_{red} by dividing X by the reference quantity X_* which is dimensionally compatible with X , and which can be derived as above. For instance, given a pressure P , we obtain

$$P_{\text{red}} = P \sigma_*^3 \varepsilon_*^{-1}.$$

Note this is an adimensional quantity. Note, also that, due to the definition of the reference temperature T_* relative to the reference energy ε_* , energy are now commensurate to temperatures. The Boltzmann factor, which is the conversion factor between units of temperature and units of energy simplifies when expressed in reduced units, a fact we can capture with the maxim $k_B* = 1$. This simplifies many formulae.

For a monoatomic Lennard-Jones system, a natural choice for m_* is the atomic mass of the considered species. We also take $\varepsilon_* = \varepsilon$ and $\sigma_* = \sigma$, (although the equilibrium length $\sigma = 2^{1/6}\sigma$ is another possible choice). In the case of Argon, we use the following values:

$$m_* = 6.634 \times 10^{-26} \text{ kg}, \quad \sigma_* = 3.405 \times 10^{-10} \text{ m}, \quad \varepsilon_* = 1.66 \times 10^{-21} \text{ J}.$$

Unless explicitly specified, all numerical results will be in this system of reduced units.

1.2 Statistical ensembles

The microscopic description is interesting from a theoretical standpoint, but it fails to be relevant when attempting to describe the behavior of atomic systems with a macroscopic number of particles, of the order of Avogadro's number (6.02×10^{23}). Besides the technical impossibility of measuring to a high accuracy the configuration of such systems, and that of recording the information required to track it (coincidentally, the total amount of digitally stored information on Earth is estimated to be 10^{23} bytes as of 2022), it is also the case that knowledge of a system at this level of detail is unnecessary to describe the quantities which are relevant to our macroscopic experience. In the instance of a gas at thermal equilibrium, examples of relevant quantities are total energy, pressure, temperature, density, which, while of course resulting from the internal state of the system, are independent of the minutiae of individual atomic motions: loosely speaking, one may describe the macroscopic state of a system by only a handful of macroscopic variables, loosing track of the myriad of microscopic degrees of freedom. An important point is that for a given macroscopic state, there are many microscopic configurations which are

compatible with our observations. This motivates defining the macroscopic state of a system as a probability distribution over phase space, which we may interpret as assigning to each microscopic configuration a likelihood that this configuration underlies the macroscopic state.

This does not tell one how to choose the distribution over microscopic states. However, it seems reasonable to assign positive probabilities to states compatible with the macroscopic constraints, and in such a way as to make the weakest possible assumptions on this microscopic state, or in other words contain the least amount of information about the system, given the macroscopic constraints. The mathematical translation of this idea is given by the principle of maximal entropy. Given a class of probability distributions compatible with the macroscopic constraints, define the macroscopic state as the one which maximizes the entropy, which is defined for a probability distribution ρ by

$$(1.4) \quad \mathfrak{S}(\rho) = - \int_{\mathcal{E}} \rho(x) \ln(\rho(x)) dx.$$

The specification of a probability distribution over states is called a thermodynamic ensemble. We will be considering the following two examples.

1.2.1 Microcanonical ensemble

The microcanonical ensemble is the suitable model for an isolated system in thermodynamic equilibrium, evolving under Hamiltonian dynamics. The number of particles N , the volume $V = L^3$, and the energy E is fixed. We will alternatively refer to the microcanonical ensemble as the NVE ensemble. Because the constant energy condition constrains the compatible microstates to level sets of H , which in general will be negligible subsets of \mathcal{E} , some care must be taken in defining the microcanonical measure, since one cannot express the macroscopic constraints by a family of probability densities. However, under suitable assumptions on V , one can define the microcanonical measure as a weak limit of uniform distributions over level ‘‘shells’’ of H :

$$\int_{\mathcal{E}} \varphi d\mu_{mc,E} := \lim_{\varepsilon \rightarrow 0} \frac{1}{|S(E, \varepsilon)|} \int_{S(E, \varepsilon)} \varphi(q, p) dq dp,$$

where

$$S(E, \varepsilon) = \{(q, p) \in \mathcal{E} \mid H(q, p) \in [E - \varepsilon, E + \varepsilon]\}.$$

This is consistent with the fact that, for a set A with finite Lebesgue measure, the probability distribution on A which maximizes the entropy is the uniform distribution on A . Alternatively, $\mu_{mc,E}$ is uniquely defined by the relation

$$\int_{\mathcal{E}} g(H(q, p)) f(q, p) dq dp = \int_{\mathbb{R}} g(E) \int_{\mathcal{E}} f(q, p) \mu_{mc,E}(dq, dp),$$

for all test functions $g : \mathbb{R} \rightarrow \mathbb{R}$ and $f : \mathcal{E} \rightarrow \mathbb{R}$. It is possible, using the coarea formula, to derive an explicit formula for $\mu_{mc,E}$, namely,

$$(1.5) \quad \mu_{mc,E}(dq, dp) = \frac{\sigma_E(dq, dp)}{|\nabla H(q, p)|},$$

where σ_E is the surface measure induced by the Lebesgue measure on the constant energy manifold

$$(1.6) \quad S(E) = \{(q, p) \in \mathcal{E} \mid H(q, p) = E\}.$$

1.2.2 Canonical ensemble

Isolated systems in thermal equilibrium are not typically those that we encounter in experiments. Instead, it is more common to observe systems which are in thermal equilibrium with respect to their environment, an ambient *heat bath* at a fixed temperature. The total energy of such systems is not fixed: small fluctuations can occur as energy is exchanged back and forth between the heat bath and the system. However, the average energy \bar{E} is fixed. This is the macroscopic constraint that defines the canonical ensemble. For a fixed N, V, \bar{E} , define the density of the the canonical measure as the maximizer:

$$\underset{\rho \in \mathcal{A}}{\operatorname{argmax}} \mathfrak{S}(\rho)$$

where \mathcal{A} is the set of admissible densities

$$\mathcal{A} = \left\{ \rho : \mathcal{E} \mapsto \mathbb{R}_+ \mid \int_{\mathcal{E}} \rho = 1, \int_{\mathcal{E}} H(q, p) \rho(q, p) dq dp = E \right\}.$$

Solving the Euler-Lagrange equation associated with this constrained optimization problem yields that the only admissible solution can be written under the form:

$$(1.7) \quad \mu(q, p) := \frac{1}{Z} e^{-\beta H(q, p)}.$$

Furthermore, one can show that μ is indeed the unique maximizer. Here, $-\beta$ and $1 + \ln Z$ are the critical Lagrange multipliers associated respectively with the energy constraint and the normalization constraint. Thus

$$Z = \int_{\mathcal{E}} e^{-\beta H(q, p)} dq dp$$

is a normalization constant called the partition function, and β is a tuning parameter related to the value of \bar{E} . The physical interpretation of β is that of an inverse temperature,

$$\beta = \frac{1}{k_B T},$$

where $k_B = 1.38 \times 10^{-23} \text{ J} \cdot \text{K}^{-1}$ is Boltzmann's constant. For obvious reasons, we prefer to refer to the canonical ensemble as the NVT ensemble (rather than the NV \bar{E})

One could of course go further and remark that when observing a fixed volume of unconfined gas in thermal equilibrium, the total number of particles N is not fixed. Instead, this fluctuates as particles are constantly exchanged with an ambient particle reservoir. Instead, the average number of particles \bar{N} is fixed. The resulting ensemble is called the grand canonical or μ V T ensemble. This, and many other constructions are possible, but we will restrict our attention to the NVE and NVT cases.

Remark 1 (Independence of canonical momenta and configurations). *We can make an observation on μ using the fact that the Hamiltonian 1.1 is separable: it is the sum of a kinetic term involving p and a configurational term involving q . Thus we can write*

$$e^{-\beta H(q, p)} = e^{-\frac{\beta}{2} p^\top M^{-1} p} e^{-\beta V(q)},$$

which implies that the canonical measure μ is of tensor form:

$$(1.8) \quad \mu = \kappa \otimes \nu,$$

where κ is a probability measure on \mathbb{R}^{dN} has a density proportional to $e^{-\frac{\beta}{2} p^\top M^{-1} p}$ and ν has a density proportional to $e^{-\beta V(q)}$ on \mathcal{D} . Recognizing a multivariate Gaussian density, we can further write, abusing the notations κ and ν to denote both the laws and their densities,

$$(1.9) \quad \kappa(p) = \det\left(\frac{M}{2\pi\beta}\right)^{\frac{1}{2}} e^{-\frac{\beta}{2} p^\top M^{-1} p}$$

$$(1.10) \quad \nu(p) = \frac{1}{Z_\nu} e^{-\beta V(q)},$$

with

$$Z_\nu = Z \det \left(\frac{M}{2\pi\beta} \right)^{\frac{1}{2}}.$$

This implies in particular that the marginal distribution in p of the canonical measure can be sampled easily, using standard algorithms for generating i.i.d. Gaussian variables, such as the Box-Muller method.

The difficult part is sampling ν . Why we should even care to do so is the object of the following paragraph.

1.2.3 From microscopic dynamics to macroscopic observables

The main interest in describing the macroscopic state of a system as a probability distribution over its microscopic configurations is that one can then express constant macroscopic quantities as averages of fluctuating microscopic observables with respect to the ensemble measure. In our context, an observable is simply a function defined over phase-space. Given a macroscopic system defined by an equilibrium ensemble μ and an observable φ , we are interested in computing its average value over the ensemble,

$$(1.11) \quad \mathbb{E}_\mu[\varphi] := \int_{\mathcal{E}} \varphi(q, p) \mu(dq, dp).$$

Two problems arise. One is, for a given macroscopic quantity of interest, how to correctly define a microscopic observable φ which underlies the macroscopic behavior. The second, once we have properly defined φ , is how to compute averages (??).

1.2.4 Examples of instantaneous observables

Let us give some examples of observables which will be of interest to us. Obvious examples include the kinetic energy,

$$E_\kappa(q, p) = \frac{1}{2} p^\top M^{-1} p,$$

the potential energy

$$E_p(q, p) = V(q),$$

and the Hamiltonian H . We will generally be considering real-valued observables, although vector-valued observables such as the velocity $v = M^{-1}p$ may be of interest. We will give two additional examples. The kinetic temperature is defined by the following expression:

$$T_\kappa(q, p) = \frac{2}{k_B d N} E_\kappa(q, p).$$

It is, up to a conversion factor of Boltzmann's constant, twice the kinetic energy per degree of freedom. In the canonical ensemble, it is easily shown that $\mathbb{E}_\mu[T_\kappa] = T$, justifying the terminology. (reference also equipartition theorem)

We will also be considering the instantaneous pressure, which is given, for a pair interaction potential of the form (1.3) and a periodic domain \mathcal{D}

$$P(q, p) = \frac{1}{|\mathcal{D}|} \left(N k_B T_\kappa - \frac{1}{d} \sum_{i=1}^N q_i^\top \nabla_{q_i} V(q) \right).$$

Neglecting the right-hand side gives the famous ideal gas law, $PV = Nk_B T$, which is a good approximation at low densities. The right hand side, otherwise known as the virial, appears to be problematic since the q_i are not periodic functions of q , which would suggest P is not a well-defined observable on \mathcal{D} . However, using the particular form of the potential, which is a function of the displacements $|q_i - q_j|$, and symmetry arising from Newton's third law, we can arrive at the following expression:

$$P(q, p) = \frac{1}{d|\mathcal{D}|} \left(\sum_{i=1}^N \frac{|p_i|}{m_i} - \sum_{i \neq j} |q_i - q_j| v'(|q_i - q_j|) \right),$$

which is indeed a periodic function of q . In the NVT ensemble, the average of the kinetic part of the pressure is a known parameter, so we may replace it by its value, considering the observable:

$$\frac{N}{\beta|\mathcal{D}|} - \frac{1}{d|\mathcal{D}|} \sum_{i=1}^N q_i^\top \nabla_{q_i} V(q).$$

1.2.5 Ergodic averages

This second problem is one of sampling a probability measure in many dimensions, which is a difficult problem in general. Our broad strategy, which will remain the same in the NVE and NVT case, is the following. We define a process $(q_t, p_t)_{t \geq 0}$ on \mathcal{E} , either deterministic or stochastic, which is invariant for the target measure μ , in the following sense:

$$(1.12) \quad \forall t \geq 0, \varphi \in B^\infty(\mathcal{E}), \int_{\mathcal{E}} \mathbb{E}^{(q,p)} [\varphi(q_t, p_t)] \mu(dq, dp) = \int_{\mathcal{E}} \varphi(q, p) \mu(dq, dp),$$

where the superscript in the expectation denotes that the process has value (q, p) at $t = 0$, and the expectation is over values of (q_t, p_t) . In other words, this is a process which, given that its initial condition is distributed according to μ , remains distributed according to μ at any later time. It is then natural to consider average values of φ over the trajectories:

$$(1.13) \quad \frac{1}{T} \int_0^T \varphi(q_t, p_t) dt,$$

which we may hope will converge to the target value. The convergence of ergodic averages to the ensemble average can be shown not to hold in generality, and is something which must be proven on a case by case basis, though general criteria can be derived. If the underlying dynamic is stochastic, then the variance of the random variables (1.13) becomes an issue, which one must keep in check by ensuring that time averages are taken over long enough trajectories. Furthermore, since the true invariant dynamics is in general in continuous time, one must devise discrete in time approximations to the true trajectories. However, empirical practice shows that ergodic averages obtained from computer simulations, even for a modest number of atoms, agrees very well with experimental data for certain types of systems, and even in the absence of theoretical guarantees.

Chapter 2

Sampling equilibrium properties

2.1 Microcanonical averages

Our aim in this section will be to describe methods to sample microcanonical averages. We first describe a few qualitative properties of Hamiltonian dynamics. These properties will serve as litmus tests to determine viable candidate numerical schemes, which we will require to preserve, either exactly or asymptotically, these qualitative properties.

2.1.1 Elementary properties of Hamiltonian dynamics

The Hamiltonian dynamics (1.2) rewrites in matrix form, writing $X_t = (q_t, p_t)$:

$$(2.1) \quad dX_t = J \nabla H(X_t) dt,$$

where J is the symplectic matrix

$$J = \begin{pmatrix} 0_{dN} & \text{Id}_{dN} \\ -\text{Id}_{dN} & 0_{dN} \end{pmatrix}$$

Applying the chain rule to any smooth function $\varphi : \mathcal{S} \mapsto \mathbb{R}$, we obtain

$$d\varphi(X_t) = dX_t^\top \nabla \varphi(X_t) = (J \nabla H(X_t))^\top \nabla \varphi(X_t) dt = (\nabla_p H \cdot \nabla_q - \nabla_q H \cdot \nabla_p) \varphi(X_t) dt$$

This motivates the following.

Definition 3 (Generator of the Hamiltonian dynamics). *We define the generator associated with the Hamiltonian dynamics to be the operator \mathcal{L}_H defined on smooth functions by*

$$(2.2) \quad \mathcal{L}_{\text{ham}} \varphi = (\nabla_p H \cdot \nabla_q - \nabla_q H \cdot \nabla_p) \varphi = (J \nabla H)^\top \nabla \varphi$$

We can split the generator as the sum of two elementary operators,

$$\mathcal{L}_{\text{ham}} = A + B,$$

with

$$(2.3) \quad A = (M^{-1}p) \cdot \nabla_q \quad B = -\nabla V(q) \cdot \nabla_p.$$

The generator allows us to quantify the rate of change of an observable φ under the evolution of the system. If we define, for $t \geq 0$, the evolution operators

$$P_t \varphi(q_0, p_0) = \varphi(\Phi_t(q_0, p_0)),$$

where Φ is the flow associated with the Hamiltonian dynamics, that is the collection of maps $(\Phi_t)_{t \geq 0}$, defined by $\Phi_t(q_0, p_0) = (q_t, p_t)$, the unique solution to (1.2) with initial conditions (q_0, p_0) , then we have formally:

$$\frac{\partial}{\partial t} P_t \varphi(q, p) = \partial_t \varphi(q_t, p_t) = \mathcal{L}_{\text{ham}} \varphi(q_t, p_t) = \mathcal{L}_{\text{ham}} P_t \varphi(q, p) = P_t \mathcal{L}_{\text{ham}} \varphi(q, p).$$

In the following result, we collect certain qualitative properties of Hamiltonian dynamics.

Proposition 1 (Properties of Hamiltonian dynamics). *Assume that the Hamiltonian H is C^2 on \mathcal{E} and that the flow Φ_t is globally defined for $t \in \mathbb{R}$. Then the following properties hold.*

i) *Group structure:*

$$\forall t, s \in \mathbb{R}, \Phi_t \circ \Phi_s = \Phi_{t+s}, \Phi_0 = \text{Id}.$$

ii) *Energy preservation:*

$$\frac{dH(q_t, p_t)}{dt} = 0.$$

iii) *Conservation of the Lebesgue measure:*

$$\forall D \subseteq \mathcal{E}, \forall t \geq 0, |\Phi_t(D)| = |D|.$$

iv) *Symplecticity:*

$$\forall t \geq 0, \nabla \Phi_t^\top J \nabla \Phi_t = J.$$

v) *Time reversibility:*

$$\Phi_t \circ \mathcal{R} \circ \Phi_t = \mathcal{R}.$$

The notation ∇ corresponds to (B.1), and the map \mathcal{R} is the momentum-reversing involution

$$\mathcal{R}(q, p) = (q, -p).$$

Hints of proof. i) This property expresses the fact that the Hamiltonian evolution is autonomous, and follows from uniqueness in the Cauchy-Lipschitz theorem. This allows one to formally interpret the flow as a group action of \mathbb{R} on \mathcal{E} .

ii) The energy conservation property simply follows from applying \mathcal{L}_{ham} to H .

iii) This property, known as Liouville's theorem, holds generally for any divergent-free flow. Its proof is based on a time differentiation of the determinant $\det(\nabla \Phi_t)$, and observing that the Hamiltonian vector field is divergence free:

$$\text{div}(J \nabla H) = \text{div}_q(\nabla_p H) - \text{div}_p(\nabla_q H) = 0.$$

- iv) The property is trivially verified at time $t = 0$. A straightforward calculation shows that the time derivative of the symplecticity condition for Φ_t is 0, which proves the claim. Let us remark that this property also implies property iii), since it shows $\det(\nabla \Phi_t)^2 \det(J) = \det(J) \implies |\det(\nabla \Phi_t)| = 1$.
- v) This again follows by uniqueness of trajectories, by observing that, fixing an initial condition (q_0, p_0) , time differentiating the trajectory $(q_{-t}, -p_{-t}) = \mathcal{R} \circ \Phi_{-t}(q_0, p_0)$ shows it is Hamiltonian. Thus it must coincide with $\Phi_t(q_0, -p_0) = \Phi_t \circ \mathcal{R}(q_0, p_0)$, or as an equality of mappings, $\mathcal{R} \circ \Phi_{-t} = \Phi_t \circ \mathcal{R}$. Precomposing by Φ_t on each side yields the result using property i). □

Remark 2. Properties i) to iv) above are valid for any dynamics of the form (2.1), thus it is possible to consider dynamics with more general Hamiltonians, which still obey them, disregarding issues of well-posedness. Property v) requires the additional condition that the Hamiltonian be separable into a kinetic and potential part and that the kinetic part be an even function of p .

Property *ii*) in the proposition above asserts that Hamiltonian trajectories remain on the constant energy manifold $S(H(q_0, p_0))$ defined in (1.6). Since this is the support of the microcanonical measure $\mu_{mc,E}$, it is natural to ask whether the Hamiltonian dynamics can be used to sample the microcanonical measure, by means of ergodic averages. A minimum requirement for this to hold is that the measure is left invariant under Hamiltonian evolution. Indeed, this is the case. We consider a Hamiltonian trajectory (q_t, p_t) such that $H(q_0, p_0) = E$. For g and f test functions,

$$\begin{aligned} \int_{\mathbb{R}} g(E) \int_{\mathcal{E}} f(q_t, p_t) d\mu_{mc,E}(dq, dp) dE &= \int_{\mathcal{E}} g(H(q, p)) f \circ \Phi_t(q, p) dq dp \\ &= \int_{\mathcal{E}} g(H \circ \Phi_{-t}(\tilde{q}, \tilde{p})) f(\tilde{q}, \tilde{p}) d\tilde{q} d\tilde{p} \\ &= \int_{\mathcal{E}} g(H(\tilde{q}, \tilde{p})) f(\tilde{q}, \tilde{p}) d\tilde{q} d\tilde{p} \\ &= \int_{\mathbb{R}} g(E) \int_{\mathcal{E}} f(\tilde{q}, \tilde{p}) d\mu_{mc,E}(d\tilde{q}, d\tilde{p}) dE. \end{aligned}$$

the absence of a Jacobian determinant term in the change of variables from the second to the third line follows from property *iii*), while the passage from the second to the third line is justified by the energy conservation property. This shows that the microcanonical measure is invariant under the Hamiltonian dynamics, but it is easy to construct examples where ergodic averages fail to converge to the correct value, as the following simple example shows.

Example 2 (A non-ergodic system). *We consider the following one-dimensional system with $\mathcal{E} = \mathbb{T} \times \mathbb{R}$, and the potential given by*

$$V(q) = \cos\left(4\pi(q - \frac{1}{2})\right).$$

The constant-energy manifold $S(0)$ consists of two disjoint compact connected components (see Figure 2.1). The observable

$$\varphi(q, p) = \mathbb{1}_{q > \frac{1}{2}} - \mathbb{1}_{q < \frac{1}{2}}$$

is constant on each component of $S(0)$, and has zero average with respect to $\mu_{mc,0}$ by symmetry, but ergodic averages do not converge, since

$$\frac{1}{T} \int_0^T \varphi(q_t, p_t) dt = \frac{1}{T} \int_0^T \varphi(q_0, p_0) dt = \varphi(q_0, p_0) \in \{\pm 1\}$$

The issue of ergodicity is in general very hard to tackle for realistic systems, and in practice is overlooked. Besides, it may happen that for observables respectful of symmetries in the constant energy manifold converge to the correct microcanonical average even in the absence of ergodicity. This is, for example, the case for the kinetic energy observable in our Example 2.

2.1.2 Numerical schemes for Hamiltonian dynamics

It is not impossible, except for a restricted class of systems, which do not typically arise in practice, to analytically integrate Hamilton's equation (1.2). For this reason, one must revert to numerical schemes, which can and will interpret as approximations of the flow map over one timestep. More precisely, for a fixed timestep Δt , if we possess an approximation of the flow

$$\tilde{\Phi}_{\Delta t} \approx \Phi_{\Delta t},$$

we will deduce discrete approximations of the evolution by iteration:

$$(2.4) \quad (q^n, p^n) := \tilde{\Phi}_{\Delta t}^n(q_0, p_0) \approx (q_{n\Delta t}, p_{n\Delta t}),$$

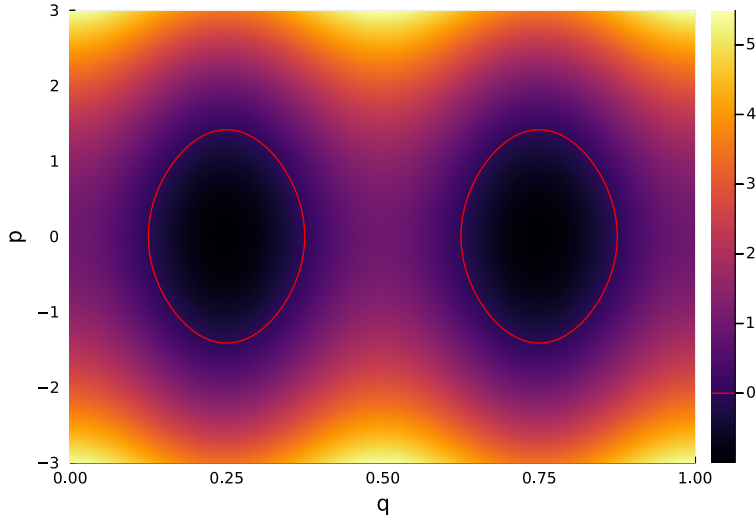


Figure 2.1: The Hamiltonian landscape for the potential V of Example 2 , with $S(0)$ plotted in red.

which can then be used as sample points for the computation of empirical averages, discrete counterparts to the ergodic averages (1.13),

$$(2.5) \quad \frac{1}{n} \sum_{k=0}^n \varphi(q^n, p^n).$$

In most common applications involving ODEs, the aim is to approximate the exact solution as precisely as possible over a given domain. In the case of sampling trajectory averages in molecular dynamics, however, the time domain is usually very large, because simulating long trajectories is a requirement to ensure that a representative portion of phase space is explored. As a consequence, it is in practice impossible to obtain precise solutions over a long time, because the evolution's sensitivity to initial conditions will cause small initial errors to rapidly blow-up. Furthermore, one does not really *care* about the exact evolution, since the dynamics are merely used as a sampling device. Instead, one key requirement is that the dynamics stay on or close to the constant energy manifold associated with a given initial condition. It can be shown through eigenanalysis that for simple linear systems, this requirement is not satisfied by standard ODE numerical methods such as the explicit and implicit Euler schemes, or the RK4 method, for which the energy may explode or implode geometrically. This has the practical effect that for reasonably sized atomic systems, numerical instabilities render the simulations nonsensical after only a few time steps, a far cry from what is needed to obtain good estimates. One must then devise dedicated numerical methods, guided by the aim to preserve qualitative properties of the Hamiltonian evolution. It turns out that splitting schemes, based on operator splitting approximations of the Hamiltonian evolution operator over one timestep, preserve crucial qualitative properties of the Hamiltonian evolution.

An important observation is that if one considers each part of (2.3) as a generator in its own right, the corresponding dynamics is analytically solvable as ballistic trajectory.

Remark 3. Consider the two dynamics defined by

$$(2.6) \quad \begin{cases} dq_t^A = M^{-1} p_t^A dt, & dp_t^A = 0, \\ dq_t^B = 0, & dp_t^B = -\nabla V(q_t^B) dt. \end{cases}$$

These are easily solved, namely

$$(2.7) \quad \begin{cases} (q_t^A, p_t^A) = (q_0^A + tp_0^A, p_0^A), \\ (q_t^B, p_t^B) = (q_0^B, p_0^B - tV(q_0^B)). \end{cases}$$

Moreover, these evolutions are of Hamiltonian form, with Hamiltonians corresponding respectively to the kinetic part and the configurational part only, and have corresponding generators A and B . We denote by $(\Phi_t^A)_{t \in \mathbb{R}}$ and $(\Phi_t^B)_{t \in \mathbb{R}}$ their respective flow maps.

This observation suggests the following general recipes to construct a class of numerical schemes for the Hamiltonian dynamics, named splitting schemes. We consider approximations of the form

$$(2.8) \quad \Phi_{\Delta t} \approx \Phi_{\Delta t_k}^{G_k} \circ \cdots \circ \Phi_{\Delta t_1}^{G_1},$$

where $G_i \in \{A, B\}$ for all i and $\sum_{G_i=A} \Delta t_i = \sum_{G_i=B} \Delta t_i = 1$. We will be considering three schemes, the simplest of which are the symplectic Euler schemes.

The symplectic Euler schemes are defined by the following update equations.

$$(2.9) \quad \begin{cases} p^{n+1} = p^n - \nabla V(q^n) \Delta t \\ q^{n+1} = q^n + M^{-1} p^{n+1} \Delta t \end{cases}$$

$$(2.10) \quad \begin{cases} q^{n+1} = q^n + M^{-1} p^n \Delta t \\ p^{n+1} = p^n - \nabla V(q^{n+1}) \Delta t \end{cases}$$

These correspond respectively to the splitting

$$\Phi_{\Delta t}^A \circ \Phi_{\Delta t}^B := \Phi_{\Delta t}^{BA}$$

and

$$\Phi_{\Delta t}^B \circ \Phi_{\Delta t}^A := \Phi_{\Delta t}^{AB}.$$

The velocity Verlet scheme is based on the symmetric splitting

$$\Phi_{\Delta t/2}^B \circ \Phi_{\Delta t}^A \circ \Phi_{\Delta t/2}^B := \Phi_{\Delta t}^{BAB}.$$

Its update equation is given by

$$(2.11) \quad \begin{cases} p^{n+\frac{1}{2}} = p^n - \frac{\Delta t}{2} \nabla V(q^n) \\ q^{n+1} = q^n + \Delta t M^{-1} p^{n+\frac{1}{2}} \\ p^{n+1} = p^{n+\frac{1}{2}} - \frac{\Delta t}{2} \nabla V(q^{n+1}). \end{cases}$$

We have advertised above that these numerical schemes preserve some qualitative properties of the Hamiltonian dynamics. We now turn to making this statement precise. Let us fix an evolution operator $\tilde{\Phi}_{\Delta t}$ corresponding to a splitting of the form (2.8) with a timestep $\Delta t > 0$. We refer to these properties using the same indexing as in Proposition 1, but where Φ_t is replaced by $\tilde{\Phi}_{\Delta t}$ regardless of t . We further say a splitting is *symmetric* if the corresponding order of operators A and B is a palindrome. The velocity Verlet splitting is symmetric, while the symplectic Euler splittings are not.

Proposition 2 (Properties of splitting schemes for Hamiltonian dynamics). *We go through the properties in Proposition 1, listing those which apply, and those which have to be modified.*

- i) *Group structure: the analogous statement is a group action of \mathbb{Z} on \mathcal{E} . This holds if the splitting is symmetric: then, $\tilde{\Phi}_{\Delta t}^{-1} = \tilde{\Phi}_{-\Delta t}$.*

- ii) *Energy preservation:* this does not hold as is, but does in a weakened sense that we discuss below.
- iii) *Conservation of the Lebesgue measure:* this holds for any splitting.
- iv) *Symplecticity:* similarly, this holds for all splittings.
- v) *Time-reversibility:* this holds for any symmetric splitting.

Hints of proofs. For every one of these properties, the strategy is the same. From Proposition 1, each one of them holds for $\Phi_{\Delta t}^A$ and for $\Phi_{\Delta t}^B$. The aim is then to show that these properties are stable, at best under composition, and at worst under symmetric composition.

- i) This simply follows from writing

$$(g_1 \circ g_2 \circ \cdots \circ g_2 \circ g_1)^{-1} = g_1^{-1} \circ g_2^{-1} \circ \cdots \circ g_2^{-1} \circ g_1^{-1},$$

and using property i) applied to $\Phi_{\Delta t}^A$ and $\Phi_{\Delta t}^B$.

- ii) This is a crucial and slightly subtle point, which we return to in more detail below.
- iii) This follows trivially by composition (or alternatively by symplecticity). For any measure preserving measurable maps f and g ,

$$|f \circ g(D)| = |g(D)| = |D|.$$

- iv) This follows from the fact that any composition of symplectic maps is symplectic. This, in turn, follows from the multivariate chain rule below, and applying the symplectic property twice:

$$\nabla(g \circ f) = ((\nabla g) \circ f) \nabla f \implies [((\nabla g) \circ f) \nabla f]^\top J [((\nabla g) \circ f) \nabla f] = \nabla f^\top J \nabla f = J.$$

- v) Fixing $f \circ \mathcal{R} \circ f = g \circ \mathcal{R} \circ g = \mathcal{R}$, we write

$$f \circ g \circ \mathcal{R} \circ g \circ f = f \circ \mathcal{R} \circ f = \mathcal{R},$$

and conclude by induction that the property holds for any symmetric splitting.

□

We have shown that splitting schemes inherit some nice geometrical properties from the underlying Hamiltonian flow, and all the more for symmetric splittings. However our final aim is to sample from the microcanonical measure, hence we should aim to sample points which remain close to the constant energy manifold $S(E)$. Ideally, we would want to guarantee that the Hamiltonian is perfectly preserved under the discrete evolution induced by these schemes. This, it turns out, is too high a hope. It happens, however, that, for each of these schemes, a *perturbed* Hamiltonian is (almost) exactly conserved, which we can interpret to mean that the discrete dynamics (2.4) are regularly and (almost) exactly sampled points from a *perturbed* dynamics corresponding to the new Hamiltonian. The order of this perturbation in the timestep Δt then allows one to quantify over finite time intervals the drift. The statements and proofs of this kind of results fall under the broad umbrella of backward numerical analysis. For a limpid and more detailed introduction, one can consult section 4 of [5]. The general idea of backward numerical analysis, given an evolution equation and an associated numerical method:

$$\dot{y} = F_0(y), \quad y^{n+1} = \tilde{\Phi}_{\Delta t}(y),$$

is to reinterpret the numerical solution y^1 not as an approximation of the exact solution $y_{\Delta t}$, but as the exact solution $\tilde{y}_{\Delta t}$ of an approximate evolution \tilde{y} , given by the ODE

$$\dot{\tilde{y}} = \tilde{F}(y),$$

where \tilde{F} is given by a perturbative expansion

$$\tilde{F} = F_0 + \Delta t F_1 + \Delta t^2 F_2 + \dots$$

To avoid any convergence issue related to infinite expansions, precise statements usually truncate the expansion at some finite order $\alpha > 0$, and require the exactitude of the numerical trajectory up to order $\alpha + 1$, say

$$\tilde{F} = F_0 + \Delta t F_1 + \dots + \Delta t^\alpha F_\alpha, \quad |\tilde{\Phi}_{\Delta t}(y_0) - \tilde{y}_{\Delta t}| = O(\Delta t^{\alpha+2}).$$

Comparing Taylor expansions in powers Δt of $\tilde{\Phi}_{\Delta t}$ and $\tilde{y}_{\Delta t}$ then allows us to explicitly compute the terms in the expansion of \tilde{F} . As an example we compute the first correction term for the symplectic Euler scheme $\Phi_{\Delta t}^{AB}$.

Example 3 (Leading-order correction for $\Phi_{\Delta t}^{AB}$). *Following our strategy, we Taylor-expand our scheme as*

$$\Phi_{\Delta t}^{AB}(q, p) = \begin{pmatrix} q + \Delta t M^{-1} p \\ p - \Delta t \nabla V(q) - \Delta t^2 \nabla^2 V(q) M^{-1} p \end{pmatrix} + O(\Delta t^3).$$

Similarly, expanding the exact solution with initial condition $(q, p) = y_0$ to the second order yields

$$\begin{aligned} \Phi_{\Delta t}(q, p) &= y_0 + \Delta t J \nabla H(y_0) + \frac{\Delta t^2}{2} \nabla [J \nabla H(y_0)] J \nabla H(y_0) + O(\Delta t^3) \\ &= y_0 + \Delta t J \nabla H(y_0) + \frac{\Delta t^2}{2} J \nabla^2 H(y_0) J \nabla H(y_0) + O(\Delta t^3) \\ &= \begin{pmatrix} q + \Delta t M^{-1} p - \frac{\Delta t^2}{2} M^{-1} \nabla V(q) \\ p - \Delta t \nabla V(q) - \frac{\Delta t^2}{2} \nabla^2 V(q) M^{-1} p \end{pmatrix} + O(\Delta t^3). \end{aligned}$$

This shows the scheme is of order one, hence

$$|\Phi_{\Delta t}(q, p) - \Phi_{\Delta t}^{AB}(q, p)| = O(\Delta t^2).$$

Comparing the two expansions allows us to recover the discrepancy term, showing that the solution of the modified equation at time Δt

$$\begin{cases} \frac{d}{dt} q = M^{-1} p + \frac{\Delta t}{2} M^{-1} \nabla V(q) \\ \frac{d}{dt} p = -\nabla V(q) + \frac{\Delta t}{2} \nabla^2 V(q) M^{-1} p \end{cases}$$

agrees with $\Phi_{\Delta t}^{AB}(q, p)$ up to order 2 in Δt . Crucially, this equation is still of Hamiltonian form, for the modified Hamiltonian

$$(2.12) \quad \tilde{H}(q, p) = H(q, p) - \frac{\Delta t}{2} V(q)^\top M^{-1} p.$$

In fact, it is a general fact that all truncations of the modified dynamics for a symplectic method is of Hamiltonian form. For a precise statement and proof, we refer to the book by Hairer, [demander a regis pour la ref], but for now we simply make note of the fact that given a numerical method, we can construct a modified Hamiltonian equation for which this numerical order is of arbitrarily high order of local consistency. This is important, because, as the following result shows, the order of the numerical method is directly linked to the long-time energy conservation properties along numerical trajectories.

Theorem 1. *Let H be an analytic Hamiltonian, and $\tilde{\Phi}_{\Delta t}$ be a symplectic numerical method of order α . If there exists $K \subset \mathcal{E}$ a compact set such that $(q^n, p^n) \in K \forall n$, there exists $\tau > 0$ such that for Δt small enough,*

$$(2.13) \quad H(q^n, p^n) = H(q^0, p^0) + O(\Delta t^\alpha)$$

for times $n \Delta t \leq e^{\tau/\Delta t}$.

For a proof, see Theorem IX.8.1 in [meme ref]. The fact that the order of the scheme is linked to the local conservation in time of the Hamiltonian is unsurprising. The main content of the above result is that this conservation is valid over very long times, provided the numerical trajectory does not explode and that the timestep is chosen to be small enough.

We have already seen that the symplectic Euler methods are of order one, and it can straightforwardly be shown that the Verlet scheme is of order two by Taylor expansion. Hence we expect the fluctuation of the Hamiltonian to be of order Δt for the symplectic Euler methods and of order Δt^2 for the Verlet scheme. Moreover, by construction, the symplectic Euler methods are of order two for the first-order modified Hamiltonian dynamics, so we expect the fluctuation of the first-order modified Hamiltonian computed in Example 3 to be of order two for the symplectic Euler methods. The leading-order correction term for the other Euler symplectic scheme can be computed using the same method, and is given by the opposite of (2.12).

In Figure 2.2, we verify this result numerically. A Lennard-Jones system of 1000 particles was simulated with a temperature $T = 1.5$, for a time $\tau = 1.0$, and at density $\rho = 0.7$. The Lennard-Jones potential was cutoff using a cubic spline interpolation between $r_a = 2.0$ and $r_c = 2.5$. We plot the maximum fluctuation of the Hamiltonian

$$\Delta H := \max_{0 \leq n \leq \lceil \tau / \Delta t \rceil} H(q^n, p^n) - \min_{0 \leq n \leq \lceil \tau / \Delta t \rceil} H(q^n, p^n)$$

as a function of the timestep Δt for each of the symplectic splitting schemes. We also plot the maximum fluctuation of the modified Hamiltonian (2.12) for the symplectic Euler schemes, which we denote in the legend by a lowercase m . The legend gives the order of the operators in the splitting, along with the slope of the least squares regression line in log-log space, which we superimpose in dotted line. In order for the trajectories to be comparable, every simulation was started from the same precomputed equilibrium starting configuration. The results concur with theoretical prediction.

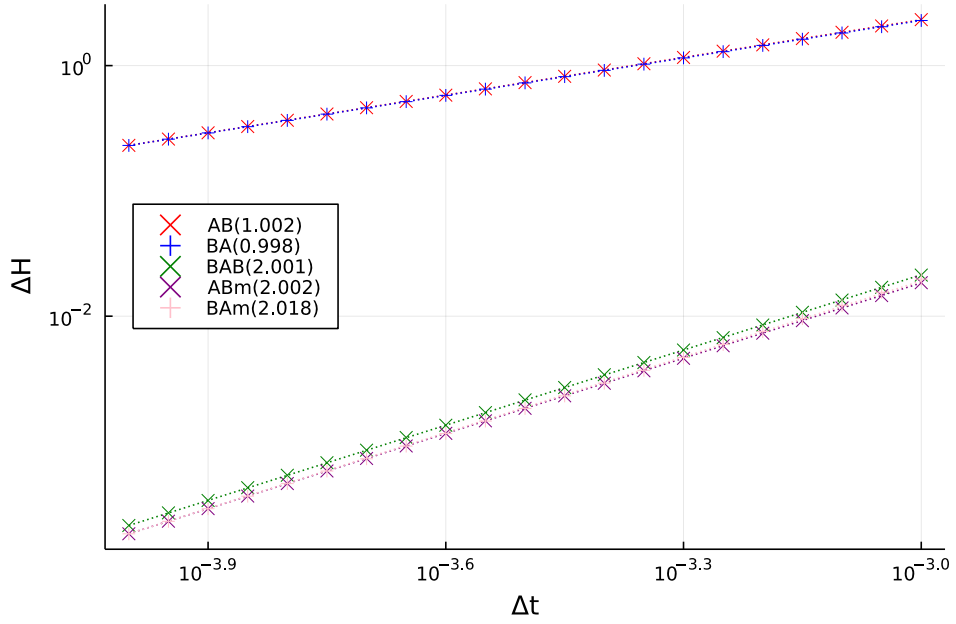


Figure 2.2: Maximum fluctuation of the Hamiltonians and leading-order modified Hamiltonians for the Symplectic Euler and Verlet schemes.

From a practical point of view, we will always use the Verlet scheme, since it offers the better energy conservation property without any computational overhead compared to the symplectic

Euler schemes. Indeed, the force calculation in the last step of (2.11) can be repurposed for the first step of the next iteration, so that there is only one force calculation per iteration, as in the symplectic Euler method. Finally let us mention that the splitting based on the ordering *ABA* of the elementary generators yields another symplectic method called the *position* Verlet scheme, which enjoys the same conservation properties as standard (velocity) Verlet. It is, however, rarely used in practice.

2.2 Canonical averages

We now turn our attention to methods to compute canonical averages, which are expectations of observables with respect to the canonical measure (1.7).

2.2.1 Langevin dynamics

We first consider the inertial Langevin dynamics, defined by the following stochastic differential equation (SDE), where γ, β are fixed positive constants.

$$(2.14) \quad \begin{cases} dq_t = M^{-1} p_t dt, \\ dp_t = -\nabla V(q_t) dt - \gamma M^{-1} p_t dt + \sqrt{\frac{2\gamma}{\beta}} dW_t, \end{cases}$$

where $(W_t)_{t \geq 0}$ is a standard dN -dimensional Brownian motion. This process is a combination of a Hamiltonian evolution with an additional action on the momenta which, if isolated, defines a dN -dimensional Ornstein-Uhlenbeck process.

This additional term be interpreted physically as the combination of two effects: a dissipation term

$$-\gamma M^{-1} p_t dt,$$

which can be understood as the effect of a viscous friction force on the particles, and a fluctuation term,

$$\sqrt{\frac{2\gamma}{\beta}} dW_t,$$

which corresponds to the input of kinetic energy into the system as thermal agitation induced by a surrounding heat bath at temperature $1/(k_B \beta)$.

However, the physical meaning can be forgotten thanks to the fact that, *in fine*, we only require that the canonical measure be invariant under this dynamic: as we shall shortly see, this is indeed the case.

Remark 4 (Generalized Langevin dynamics). *There are several ways to generalize this process: one is to consider a generic, possibly non-separable, Hamiltonians, as in Remark 2, rather than the classical Hamiltonian used above. The other is to allow the fluctuation-dissipation term to be parametrized by coefficients γ and σ depending on the state variable, and which obey a relation ensuring the invariance of μ . Hence in full generality, we could consider the following system of SDEs:*

$$(2.15) \quad \begin{cases} dq_t = \nabla_p H(q_t, p_t) dt, \\ dp_t = -\nabla_q H(q_t, p_t) dt - \gamma(q_t, p_t) \nabla_p H(q_t, p_t) dt + \sigma(q_t, p_t) dW_t, \end{cases}$$

where γ and σ are $dN \times dN$ matrix-valued functions. In fact one can also consider the case where W_t is a r -dimensional Brownian motion and σ is a $dN \times r$ matrix-valued function. The Dissipative Particle Dynamics (DPD) is a generalized Langevin equation of this form, where γ and σ are position-dependent and the Brownian motion is $dN(N-1)/2$ -dimensional, which corresponds to the number of pairs of non-orthogonal momentum degrees of freedom.

The generator of the Langevin dynamics is the operator

$$(2.16) \quad \mathcal{L}_\gamma = M^{-1} p \cdot \nabla_q - \nabla V(q) \cdot \nabla_p - \gamma M^{-1} p \cdot \nabla_p + \frac{\gamma}{\beta} \Delta_p,$$

and we denote the evolution operator using exponential notation:

$$(2.17) \quad e^{t\mathcal{L}_\gamma} \varphi(q, p) := \mathbb{E}_{(q,p)} [\varphi(q_t, p_t)],$$

where the expectation is over all trajectories of the dynamics (2.14), conditioned on $(q_0, p_0) = (q, p)$.

2.2.2 Invariance of the canonical measure

Using the generator, one can easily express the evolution of a probability distribution under the Langevin dynamics. We assume that the solution $(q_t, p_t)_{t \geq 0}$ to (2.14) has a distribution with a smooth density ρ_0 over \mathcal{E} at time $t = 0$, and denote ρ_t the probability density of (q_t, p_t) . For any test observable φ , we have

$$\int_{\mathcal{E}} \varphi(q, p) \rho_t(q, p) dq dp = \int_{\mathcal{E}} \mathbb{E}^{(q,p)} [\varphi(q_t, p_t)] \rho_0(q, p) dq dp = \int_{\mathcal{E}} e^{t\mathcal{L}_\gamma} \varphi(q, p) \rho_0(q, p) dq dp,$$

where the superscript is as in (1.12). Thus,

$$\frac{\partial}{\partial t} \int_{\mathcal{E}} \varphi(q, p) \rho_t(q, p) dq dp = \int_{\mathcal{E}} e^{t\mathcal{L}_\gamma} \mathcal{L}_\gamma \varphi(q, p) \rho_0(q, p) dq dp = \int_{\mathcal{E}} \mathcal{L}_\gamma \varphi(q, p) \rho_t(q, p) dq dp$$

If we define $\mathcal{L}_\gamma^\dagger$ as the adjoint of \mathcal{L}_γ on the flat space $L^2(\mathcal{E})$, that is,

$$(2.18) \quad \int_{\mathcal{E}} \mathcal{L}_\gamma \varphi \psi = \int_{\mathcal{E}} \varphi \mathcal{L}_\gamma^\dagger \psi \quad \text{for all test functions } \phi, \psi,$$

we have the Fokker-Planck equation,

$$(2.19) \quad \frac{\partial}{\partial t} \int_{\mathcal{E}} \varphi(q, p) \rho_t(q, p) dq dp = \int_{\mathcal{E}} \varphi(q, p) \mathcal{L}_\gamma^\dagger \rho_t(q, p) dq dp,$$

which rewrites formally as

$$(2.20) \quad \frac{\partial}{\partial t} \rho_t = \mathcal{L}_\gamma^\dagger \rho_t.$$

Using this equation, we can easily show that the canonical distribution is invariant under this dynamics, which is equivalent to the condition

$$\mathcal{L}_\gamma^\dagger \mu = 0.$$

In fact, it is useful to reformulate this condition in the weighted space $L^2(\mu)$. Indeed, the stationary Fokker-Planck equation rewrites

$$\int_{\mathcal{E}} \mathcal{L}_\gamma \varphi d\mu = 0 \quad \forall \varphi,$$

or equivalently,

$$\mathcal{L}_\gamma^* \mathbb{1}_{\mathcal{E}} = 0,$$

where \mathcal{L}_γ^* is the adjoint of \mathcal{L}_γ in $L^2(\mu)$ under the scalar product

$$\langle \varphi, \psi \rangle_\mu := \int_{\mathcal{E}} \varphi \psi d\mu.$$

This, in turn, follows easily from the following lemma.

Lemma 1. *The $L^2(\mu)$ adjoints of the elementary differential operators are given by the formulae*

$$(2.21) \quad \begin{cases} \partial_{q_i}^* = -\partial_{q_i} + \beta \partial_{q_i} V, \\ \partial_{p_i}^* = -\partial_{p_i} + \beta (M^{-1}p)_i. \end{cases}$$

These are easily found by integration by parts. In particular, we find that

$$\partial_{q_i} \partial_{p_i}^* - \partial_{p_i} \partial_{q_i}^* = \beta ((M^{-1}p)_i \partial_{q_i} - \partial_{q_i} V \partial_{p_i}),$$

whence, by summing over i , we get

$$(2.22) \quad \mathcal{L}_{\text{ham}} = \frac{1}{\beta} (\nabla_q \cdot \nabla_p^* - \nabla_p \cdot \nabla_q^*),$$

which is an antisymmetric operator. Similarly,

$$\partial_{p_i} \partial_{p_i}^* = \beta (M^{-1}p)_i \partial_{p_i} - \partial_{p_i}^2,$$

hence

$$(2.23) \quad C = -\frac{1}{\beta} \nabla_p \cdot \nabla_p^*,$$

which is a symmetric operator. In summary, we have that

$$(2.24) \quad \mathcal{L}_\gamma^* = -\mathcal{L}_{\text{ham}} + \gamma C = -(A + B) + \gamma C.$$

It follows immediately that $\mathcal{L}_\gamma^* \mathbb{1}_{\mathcal{E}} = 0$. Notice that since $\mathcal{L}_{\text{ham}}^* \mathbb{1}_{\mathcal{E}} = 0$, the canonical measure is also invariant under the Hamiltonian dynamics. However, because the latter is restricted to a manifold with zero measure with respect to μ , Hamiltonian ergodic averages cannot in general converge to the correct value.

Remark 5 (Fluctuation-dissipation relation for generalized Langevin dynamics). *We come back to the general Langevin dynamics (2.15). In this case the generator is given by*

$$\mathcal{L}_{\gamma, \sigma} = \mathcal{L}_{\text{ham}} - (\gamma \nabla_p H) \cdot \nabla_p + \frac{1}{2} (\sigma \sigma^\top) : \nabla_p^2.$$

The canonical measure is invariant under the action of the Hamiltonian part, so having

$$\tilde{\mathcal{L}}_{\text{FD}} := -(\gamma \nabla_p H) \cdot \nabla_p + \frac{1}{2} (\sigma \sigma^\top) : \nabla_p^2$$

such that $\tilde{\mathcal{L}}_{\text{FD}}^ \mathbb{1}_{\mathcal{E}} = 0$ is enough to guarantee the invariance of the canonical measure. If γ and σ are momentum-dependent, then this condition is a complicated differential-in- p relation between the coefficients of γ and σ , which can be explicitly computed by integration by parts in the expression*

$$\int_{\mathcal{E}} (\tilde{\mathcal{L}}_{\text{FD}} \varphi) \psi e^{-\beta H},$$

with $\varphi, \psi \in C_c^\infty(\mathcal{E})$ test functions. In the case where γ and σ are only position-dependent however, as is often the case in practice, then the expression simplifies greatly, and becomes simply an algebraic relationship between γ and σ ,

$$(2.25) \quad \sigma \sigma^\top = \frac{2\gamma}{\beta}.$$

2.2.3 Overdamped limit of Langevin dynamics

As already pointed out, the fact that the kinetic marginal of μ is a Gaussian distribution makes sampling canonical momenta trivial. Instead, the main problem is sampling from ν . It follows directly from the invariance of μ under trajectories of the Langevin dynamics that ν is invariant under the configurational trajectories of the Langevin dynamics. It would be convenient, however, to have at our disposal a dynamics on \mathcal{D} which has ν as an invariant measure. It turns out this is possible, by observing that the invariance of μ is independent of the parameter γ , and taking the limit $\gamma \rightarrow \infty$. This requires a bit of care. Notice the SDE on the momenta in (2.14) rewrites

$$dp_t = -\nabla V(q_t)dt - \gamma dq_t + \sqrt{\frac{2\gamma}{\beta}}dW_t,$$

thus integrating gives

$$q_t - q_0 = \frac{p_0 - p_t}{\gamma} - \frac{1}{\gamma} \int_0^t \nabla V(q_s)ds + \sqrt{\frac{2}{\gamma\beta}}W_t.$$

The scaling invariance of the Brownian motion $(\sqrt{\alpha}W_{t/\alpha^2})_{t \geq 0} \sim (W_t)_{t \geq 0}$ suggests considering the timescale $\gamma\beta t$, thus

$$q_{\gamma\beta t} - q_0 = \frac{p_0 - p_{\gamma\beta t}}{\gamma} - \frac{1}{\gamma} \int_0^{\gamma\beta t} \nabla V(q_s)ds + \sqrt{2}\widetilde{W}_t,$$

where \widetilde{W} is again a Brownian motion. Using the change of variables $s = \gamma\beta u$ in the integral term yields

$$(2.26) \quad q_{\gamma\beta t} - q_0 = \frac{p_0 - p_{\gamma\beta t}}{\gamma} - \beta \int_0^t \nabla V(q_{\gamma\beta u})du + \sqrt{2}\widetilde{W}_t,$$

At this point, we formally take $\gamma \rightarrow \infty$, which suggests the following SDE for the rescaled in time process,

$$(2.27) \quad dq_t = -\beta \nabla V(q_t)dt + \sqrt{2}dW_t.$$

This equation defines the overdamped Langevin, or Brownian, dynamics. To justify the limit in a rigorous manner, one would hope to show that the rescaled process (2.26) converges in law to a weak solution of the SDE (2.27), in some functional space. However, this is technical overkill, since, we only need to consider dynamics as sampling devices. In fact, the physical interpretation of this equation is not entirely clear in terms of the dimensions of the quantities involved. We can just as well take equation (2.27) as given, and be satisfied by the following fact.

Proposition 3. *The configurational Gibbs measure ν is invariant under the dynamics (2.27).*

This follows along the same lines as for the Langevin dynamics. The generator (now acting on observables defined on \mathcal{D}) is the operator

$$(2.28) \quad \mathcal{L}\varphi = -\beta \nabla V \cdot \nabla \varphi + \Delta \varphi.$$

Again, we consider the weighted space $L^2(\nu)$. Adjoints of elementary differential operators are still given by the first line of (2.21), and it is then easily seen that

$$(2.29) \quad \mathcal{L} = -\nabla^* \cdot \nabla$$

is a symmetric operator. Again we have $\mathcal{L}^* \mathbb{1}_{\mathcal{D}} = 0$, so ν satisfies the stationary Fokker-Planck equation under this dynamics.

Remark 6. Instead of rescaling time by $\beta\gamma$, we could have rescaled by γ , which would yield the dynamics

$$(2.30) \quad dq_t = -\nabla V(q_t)dt + \sqrt{\frac{2}{\beta}}dW_t.$$

Which formulation to choose is a matter of preference, since both yield a dynamics invariant under ν , as seen from the identity (where we still write \mathcal{L} for the generator)

$$\mathcal{L} = -\frac{1}{\beta}\nabla^* \cdot \nabla.$$

We end this chapter by stating some key properties of the continuous dynamics, before moving to the description of splitting schemes.

2.2.4 Convergence to equilibrium

Once we have shown that the Langevin dynamics and its overdamped limit are reasonable candidates to sample from the canonical measure and its configurational marginal, we should ensure that the target measure is reached, and not simply invariant for the dynamics, as the cautionary example of the Hamiltonian dynamics shows. This is the question of ergodicity, and results of this nature chiefly come in two flavors.

- (i) Probabilistic ergodic theorems that ask about the convergence of random variables like (1.13), that give analogs of the Law of Large Numbers for the correlated process $\varphi(q_t, p_t)$.
- (ii) More analytic results which express the convergence of the law of the process at time t towards a stationary solution to the Fokker-Planck equation. These can usually be expressed as decay estimates on the evolution Semigroup (2.17), in a judiciously chosen functional setting.

We will not get into details as these questions can quickly get rather technical, but rather give vague ideas of the setting, and point the reader to more thorough sources. Results such as (i) typically leverage the strong Law of Large Numbers by dissecting the trajectory into a discrete number of (loosely) *i.i.d.* excursions through phase space, guaranteeing the almost sure convergence of trajectory averages. As such, proving the positive recurrence of the dynamics is crucial to showing that these excursions are well-behaved, while also implying that the invariant measure is unique. One idea, exploited by Klieman in [8], is to recast the Langevin dynamics as a control equation (where W_t acts as the control). He is thus able to leverage criteria on \mathcal{L}_γ from geometric control theory to ensure the almost sure convergence of trajectory averages. Results such as (ii) depend on the functional setting. Let us simply state the following result, based on hypocoercive estimates. For an introduction to these ideas, and references, we point to Section 2.1.1 in [10].

Proposition 4 (Exponential decay rate on the Semigroup). *Let $H^1(\mu)$ be the weighted Sobolev space*

$$(2.31) \quad H^1(\mu) = \{f \in L^2(\mu) \mid \nabla f \in L^2(\mu)^{2dN}\},$$

with the norm

$$\|f\|_{H^1(\mu)}^2 = \|f\|_{L^2(\mu)}^2 + \|\nabla_p f\|_{L^2(\mu)}^2 + \|\nabla_q f\|_{L^2(\mu)}^2.$$

We define $\mathcal{H}^1(\mu)$ as the subspace

$$\mathcal{H}^1(\mu) = \left\{ f \in H^1(\mu) \mid \int_{\mathcal{E}} f d\mu = 0 \right\}$$

of centered observables, endowed with the same norm. Then there exist constants $C_\gamma, \lambda_\gamma > 0$ such that

$$(2.32) \quad \|e^{t\mathcal{L}_\gamma}\|_{\mathcal{B}(\mathcal{H}(\mu))} \leq C_\gamma e^{-t\lambda_\gamma}.$$

For the overdamped case, exponential decay rates can be obtained more directly. In both cases, conditions have to be met by V , such as a Poincaré inequality for ν , which are however trivially verified in the case where \mathcal{D} is compact.

2.2.5 Asymptotic variance for ergodic averages

Since ergodic averages are computed over a finite time-interval, the corresponding random variable will have some variance. Let us show how to relate this variance to the dynamics, provided a Central Limit Theorem holds. For simplicity, we assume that $(q_0, p_0) \sim \mu$, and let $\varphi \in H^1(\mu)$ be an observable of interest. We also denote by

$$(2.33) \quad \Pi\varphi = \varphi - \int_{\mathcal{E}} \varphi d\mu$$

the centering projector associated with μ . The Central Limit Theorem asserts that the following convergence in law holds,

$$(2.34) \quad \frac{1}{\sqrt{T}} \int_0^T \Pi\varphi(q_t, p_t) dt \xrightarrow{\text{law}} \mathcal{N}(0, \sigma_\varphi^2),$$

where σ_φ^2 is the asymptotic variance associated to φ under the dynamics, which is thus given by the limit of the variance on the left-hand side. Let us compute:

$$\sigma_T := \mathbb{E}_\mu \left[\left(\frac{1}{\sqrt{T}} \int_0^T \Pi\varphi(q_t, p_t) dt \right)^2 \right] = \frac{1}{T} \int_0^T \int_0^T \mathbb{E}_\mu [\Pi\varphi(q_t, p_t) \Pi\varphi(q_s, p_s)] ds dt.$$

By stationarity, for $t > s$, $\Pi\varphi(q_t, p_t) \Pi\varphi(q_s, p_s) \sim \Pi\varphi(q_{t-s}, p_{t-s}) \Pi\varphi(q_0, p_0)$, hence we may write, by Fubini,

$$\begin{aligned} \sigma_T &= \frac{2}{T} \int_0^T \int_0^t \mathbb{E}_\mu [\Pi\varphi(q_{t-s}, p_{t-s}) \Pi\varphi(q_0, p_0)] ds dt \\ &= \frac{2}{T} \int_0^T \int_s^T \mathbb{E}_\mu [\Pi\varphi(q_s, p_s) \Pi\varphi(q_0, p_0)] dt ds \\ &= 2 \int_0^T \mathbb{E}_\mu [\Pi\varphi(q_s, p_s) \Pi\varphi(q_0, p_0)] \left(1 - \frac{s}{T}\right) ds \\ &= 2 \int_0^T \mathbb{E}_\mu [(e^{s\mathcal{L}_\gamma} \Pi\varphi)(\Pi\varphi)] \left(1 - \frac{s}{T}\right) ds \end{aligned}$$

Using Cauchy-Schwartz in $L^2(\mu)$ and an exponential decay estimate on the evolution semigroup like (2.32), we obtain a bound of the form

$$\int_0^T \left| \mathbb{E}_\mu [(e^{s\mathcal{L}_\gamma} \Pi\varphi)(\Pi\varphi)] \frac{s}{T} \right| ds \leq \int_0^\infty C_\gamma e^{-\lambda_\gamma s} \|\Pi\varphi\|_{L^2(\mu)}^2 \frac{s}{T} ds$$

for some positive constants C and α , which converges uniformly to 0 as $T \rightarrow \infty$. It follows that

$$(2.35) \quad \sigma_\varphi^2 = \int_0^\infty \mathbb{E}_\mu [(e^{s\mathcal{L}_\gamma} \Pi\varphi)(\Pi\varphi)] ds.$$

We use the following equality of bounded operators on $H^1(\mu)$, which is the continuous analog of a Neumann series:

$$(2.36) \quad (-\mathcal{L}_\gamma)^{-1} = \int_0^\infty e^{s\mathcal{L}_\gamma} ds,$$

which again is justified by the exponential decay rate of evolution semigroup, and where the integral on the right is in the Bochner sense. Using this identity, we can write the asymptotic variance more concisely,

$$(2.37) \quad \sigma_\varphi^2 = \mathbb{E}_\mu [(\Pi\varphi)(-\mathcal{L}_\gamma)^{-1}(\Pi\varphi)].$$

Note that the exact same computations can be performed for the overdamped Langevin dynamics. It follows from [1], (Theorem 2.1) that a sufficient condition for a CLT to hold is that $\Pi\varphi \in \text{Ran } \mathcal{L}_\gamma$, which is the case provided we can express the inverse of \mathcal{L}_γ using (2.36).

2.2.6 Splitting schemes for the Langevin dynamics

Similar to the Hamiltonian case, the generator (2.16) splits into three elementary generators, namely

$$\mathcal{L}_\gamma = A + B + \gamma C = \mathcal{L}_{\text{ham}} + \gamma C,$$

with

$$(2.38) \quad C = -M^{-1}p \cdot \nabla_p + \frac{1}{\beta}\Delta_p.$$

These generators individually give rise to dynamics which we can express explicitly, defined by the following evolution operators:

$$(2.39) \quad \begin{cases} e^{tA}\varphi(q, p) = \varphi(q + tM^{-1}p, p), \\ e^{tB}\varphi(q, p) = \varphi(q, p - t\nabla V(q)), \\ e^{t\gamma C}\varphi(q, p) = \mathbb{E} \left[\varphi \left(q, e^{-\gamma M^{-1}t}p + \sqrt{\frac{M}{\beta}(1 - e^{-2\gamma M^{-1}t})}G \right) \right], \end{cases}$$

where G is a standard dN -dimensional Gaussian. The third equality translates an equality in law between an Itô integral and a Gaussian random variable, and follows by applying Itô's formula to the rescaled process

$$e^{\gamma M^{-1}t}X_t,$$

where X_t is the Ornstein-Uhlenbeck process:

$$(2.40) \quad dX_t = -\gamma M^{-1}X_t dt + \sqrt{\frac{2\gamma}{\beta}}dW_t.$$

The dynamics associated with the A and B part are deterministic Hamiltonian dynamics already identified in (2.7). Just as in the Hamiltonian case, we can define schemes for the Langevin dynamics based on approximating the evolution operator (2.17) over one timestep by splitting the generator \mathcal{L}_γ , and combining the corresponding evolution operators (2.39) in a sequence. We refer to such a splitting approximation by the sequence in which the individual propagators are composed. It is useful at this point to introduce the stochastic flow map associated with the Ornstein-Uhlenbeck dynamics.

$$(2.41) \quad \Phi_t^C(q, p, \xi) = \left(q, e^{-\gamma M^{-1}t}p + \sqrt{\frac{M}{\beta}(1 - e^{-2\gamma M^{-1}t})}\xi \right),$$

where $\xi \in \mathbb{R}^{dN}$, the point being $\mathbb{E}[\varphi(\Phi_t^C(q, p, G))] = e^{t\gamma C}\varphi(q, p)$ when G is standard Gaussian. Given an ordering of operators,

$$(2.42) \quad (R_1, \dots, R_k) \in \{A, B, \gamma C\}^k,$$

we can consider the mapping obtained by composing the elementary flows, noted as

$$(2.43) \quad \Phi^{R_1, \dots, R_k} := \Phi_{\Delta t/n_{R_k}}^{R_k} \circ \dots \circ \Phi_{\Delta t/n_{R_1}}^{R_1},$$

where

$$n_R := \#\{1 \leq j \leq n | R_j = R\}$$

for $R \in \{A, B, \gamma C\}$, and which we may consider by a slight abuse to be the mapping which takes a point in phase space and $n_{\gamma C}$ vectors in \mathbb{R}^{dN} ($\xi_1, \dots, \xi_{n_{\gamma C}}$), yielding a point in phase space by successively applying the flow, and, if need be, stochastic flow, mappings corresponding to the reverse ordering of (2.42). Applying this mapping with a vector of independent standard Gaussians

yields a stochastic mapping, which defines the update rule for the splitting scheme associated with the ordering (2.42). An important property which follows from writing the update rule using the mapping (2.43) is that numerical trajectories formed by iterating this update rule with independent vectors of standard Gaussians form a Markov chain. The hope is that the invariant measure corresponding to this Markov chain (provided it is unique) is a close approximation to the canonical measure, as well as being ergodic. It is less cumbersome to write such schemes at the level of the evolution operator associated with the Markov chain,

$$(2.44) \quad P_{\Delta t} \varphi(q, p) = \mathbb{E} [\varphi(q^1, p^1) | q^0 = q, p^0 = p].$$

The evolution operator associated with the splitting (2.42) is

$$(2.45) \quad P_{\Delta t} = e^{\frac{\Delta t}{n_{R^1}} R_1} \cdots e^{\frac{\Delta t}{n_{R^k}} R_k}.$$

Note that the order is reversed compared to the stochastic flow formulation. We will refer to such schemes by the name obtained by concatenating the names of each operator appearing in the ordering, using O instead of γC . For instance, the BAO scheme is given by the following update rule, which corresponds to applying the symplectic Euler scheme over one timestep, followed by one timestep of the Ornstein-Uhlenbeck stochastic flow (2.41).

Example 4 (BAO scheme). *The update rule is given by the following equations, where we introduce the intermediate momentum variable $p^{n+\frac{1}{2}}$:*

$$(2.46) \quad \begin{cases} p^{n+\frac{1}{2}} = p^n - \Delta t \nabla V(q^n) \\ q^{n+1} = q^n + \Delta t M^{-1} p^{n+\frac{1}{2}} \\ p^{n+1} = \alpha_{\Delta t} p^{n+\frac{1}{2}} + \sigma_{\Delta t} G^n, \end{cases}$$

where G^n is a standard dN -dimensional Gaussian, and $\alpha_{\Delta t}$, $\sigma_{\Delta t}$ are given by

$$(2.47) \quad \alpha_{\Delta t} = e^{-\gamma M^{-1} \Delta t}, \quad \sigma_{\Delta t} = \sqrt{\frac{M}{\beta} (1 - \alpha_{\Delta t}^2)}.$$

Similarly, we define the BAOAB scheme.

Example 5 (BAOAB scheme). *The update rule is given by the following equations, with additional intermediate coordinate and momentum variables:*

$$(2.48) \quad \begin{cases} p^{n+\frac{1}{3}} = p^n - \frac{\Delta t}{2} \nabla V(q^n) \\ q^{n+\frac{1}{2}} = q^n + \frac{\Delta t}{2} M^{-1} p^{n+\frac{1}{3}} \\ p^{n+\frac{2}{3}} = \alpha_{\Delta t} p^{n+\frac{1}{3}} + \sigma_{\Delta t} G^n \\ q^{n+1} = q^{n+\frac{1}{2}} + \frac{\Delta t}{2} M^{-1} p^{n+\frac{2}{3}} \\ p^{n+1} = p^{n+\frac{2}{3}} - \frac{\Delta t}{2} \nabla V(q^{n+1}), \end{cases}$$

where, again, G^n is a standard dN -dimensional Gaussian.

Now we have a recipe to make an infinite number of numerical schemes, which can easily be implemented in a computer. We could even go further and consider methods with an uneven distribution for the secondary timesteps, the introduction of negative secondary timesteps for the A and B steps, and so on. This room for creativity highlights the need for criteria to assess the quality of such schemes. Several considerations have to be weighed.

- (i) Our aim is to compute long trajectories, which are needed to ensure that phase space is properly explored, as well as to obtain better statistical properties for averages (2.5). Thus, for a fixed computational budget, we desire a scheme which allows us to take as large a timestep Δt as possible. This is the issue of numerical stability.
- (ii) The use of a positive timestep Δt implies in general that the invariant measure for the Markov chain corresponding to a given scheme is not the canonical measure. This issue is called systematic error, or bias, and one would desire a scheme which minimizes this bias.
- (iii) The main computational cost in computing iterates of these numerical schemes is the evaluation of the gradient of the potential used for the B steps. As such, it is desirable to have a scheme which requires as few evaluations of this gradient per iteration. Some care must be taken when implementing these, to ensure that already computed gradients are not re-computed: for instance, the gradient in the last step of the BOAB scheme, is equal to the one in the first step of the next iteration.
- (iv) Notice that the parameter γ is free for the practitioner to choose. A natural question is to determine the properties of the marginal dynamics in q in the limit $\gamma \rightarrow +\infty$, and in particular if we obtain a consistent discretization of the overdamped Langevin dynamics. Conversely, one could ask about properties of the dynamics as we take the Hamiltonian limit $\gamma \rightarrow 0$.

Remark 7 (Overdamped and Hamiltonian limits in splitting schemes). *Concern (iv) is simple to address. Since*

$$\lim_{\gamma \rightarrow 0} \alpha_{\Delta t} = 1 \quad \lim_{\gamma \rightarrow +\infty} \alpha_{\Delta t} = 0,$$

every O-step can simply be dropped as $\gamma \rightarrow 0$ from the sequence of operators defining the splitting. This yields a symplectic scheme for the Hamiltonian parts of the dynamics, whose properties can be analyzed as before. For this reason, the ordering of the Hamiltonian parts of the splitting of most commonly used schemes correspond to that of a velocity Verlet method. As $\gamma \rightarrow \infty$, every O-step reduces to resampling the momentum according to the Maxwell-Boltzmann distribution. The properties of the resulting scheme depend on the particular ordering of the splitting at hand. For instance, if every A step is preceded by an O step, then the potential is entirely ignored by the evolution, and the trajectories form an isotropic random walk. This is for instance the case of the BOA scheme. On the other hand, it may happen that one obtains a discretization of the overdamped Langevin dynamics. For example, the update equation for the overdamped limit of the BAOA scheme in the case $M = \text{Id}$ rewrites

$$q^{n+1} = q^n - \frac{\Delta t^2}{2} \nabla V(q^n) + \frac{1}{2} \sqrt{\frac{\Delta t^2}{\beta}} (G^n + G^{n+1}),$$

with (G^n) an i.i.d. standard Gaussian sequence. Because of the two-step correlations in the Gaussian increments, the numerical trajectories are not Markovian,. Nevertheless the scheme is reminiscent of a discretization of the overdamped equation (2.30), but with an effective timestep $\frac{\Delta t^2}{2}$. This quadratic rescaling of the timestep is common, and has to be related to the fact that the overdamped equation is defined through a diffusive rescaling. This discretization also corresponds to the overdamped limit of the BAOAB scheme, which is unsurprising in view of the results of the next chapter.

2.2.7 Error analysis for splitting schemes

We turn our attention to analyzing the error arising from the estimation of canonical expectations by discrete ergodic averages. We consider estimations of the form

$$\widehat{\varphi}_{N_{\text{iter}}} := \frac{1}{N_{\text{iter}}} \sum_{i=0}^{N_{\text{iter}}-1} \varphi(q^i, p^i),$$

where $(q^n, p^n)_{n \geq 0}$ is a numerical trajectory of a Markov chain which is ergodic with respect to a unique stationary distribution $\pi_{\Delta t}$ on \mathcal{E} , which approximates μ . For simplicity, we will assume that (q^0, p^0) is distributed according to $\pi_{\Delta t}$, so that the whole numerical trajectory is stationary. This requires in practice that the system be equilibrated before starting to sample the observables of interest. We decompose the error as follows:

$$\widehat{\varphi}_{N_{\text{iter}}} - \int_{\mathcal{E}} \varphi \, d\mu = \widehat{\varphi}_{N_{\text{iter}}} - \int_{\mathcal{E}} \varphi \, d\pi_{\Delta t} + \int_{\mathcal{E}} \varphi \, d\pi_{\Delta t} - \int_{\mathcal{E}} \varphi \, d\mu.$$

Two terms contribute to the error.

Statistical Error

The first term

$$\widehat{\varphi}_{N_{\text{iter}}} - \int_{\mathcal{E}} \varphi \, d\pi_{\Delta t}$$

is the statistical error due to the truncation of computed trajectories to a finite time $T_{\text{sim}} := N_{\text{iter}} \Delta t$. By the Central Limit Theorem for Markov Chains, asymptotically, the statistical error is of order

$$\frac{\sigma_{\varphi, \Delta t}}{\sqrt{N_{\text{iter}}}},$$

where $\sigma_{\varphi, \Delta t}$ is the asymptotic variance of the Markov chain, which is given by the following expression, under suitable assumptions, by

$$\sigma_{\varphi, \Delta t}^2 = \text{Var}_{\pi_{\Delta t}}(\varphi) + 2 \sum_{k=1}^{\infty} \text{Cov}_{\pi_{\Delta t}}(\varphi(q^0, p^0) \varphi(q^k, p^k)).$$

The proof of the above expression is in spirit the same as the one in the continuous case, exploiting the stationarity in law of the trajectory. Using the evolution and projection operators associated with the Markov chain, which are respectively defined by

$$(2.49) \quad P_{\Delta t} \varphi(q, p) = \mathbb{E}[\varphi(q^1, p^1) | (q^0, p^0) = (q, p)], \quad \Pi_{\Delta t} \varphi = \varphi - \int_{\mathcal{E}} \varphi \, d\pi_{\Delta t},$$

we can rewrite the asymptotic variance in a more analytic form, namely

$$(2.50) \quad \sigma_{\varphi, \Delta t}^2 = 2 \int_{\mathcal{E}} (\Pi_{\Delta t} \varphi)(\text{Id} - P_{\Delta t})^{-1} (\Pi_{\Delta t} \varphi) \, d\pi_{\Delta t} - \int_{\mathcal{E}} (\Pi_{\Delta t} \varphi)^2 \, d\pi_{\Delta t},$$

where we used formally the Neumann series

$$\sum_{k=0}^{\infty} P_{\Delta t} = (\text{Id} - P_{\Delta t})^{-1},$$

which has to be justified rigorously, usually using a geometric decay estimate for $P_{\Delta t}^n$, seen as an operator on $L_0^2(\pi_{\Delta t}) = \Pi_{\Delta t} L^2(\pi_{\Delta t})$. This implies that

$$\Delta t \sigma_{\varphi, \Delta t}^2 = 2 \int_{\mathcal{E}} (\Pi_{\Delta t} \varphi) \left(\frac{\text{Id} - P_{\Delta t}}{\Delta t} \right)^{-1} (\Pi_{\Delta t} \varphi) \, d\pi_{\Delta t} + O(\Delta t).$$

For reasonable discretizations of the Langevin dynamics, we expect that

$$\frac{\text{Id} - P_{\Delta t}}{\Delta t} = -\mathcal{L}_\gamma + O(\Delta t),$$

which suggests that at dominant order in Δt approaching 0, $\Delta t \sigma_{\varphi, \Delta t}^2$ behaves like

$$2 \int_{\mathcal{E}} (\Pi \varphi) (-\mathcal{L}_\gamma)^{-1} (\Pi \varphi) \, d\mu = \sigma_\varphi^2,$$

where we recall the asymptotic variance for the continuous dynamics (2.37) Hence the statistical error can be estimated, for Δt small enough, by

$$\frac{\sigma_{\varphi, \Delta t}}{\sqrt{N_{\text{iter}}}} = \frac{\sigma_{\varphi, \Delta t} \sqrt{\Delta t}}{\sqrt{T_{\text{sim}}}} \approx \frac{\sigma_{\varphi}}{\sqrt{T_{\text{sim}}}}.$$

Loosely speaking, the statistical error for the discrete ergodic estimator is governed at dominant order by the corresponding asymptotic variance for the underlying continuous dynamics, as well as the *physical* time of the simulation. This confirms that to minimize statistical error, and given a fixed budget of simulation steps, one should maximize T_{sim} and thus Δt , as discussed in consideration (i). However, increasing the timestep comes at the following cost.

Systematic Error

The second term,

$$\int_{\mathcal{E}} \varphi d\pi_{\Delta t} - \int_{\mathcal{E}} \varphi d\mu,$$

is independent of the simulation time, and expresses the fact, highlighted in consideration (ii), that the invariant measure $\pi_{\Delta t}$ for the discrete evolution will in general be offset from μ , in the sense that the average of an observable φ under $\pi_{\Delta t}$ can be expressed by an expansion of the form

$$(2.51) \quad \int_{\mathcal{E}} \varphi(q, p) \pi_{\Delta t}(dq, dp) = \int_{\mathcal{E}} \varphi(q, p) \mu(dq, dp) + \Delta t^\alpha \int_{\mathcal{E}} \varphi(q, p) f_\alpha(q, p) \mu(dq, dp) + O(\Delta t^{\alpha+1}),$$

where $\alpha > 0$ and f_α is the dominant correction term, which can be explicitly computed for splitting schemes. We postpone further discussion of these types of weak error estimates to the next chapter, in which we analyze the systematic error in the BAOA scheme.

2.2.8 Unbiased sampling

It turns out that one can devise schemes which have no systematic error: the Markov chain generating the trajectories has invariant measure exactly μ . These methods are based on the Metropolis-Hastings algorithm, which gives a general method to sample a given target distribution.

The Metropolis-Hastings algorithm

We aim to sample from a given target measure on \mathbb{R}^d . We suppose we have at our disposal a way to generate proposal points from a given point $\in \mathbb{R}^d$. This amounts to defining a transition kernel, the *proposal*, which we may take to be a map

$$T : \mathbb{R}^d \times \mathbb{R}^d \longrightarrow \mathbb{R}_+,$$

such that for any $x \in \mathbb{R}^d$, $T(x, \cdot)$ is a probability density on \mathbb{R}^d , and which is cheap to sample from (very often these are taken to be some form of Gaussian distribution). We also assume that we always have $T(x, y) > 0$. (This is always the case if the kernel is Gaussian). We also fix a function $r : \mathbb{R}_+ \rightarrow (0, 1]$, the *rule*, which satisfies the property

$$(2.52) \quad x \cdot r\left(\frac{1}{x}\right) = r(x)$$

We then define a Markov chain by iterating the following algorithm, starting from an arbitrary point $q^0 \in \mathbb{R}^d$.

Algorithm 1 (Metropolis-Hastings). *From a given point q^n*

- (1) *Sample a proposal \tilde{q}^{n+1} according to the probability law $T(q^n, \cdot)$.*

(2) Compute

$$R(\tilde{q}^{n+1}, q^n) = r \left(\frac{\pi(\tilde{q}^{n+1})T(\tilde{q}^{n+1}, q^n)}{\pi(q^n)T(q^n, \tilde{q}^{n+1})} \right).$$

(3) With probability $R(\tilde{q}^{n+1}, q^n)$, set $q^{n+1} = \tilde{q}^{n+1}$, otherwise, set $q^{n+1} = q^n$.

(4) Go back to step (1) with $q^n \leftarrow q^{n+1}$.

Since T defines a Markov chain, we may always write $\tilde{q}^{n+1} = \Phi(q^n, \xi^n)$ for some family of *i.i.d.* variables $(\xi^n)_{n \geq 0}$. We can then write q^{n+1} in a concise form:

$$(2.53) \quad q^{n+1} = \Phi(q^n, \xi^n) + \mathbb{1}_{U^n > R(\Phi(q^n, \xi^n), q^n)} (q^n - \Phi(q^n, \xi^n)) = \Psi(q^n, \xi^n, U^n),$$

where the U^n are *i.i.d.* uniform on $[0, 1]$, such that the (ξ^n, U^n) are an independent family. This shows that the algorithm defines a Markov chain. Furthermore, we may compute

$$\begin{aligned} \pi(x)\mathbb{P}(q^1 = y | q^0 = x) &= \pi(x)T(x, y)R(x, y) \\ &= \pi(x)T(x, y)r \left(\frac{\pi(y)T(y, x)}{\pi(x)T(x, y)} \right) \\ (2.54) \quad &= \pi(y)T(y, x) \frac{\pi(x)T(x, y)}{\pi(y)T(y, x)} r \left(\frac{\pi(y)T(y, x)}{\pi(x)T(x, y)} \right) \\ &= \pi(y)T(y, x)r \left(\frac{\pi(x)T(x, y)}{\pi(y)T(y, x)} \right) \text{ (Using (2.52))} \\ &= \pi(y)\mathbb{P}(q^1 = x | q^0 = y). \end{aligned}$$

Thus, the chain is reversible with respect to π which is then an invariant measure. Note that the algorithm is applicable even when we do not know how to evaluate π , but only the ratios $\pi(x)/\pi(y)$, which is in particular the case for Gibbs measures.

Remark 8 (Rules for Metropolis-Hastings). *Possible choices for r are:*

1. *The Metropolis rule,*

$$r(x) = \min \{1, x\},$$

2. *The Barker rule,*

$$r(x) = \frac{x}{1+x},$$

3. *Any combination of these of the form, for $\gamma > 0$,*

$$r(x) = \frac{x}{1+x} \left(1 + 2 \left(\frac{1}{2} \min \left(r, \frac{1}{r} \right) \right)^\gamma \right).$$

Remark 9 (Issues with Metropolized-schemes). *The Metropolis-Hastings algorithm provides a general recipe to define an unbiased Markov chain for the overdamped Langevin dynamics: one only needs to specify a proposition kernel, an acceptance rule, and a way to compute the ratio of the corresponding transition probabilities. For example, the so-called MALA scheme is very common, which combines a proposal function based on the Euler-Maruyama discretization of the dynamics (2.27), and a Metropolis acceptance rule. The use of the Metropolis-Hastings algorithm is not free. Because of the rejection rate, the correlations between samples decays at a slower rate, resulting in a higher asymptotic variance for estimators based on ergodic averages. This implies that the use of a Metropolized scheme is only beneficial if the simulation time regime in which the systematic error overcomes the statistical error is computationally attainable. For most systems of interest, this is not the case. Furthermore, the possibility of rejection effectively slows down the dynamics, which may degrade the quality of estimates for dynamical quantities. The effect of the Metropolization procedure with the MALA scheme on the estimation of self-diffusion properties has been analyzed in [3], and improved rules and proposals for the computation of transport properties are discussed in detail in [4].*

2.2.9 Numerical illustrations

We now turn to a few numerical illustrations of the discussions above. In Figure 2.3, we compute numerically compute the pressure as a function of the density for the Lennard-Jones fluid, using the parameters for Argon, at two different temperatures. The resulting profile gives a numerical estimation of the equation of state of Argon, and comparison with experimental data shows that the agreement is very good at low densities and room temperature. The size of the systems was $N = 2744$ atoms, using a sharp cutoff at $r_c = 1.364$ nm, and a BOAB splitting scheme with $\Delta t = 0.01$ ps. A reduced value of $\gamma = 1.0$ was used for the friction parameter. We verified by using a block averaging procedure for the trajectories at both ends of the density range that the standard error bars are negligible.

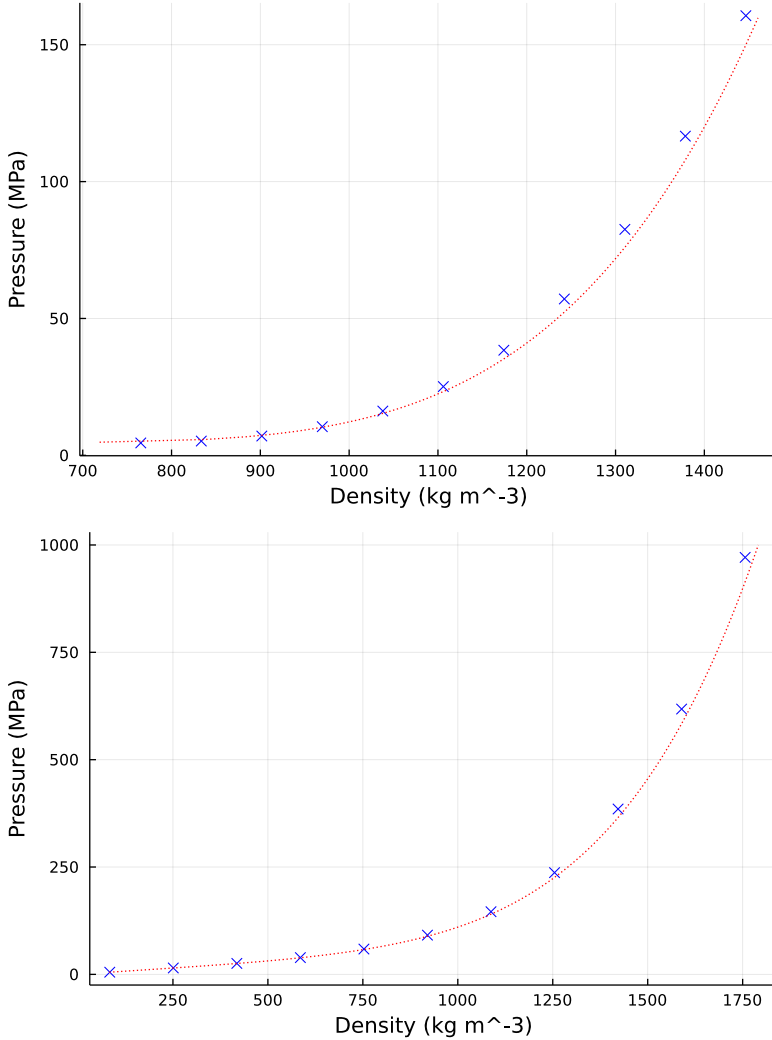


Figure 2.3: Simulated equations of state of Argon at 150 K (liquid phase, left) and 300 K (supercritical phase, right). Experimental reference curves are plotted in red, simulated data points are scattered in blue.

In Figures 2.4 and 2.5, we highlight the systematic error in several observables. Simulations were run for systems of $N = 27$ Lennard-Jones particles, at a temperature $T = 1.25$ and at a reduced density $\rho = 0.25$. A cutoff of the potential at a distance $r_c = 2.0$ was imposed,

with a linear correction term ensuring that V be C^1 . Additionally, regression lines were added by extrapolating the behavior at small Δt based on the theoretical expansions (2.51), and constraining the regression lines to converge in the limit $\Delta t \rightarrow 0$. This was achieved by a linear least squares regression procedure. The result also illustrate that a possibility to reduce the systematic error is to compute a desired average for several timesteps, and computing an extrapolated value at $\Delta t = 0$ based on the theoretical knowledge of the behavior of the systematic error as $\Delta t \rightarrow 0$. This is known as Romberg extrapolation (ref?).

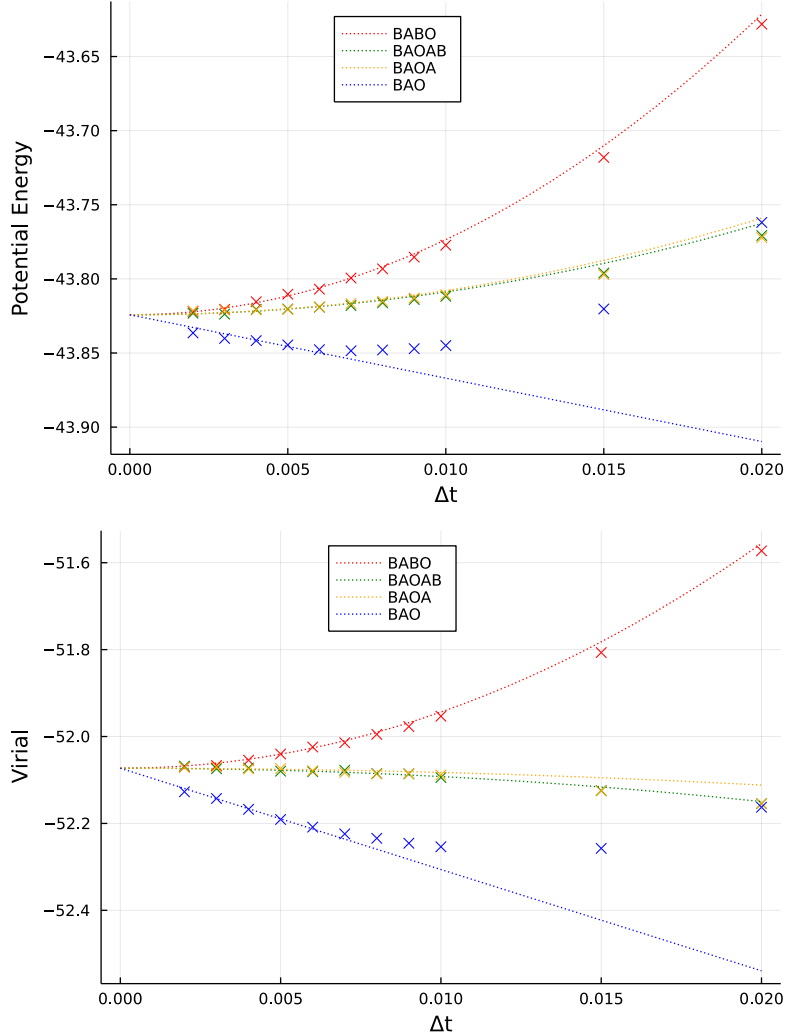


Figure 2.4: Systematic error in configurational quantities for a Lennard-Jones fluid.

For the two configurational quantities we investigated, the virial and potential energy, we observe an overlap in the bias between the BAOAB and BAOA schemes. It so happens that this overlap can be simply explained by a result relating the invariant measures of certain pairs of numerical schemes (Lemma 2). In fact, a preprint [7] was recently posted, showing that a certain widely used scheme in the molecular dynamics community was equivalent to the BAOA scheme, and that the latter sampled the same configurational marginal as the BAOAB scheme. This prompted the need for a more thorough investigation of the properties of the BAOA scheme, which we discuss in the next chapter.

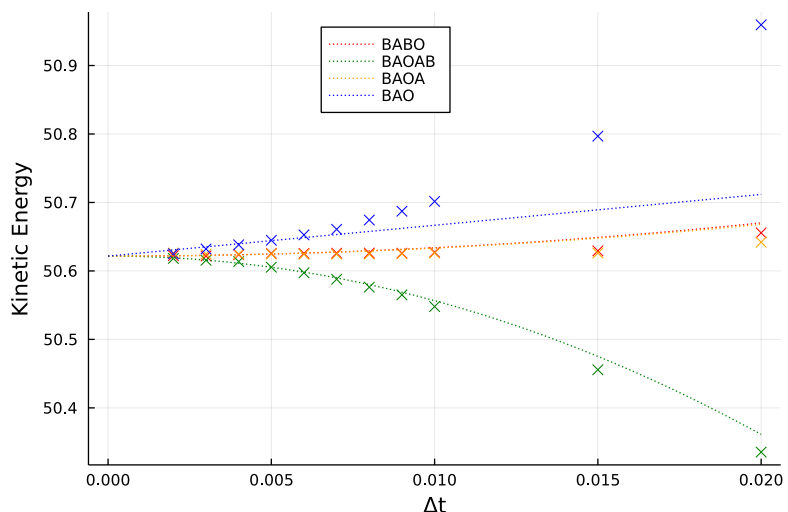


Figure 2.5: Systematic error in kinetic energy for a Lennard-Jones fluid.

Chapter 3

Study of the BAOA scheme

We consider time discretization schemes of underdamped Langevin dynamics known as the BAOA and BAOAB schemes, in order to compare the sampling bias induced by the timestep Δt for these two methods. Analysis of the timestep bias for the BAOAB scheme is given in [10], however it does not appear that the BAOA bias is so well understood. It has been observed numerically in [7] (Section III.B) that the bias on the kinetic marginal distribution is much lower using the BAOA method. We attempt to explain this from a theoretical point of view, before illustrating our results in numerical examples. Building on known results for the BAOAB scheme, we show the following results.

- (i) In section 3.0.2, we express the invariant measure of the BAOA scheme in terms of the invariant measure of the BAOAB scheme (Proposition 5), and using this expression, we show, as in [7] (Section II.C), the equality between their respective configurational marginal distributions (Corollary 1).
- (ii) In section 3.0.3, we show that the dominant error term for BAOA averages is only of order one in Δt , confirming that the BAOAB method is in general of higher order (Corollary 2).
- (iii) We show in section 3.0.4 that for kinetic observables, however, the error is of second order in Δt , so that both marginal distributions are second-order accurate (Corollary 3).
- (iv) In section 3.0.5, we give an expression for the dominant error term in the kinetic marginal distribution of the BAOA scheme (Proposition 6). In fact, we conjecture that, at least in dimension one, this term cancels, leading to an order of at least Δt^3 (Conjecture 1).
- (v) Lastly, in section 3.0.6, we analyze the difference between the kinetic marginal distribution under the BAOA and BAOAB scheme (Proposition 7), and explain why this difference leads to a systematic underestimation of the kinetic variance in BAOAB trajectories (Remark 11).

3.0.1 Definitions and notations

We consider two splitting schemes for (2.14), as defined by the following evolution operators:

$$(3.1) \quad \begin{cases} P_{\Delta t} = e^{\Delta t B} e^{\frac{\Delta t}{2} A} e^{\Delta t \gamma C} e^{\frac{\Delta t}{2} A}, \\ Q_{\Delta t} = e^{\frac{\Delta t}{2} B} e^{\frac{\Delta t}{2} A} e^{\Delta t \gamma C} e^{\frac{\Delta t}{2} A} e^{\frac{\Delta t}{2} B}. \end{cases}$$

These correspond respectively to the BAOA and the BAOAB scheme. We also denote $\mu_{\Delta t, P}, \mu_{\Delta t, Q}$ the invariant measures for the Markov chains associated with (3.1). We assume these have smooth densities which we also denote $\mu_{\Delta t, P}, \mu_{\Delta t, Q}$, and that a certain ergodicity condition holds (see Lemma 2). Additionally we denote by $\nu_{\Delta t, P}, \nu_{\Delta t, Q}, \kappa_{\Delta t, P}, \kappa_{\Delta t, Q}$ the associated marginals and densities with obvious notation inspired by (1.8).

3.0.2 Relating invariant measures of discretization schemes

In this paragraph, we provide a formula for $\mu_{\Delta t, P}$ in terms of $\mu_{\Delta t, Q}$. This result allows one to very simply show the equality in the configurational marginals between these two measures, as noted in [7]. The main tool is the following result, which is a reformulation of the TU lemma (Lemma 9 from [10]).

Lemma 2. *Let $P_{\Delta t}, Q_{\Delta t}$ be bounded operators on $B^\infty(\mathcal{E})$. Assume that, for any $n \geq 1$,*

$$R_{\Delta t} P_{\Delta t}^n = Q_{\Delta t}^n S_{\Delta t},$$

where $R_{\Delta t}$ and $S_{\Delta t}$ are bounded operators on $B^\infty(\mathcal{E})$, such that $R_{\Delta t} \mathbb{1} = \mathbb{1}$, and that the following ergodic condition holds: for any $\varphi \in B^\infty(\mathcal{E})$, and almost all $(q, p) \in \mathcal{E}$,

$$\begin{aligned} \lim_{n \rightarrow \infty} P_{\Delta t}^n \varphi(q, p) &= \int_{\mathcal{E}} \varphi(q, p) \mu_{\Delta t, P}(dq, dp) \\ \lim_{n \rightarrow \infty} Q_{\Delta t}^n \varphi(q, p) &= \int_{\mathcal{E}} \varphi(q, p) \mu_{\Delta t, Q}(dq, dp). \end{aligned}$$

Then we have the relation $\mu_{\Delta t, P}$ and $\mu_{\Delta t, Q}$ via the following relation:

$$\int_{\mathcal{E}} \varphi(q, p) \mu_{\Delta t, P}(dq, dp) = \int_{\mathcal{E}} (S_{\Delta t} \varphi)(q, p) \mu_{\Delta t, Q}(dq, dp)$$

Proof. Fix an initial probability measure ρ on \mathcal{E} , absolutely continuous with respect to the Lebesgue measure. Then we may write, using dominated convergence to pass to the limit:

$$\begin{aligned} &\int_{\mathcal{E}} R P_{\Delta t}^n \varphi(q, p) \rho(dq, dp) \\ &= \int_{\mathcal{E}} P_{\Delta t}^n \varphi(q, p) R^\dagger \rho(dq, dp) \\ &\xrightarrow{n \rightarrow \infty} \int_{\mathcal{E}} \left(\int_{\mathcal{E}} \varphi(q, p) \mu_{\Delta t, P}(dq, dp) \right) R^\dagger \rho(d\tilde{q}, d\tilde{p}) \\ &= \int_{\mathcal{E}} \varphi(q, p) \mu_{\Delta t, P}(dq, dp) \int_{\mathcal{E}} R \mathbb{1} d\rho \\ &= \int_{\mathcal{E}} \varphi(q, p) \mu_{\Delta t, P}(dq, dp) \end{aligned}$$

Furthermore, applying the ergodic condition to the bounded function $S\varphi$ gives

$$\int_{\mathcal{E}} Q_{\Delta t}^n (S\varphi)(q, p) \rho(dq, dp) \xrightarrow{n \rightarrow \infty} \int_{\mathcal{E}} \left(\int_{\mathcal{E}} S\varphi(q, p) \mu_{\Delta t, Q}(dq, dp) \right) \rho(d\tilde{q}, d\tilde{p}) = \int_{\mathcal{E}} S\varphi(q, p) \mu_{\Delta t, Q}(dq, dp).$$

Since $R P_{\Delta t}^n = Q_{\Delta t}^n S$, identifying the two limits yields (2) □

Applying Lemma 2 to (3.1) yields the following result.

Proposition 5. *The following relation between the densities $\mu_{\Delta t, P}$ and $\mu_{\Delta t, Q}$ holds.*

$$(3.2) \quad \mu_{\Delta t, P}(q, p) = \mu_{\Delta t, Q} \left(q, p - \frac{\Delta t}{2} V(q) \right).$$

Proof. From the expressions (3.1), we immediately get:

$$(3.3) \quad P_{\Delta t}^n e^{\frac{\Delta t}{2}B} = e^{\frac{\Delta t}{2}B} Q_{\Delta t}^n,$$

whereby applying Lemma 2, we get for any test function φ ,

$$(3.4) \quad \int_{\mathcal{E}} e^{\frac{\Delta t}{2}B} \varphi d\mu_{P,\Delta t} = \int_{\mathcal{E}} \varphi d\mu_{Q,\Delta t}$$

Using equation (3.4) with $\psi = e^{-\frac{\Delta t}{2}B} \varphi$ yields an exact expression for $\mu_{\Delta t,P}$ in terms of $\mu_{\Delta t,Q}$:

$$(3.5) \quad \int_{\mathcal{E}} \varphi d\mu_{\Delta t,P} = \int_{\mathcal{E}} e^{-\frac{\Delta t}{2}B} \varphi d\mu_{\Delta t,Q}.$$

Since φ is arbitrary, we infer that at the level of densities,

$$(3.6) \quad \mu_{\Delta t,P}(q,p) = \left(e^{-\frac{\Delta t}{2}B} \right)^{\dagger} \mu_{\Delta t,Q}(q,p),$$

where \dagger denotes the adjoint on the flat space $L^2(\mathcal{E})$. A simple computation shows that

$$e^{-\frac{\Delta t}{2}B^{\dagger}} = e^{\frac{\Delta t}{2}B},$$

since $B^{\dagger} = -B$. Hence,

$$(3.7) \quad \mu_{\Delta t,P}(q,p) = e^{\frac{\Delta t B}{2}} \mu_{\Delta t,Q}(q,p) = \mu_{\Delta t,Q} \left(q, p - \frac{\Delta t}{2} \nabla V(q) \right),$$

which is the desired conclusion. \square

Relation (3.7) is enough to show an equality between the configurational marginal distributions $\nu_{\Delta t,P}$ and $\nu_{\Delta t,Q}$, as noted in [7].

Corollary 1. *The marginal distributions in the q variable of $\mu_{\Delta t,P}$ and $\mu_{\Delta t,Q}$ coincide:*

$$(3.8) \quad \nu_{\Delta t,Q}(q) = \nu_{\Delta t,P}(q).$$

Proof. Write, for any $q \in \mathcal{D}$,

$$\begin{aligned} \nu_{\Delta t,Q}(q) &= \int_{\mathbb{R}^{dN}} \mu_{\Delta t,Q}(q,p) dp \\ &= \int_{\mathbb{R}^{dN}} \mu_{\Delta t,Q} \left(q, p - \frac{\Delta t}{2} \nabla V(q) \right) dp \\ &= \int_{\mathbb{R}^{dN}} \mu_{\Delta t,P}(q,p) dp \\ &= \nu_{\Delta t,P}(q), \end{aligned}$$

which proves the claim. \square

3.0.3 Error estimate on the phase space measure

We now turn to obtaining the dominant order in the sampling bias of $\mu_{\Delta t,P}$, building on previously known results for $\mu_{\Delta t,Q}$, and the relation (3.2). Error estimates on $\mu_{\Delta t,Q}$ have been investigated in [10] (Section 1.4). In particular, the following expansion of $\mu_{\Delta t,Q}$ is derived, which will be central in our analysis.

Theorem 2 (Theorem 13 in [10]). *There exists a smooth function f_2 such that for any smooth ψ ,*

$$(3.9) \quad \int_{\mathcal{E}} \psi(q, p) \mu_{\Delta t, Q}(q, p) dq dp = \int_{\mathcal{E}} \psi(q, p) \mu(q, p) dq dp + \Delta t^2 \int_{\mathcal{E}} \varphi(q, p) f_2(q, p) \mu(q, p) dq dp + \Delta t^4 r_{\psi, \gamma, \Delta t},$$

where the remainder $r_{\psi, \gamma, \Delta t}$ is uniformly bounded for Δt sufficiently small. Moreover, an expression for the dominant error term is obtained,

$$(3.10) \quad \begin{cases} f_2 = \tilde{f}_2 - \frac{1}{8}(A + B)g \\ \mathcal{L}_\gamma^* \tilde{f}_2 = \frac{1}{12}(A + B) \left[\left(A + \frac{B}{2} \right) g \right], \\ g := \beta(M^{-1}p) \cdot \nabla V(q) \end{cases}$$

where \mathcal{L}_γ^* is the adjoint of \mathcal{L}_γ on the weighted space $L^2(\mu)$.

Smoothness here is meant in a technical sense (see Definition 8 in [10]), which we refrain from detailing here. Using this expansion, one can derive the dominant order error for the BAOA scheme.

Corollary 2. *For any smooth observable φ ,*

$$(3.11) \quad \int_{\mathcal{E}} \varphi(q, p) \mu_{\Delta t, P}(q, p) dq dp = \int_{\mathcal{E}} \varphi(q, p) \left(1 + \frac{\Delta t}{2} g(q, p) \right) \mu(q, p) dq dp + O(\Delta t^2),$$

where g is given by (3.10).

Proof. Combining (3.9) with (3.2), we get the following estimation for averages with respect to $\mu_{\Delta t, P}$:

$$(3.12) \quad \int_{\mathcal{E}} \varphi(q, p) \mu_{\Delta t, P}(q, p) dq dp = \int_{\mathcal{E}} \varphi(q, p) \mu \left(q, p - \frac{\Delta t}{2} \nabla V(q) \right) dq dp + O(\Delta t^2).$$

Taylor expanding μ gives

$$\mu \left(q, p - \frac{\Delta t}{2} \nabla V(q) \right) = \mu(q, p) \left(1 + \frac{\Delta t}{2} \beta(M^{-1}p) \cdot \nabla V(q) + O(\Delta t^2) \right) = \mu(q, p) \left(1 + \frac{\Delta t}{2} g + O(\Delta t^2) \right),$$

hence we get

$$(3.13) \quad \int_{\mathcal{E}} \varphi(q, p) \mu_{\Delta t, P}(q, p) dq dp = \int_{\mathcal{E}} \varphi(q, p) \mu(q, p) \left(1 + \frac{\Delta t}{2} g(q, p) + O(\Delta t^2) \right) dq dp,$$

which proves the claim. \square

3.0.4 Error estimates on the kinetic marginal distributions

Equation (3.11) expresses the fact that the invariant measure $\mu_{\Delta t, P}$ is only exact at first order in Δt , which is one less than $\mu_{\Delta t, Q}$. So in full generality, one can expect an error of order Δt on averages obtained from BAOA trajectories, versus Δt^2 for averages computed from BAOAB trajectories. However, if we restrict ourselves to marginal observables, that is observables which only depend on the configurational coordinate or the kinetic coordinate, the first order error term vanishes. Indeed, we have the following.

Corollary 3. *Let $\varphi(q, p) = \varphi(q)$ or $\varphi(q, p) = \varphi(p)$ be a marginal observable. Then*

$$\int_{\mathcal{E}} \varphi dq d\mu_{\Delta t, P} = \int_{\mathcal{E}} \varphi dq d\mu + O(\Delta t^2).$$

Proof. By (3.11), it is sufficient to show

$$(3.14) \quad \int_{\mathcal{E}} \varphi g \, d\mu = 0.$$

This follows from the following cancellations.

$$(3.15) \quad \int_{\mathbb{R}^{dN}} g(q, p) \mu(q, p) \, dp = \int_{\mathcal{D}} g(q, p) \mu(q, p) \, dq = 0.$$

Indeed,

$$\int_{\mathbb{R}^{dN}} \beta(M^{-1}p) \cdot \nabla V(q) \mu(q, p) \, dp = 0,$$

since the integrand is an odd function of p , and the marginal of μ in p is a centered Gaussian density. Also,

$$\int_{\mathcal{D}} \beta(M^{-1}p) \cdot \nabla V(q) \mu(q, p) \, dq = - \int_{\mathcal{D}} (M^{-1}p) \cdot \nabla_q \mu(q, p) \, dq = 0,$$

by an integration by parts. By first integrating (3.14) over the coordinate independent of φ , one of the cancellations (3.15) yields the result. \square

Corollary 2 gives no new information concerning configurational observables, since we already know by Corollary 1 that these have the same averages under $\mu_{\Delta t, P}$ and $\mu_{\Delta t, Q}$, and that by Theorem 2, these have error of order Δt^2 . However, kinetic observables may yield different averages.

3.0.5 Analysis of the second order error term for kinetic averages under $\mu_{\Delta t, P}$

It was observed numerically in [7] that the averages of the kinetic and configurational temperatures computed with a BAOA scheme have a bias of order greater than Δt , as expected from the argument above. In fact, for the kinetic temperature, the order appears to be greater than Δt^2 , in contrast to averages computed with the BAOAB method. Understanding this behavior theoretically requires comparing second order error terms.

We show the following result, which identifies the second-order error term for kinetic observables.

Proposition 6. *Let $\psi(q, p) = \psi(p)$ be a smooth kinetic observable. Then,*

$$(3.16) \quad \int_{\mathcal{E}} \psi(p) \mu_{\Delta t, P}(q, p) \, dq \, dp = \int_{\mathcal{E}} \psi(p) \mu(q, p) \, dp \, dq + \Delta t^2 \int_{\mathcal{E}} \psi(p) \tilde{f}_2(q, p) \mu(q, p) \, dq \, dp + O(\Delta t^3),$$

where \tilde{f}_2 is given by (3.10).

From Theorem 13 of [10], this error term is identical to the dominant error term for OBABO averages, and minus the dominant error term for OABAO averages.

Proof. By writing

$$\int_{\mathcal{E}} \psi(q, p) \mu_{\Delta t, P}(q, p) \, dq \, dp - \int_{\mathcal{E}} \psi(q, p) \mu(q, p) \, dp \, dq = \int_{\mathcal{E}} \left(\psi(q, p) - \int_{\mathcal{E}} \psi \, d\mu \right) \mu_{\Delta t, P}(q, p) \, dq \, dp,$$

we may assume without loss of generality that ψ has average 0 with respect to μ .

Using (3.9), we get

$$\int_{\mathcal{E}} \psi(p) \mu_{\Delta t, Q}(q, p) \, dq \, dp = \Delta t^2 \int_{\mathcal{E}} \psi(p) f_2(q, p) \mu(q, p) \, dq \, dp + O(\Delta t^3),$$

so that using our relation (3.2), we get

$$\int_{\mathcal{E}} \psi(p) \mu_{\Delta t, P}(q, p) dq dp = \int_{\mathcal{E}} \psi(p) e^{\frac{\Delta t}{2} B} \mu(q, p) dq dp + \Delta t^2 \int_{\mathcal{E}} \psi(p) e^{\frac{\Delta t}{2} B} [f_2(q, p) \mu(q, p)] dq dp + O(\Delta t^3).$$

This rewrites, at dominant order,

$$\int_{\mathcal{E}} \psi(p) \mu \left(q, p - \frac{\Delta t}{2} \nabla V(q) \right) dq dp + \Delta t^2 \int_{\mathcal{E}} \psi(p) f_2(q, p) \mu(q, p) dq dp + O(\Delta t^3).$$

Expanding μ to the second order yields

$$\begin{aligned} & \mu \left(q, p - \frac{\Delta t}{2} \nabla V(q) \right) + O(\Delta t^3) \\ &= \mu(q, p) \left[1 + \beta \frac{\Delta t}{2} (M^{-1}p) \cdot \nabla V(q) + \frac{\Delta t^2}{8} [(\beta M^{-1}p) \otimes (\beta M^{-1}p) \nabla V(q)] \cdot \nabla V(q) - \beta \frac{\Delta t^2}{8} (M^{-1} \nabla V(q)) \cdot \nabla V(q) \right] \\ &= \mu(q, p) \left[1 + \beta \frac{\Delta t}{2} (M^{-1}p) \cdot \nabla V(q) + \frac{\Delta t^2}{8} (g^2(q, p) - \beta (M^{-1} \nabla V(q)) \cdot \nabla V(q)) \right]. \end{aligned}$$

Using $\int \psi d\mu = 0$ and the cancellation (3.15) on q to remove the first order term, we obtain:

$$(3.17) \quad \int_{\mathcal{E}} \psi(p) \mu_{\Delta t, P}(q, p) dq dp = \Delta t^2 \int_{\mathcal{E}} \psi(p) \left(\frac{1}{8} (g^2(q, p) - \beta (M^{-1} \nabla V(q)) \cdot \nabla V(q)) + f_2(q, p) \right) \mu(q, p) dq dp + O(\Delta t^3).$$

Simplifications are possible. First, observe that

$$-\beta (M^{-1} \nabla V(q)) \cdot \nabla V(q) = B g(q, p),$$

so that, using the expression for f_2 given in (3.10), we get

$$(3.18) \quad \int_{\mathcal{E}} \psi(p) \mu_{\Delta t, P}(q, p) dq dp = \Delta t^2 \int_{\mathcal{E}} \psi(p) \left(\frac{1}{8} (g^2(q, p) - Ag(q, p)) + \tilde{f}_2(q, p) \right) \mu(q, p) dq dp + O(\Delta t^3).$$

Next, we examine the term

$$(g^2(q, p) - Ag(q, p)) \mu(q, p) = [\beta^2 ((M^{-1}p) \cdot \nabla V(q))^2 - \beta (M^{-1}p) \cdot (\nabla^2 V(q) M^{-1}p)] \mu(q, p),$$

by a straightforward calculation, where ∇^2 denotes the Hessian matrix. This expression is a finite sum of diagonal terms coming from both terms inside the brackets, and off-diagonal terms coming only from the rightmost term inside the bracket. Importantly, these all vanish when integrated against the configurational marginal of μ . To make this precise, we index p and q as

$$p = (p_i)_{1 \leq i \leq dN}, \quad q = (q_i)_{1 \leq i \leq dN}.$$

Fixing indices $i \neq j$, the diagonal term corresponding to i is

$$(3.19) \quad \left[\beta^2 (M^{-1}p)_i^2 \left(\frac{\partial}{\partial q_i} V(q) \right)^2 - \beta (M^{-1}p)_i^2 \frac{\partial^2}{\partial q_i^2} V(q) \right] \mu(q, p) = (M^{-1}p)_i^2 \frac{\partial^2}{\partial q_i^2} \mu(q, p),$$

and the off-diagonal term corresponding to (i, j) is

$$(3.20) \quad -\beta (M^{-1}p)_i (M^{-1}p)_j \frac{\partial}{\partial q_i} V(q) \frac{\partial}{\partial q_j} V(q) \mu(q, p) = -\frac{1}{\beta} (M^{-1}p)_i (M^{-1}p)_j \frac{\partial^2}{\partial q_i \partial q_j} \mu(q, p).$$

Factoring out the q -independent terms, and using the cancellations

$$(3.21) \quad \int_{\mathcal{D}} \frac{\partial^2}{\partial q_i^2} \mu(q, p) dq = \int_{\mathcal{D}} \frac{\partial^2}{\partial q_i \partial q_j} \mu(q, p) dq = 0,$$

which follow by integration by parts, we infer

$$(3.22) \quad \int_{\mathcal{E}} \psi(p) \mu_{\Delta t, P}(q, p) dq dp = \Delta t^2 \int_{\mathcal{E}} \psi(p) \tilde{f}_2(q, p) \mu(q, p) dq dp + O(\Delta t^3),$$

which concludes the proof. \square

Remark 10. Using exponential decay estimates on the evolution semigroup $(e^{t\mathcal{L}_\gamma})_{t \geq 0}$ like (2.32), one can show that the inverse operator \mathcal{L}_γ^{-1} is well-defined for smooth centered observables. Thus $\mathcal{L}_\gamma^{-1}\psi$ is well defined, say $\mathcal{L}_\gamma\Psi(q, p) = \psi(p)$. Hence, (3.16) rewrites

$$\begin{aligned} \int_{\mathcal{E}} \psi(p) \mu_{\Delta t, P}(q, p) dq dp &= \Delta t^2 \int_{\mathcal{E}} \mathcal{L}_\gamma\Psi(q, p) \tilde{f}_2(q, p) \mu(q, p) dq dp + O(\Delta t^3) \\ &= \Delta t^2 \int_{\mathcal{E}} \Psi(q, p) \mathcal{L}_\gamma^* \tilde{f}_2(q, p) \mu(q, p) dq dp + O(\Delta t^3) \\ &= \frac{\Delta t^2}{12} \int_{\mathcal{E}} \Psi(q, p) \left[(A + B) \left(A + \frac{B}{2} \right) g \right] (q, p) \mu(q, p) dq dp + O(\Delta t^3), \end{aligned}$$

using (3.10), which provides an alternative expression for the dominant error term. Numerical evidence (see Figure 3.11) suggests that the error on BAOA and BAOAB averages is at dominant order independent of γ . Since the error term on BAOA given in (3.16) depends on γ , this suggests that this term is zero, motivating the following conjecture.

Conjecture 1. For any smooth centered kinetic observable $\psi(p)$, we have

$$(3.23) \quad \int_{\mathcal{E}} (\mathcal{L}_\gamma^{-1}\psi)(q, p) \left[(A + B) \left(A + \frac{B}{2} \right) g \right] (q, p) \mu(q, p) dq dp = 0.$$

This would in particular imply that the kinetic marginal $\kappa_{\Delta t, P}$ is correct at order at least three in Δt , and is the subject of further investigation.

3.0.6 Analysis of the discrepancy between the dominant error terms on the kinetic marginals.

Numerical evidence presented in [7] shows a significant discrepancy between $\kappa_{\Delta t, P}$ and $\kappa_{\Delta t, Q}$. Specifically, $\kappa_{\Delta t, Q}$ in the case $d = N = 1$ tends to present a sharper peak than $\kappa_{\Delta t, P}$, thus underestimating the variance in the kinetic marginal. We show this in this paragraph this behavior is generic, in the sense that it does not, up to a shape parameter, depend on V . The arguments above show that

$$(3.24) \quad \begin{aligned} \int_{\mathcal{E}} \psi(p) \mu_{\Delta t, P}(q, p) dq dp &= \int_{\mathbb{R}^{dN}} \psi(p) \kappa_{\Delta t, P}(p) dp \\ &= \int_{\mathbb{R}^{dN}} \psi(p) \kappa(p) dp + \Delta t^2 \int_{\mathbb{R}^{dN}} \psi(p) \left(\int_{\mathcal{D}} \tilde{f}_2(q, p) \nu(q) dq \right) \kappa(p) dp + O(\Delta t^3), \end{aligned}$$

where we used the product form (1.8) for μ . Similarly,

$$(3.25) \quad \int_{\mathcal{E}} \psi(p) \kappa_{\Delta t, Q}(p) dp = \int_{\mathbb{R}^{dN}} \psi(p) \kappa(p) dp + \Delta t^2 \int_{\mathbb{R}^{dN}} \psi(p) \left(\int_{\mathcal{D}} f_2(q, p) \nu(q) dq \right) \kappa(p) dp + O(\Delta t^3),$$

so that

$$\begin{aligned} \int_{\mathcal{E}} \psi(p) (\kappa_{\Delta t, P}(p) - \kappa_{\Delta t, Q}(p)) dp &= \Delta t^2 \int_{\mathbb{R}^{dN}} \psi(p) \left(\int_{\mathcal{D}} (\tilde{f}_2(q, p) - f_2(q, p)) \nu(q) dq \right) \kappa(p) dp + O(\Delta t^3) \\ &= \frac{\Delta t^2}{8} \int_{\mathbb{R}^{dN}} \psi(p) \left(\int_{\mathcal{D}} (A + B) g(q, p) \nu(q) dq \right) \kappa(p) dp + O(\Delta t^3). \end{aligned}$$

Hence at the level of densities, we have at dominant order,

$$\kappa_{\Delta t, P}(p) - \kappa_{\Delta t, Q}(p) = \frac{\Delta t^2 \kappa(p)}{8} \int_{\mathcal{D}} (A + B) g(q, p) \nu(q) dq + O(\Delta t^3),$$

using the expressions for f_2 and \tilde{f}_2 given in (3.10). The following proposition gives an alternative expression for this discrepancy term.

Proposition 7. *We have the following expression for the discrepancy term.*

$$(3.26) \quad \kappa_{\Delta t, P}(p) - \kappa_{\Delta t, Q}(p) = \frac{\Delta t^2}{8} \text{Tr} \left(\left((\beta M^{-1} p)^{\otimes 2} - \beta M^{-1} \right)^T \text{Cov}_{\nu}(\nabla V) \right) \kappa(p) + O(\Delta t^3).$$

Proof. For simplicity we assume $Z_{\nu} = \frac{\Delta t^2}{8} = \kappa(p) = 1$. This has no incidence on our computations. We write:

$$(3.27) \quad (A + B)g(q, p)\nu(q) = \beta \left[(M^{-1}p) \cdot (\nabla^2 V(q)M^{-1}p) - (M^{-1}\nabla V(q)) \cdot \nabla V(q) \right] e^{-\beta V(q)}.$$

Setting $\tilde{p} = M^{-1}p$, we get

$$(3.28) \quad (A + B)g(q, M\tilde{p})\nu(q) = \beta \left[\tilde{p} \cdot (\nabla^2 V(q)\tilde{p}) - (M^{-1}\nabla V(q)) \cdot \nabla V(q) \right] e^{-\beta V(q)}.$$

This is a sum of terms of the form

$$T_{ij}(q, p) = \left[\beta \tilde{p}_i \tilde{p}_j \frac{\partial^2}{\partial q_i \partial q_j} V(q) - \beta M_{i,j}^{-1} \frac{\partial}{\partial q_i} V(q) \frac{\partial}{\partial q_j} V(q) \right] e^{-\beta V(q)}.$$

Upon integrating this term over \mathcal{D} , we can integrate the left-most term by parts (boundary terms cancel out by periodicity or by growth conditions on V), to obtain

$$\int_{\mathcal{D}} T_{ij}(q, p) dq = \int_{\mathcal{D}} \left[\beta^2 \tilde{p}_i \tilde{p}_j \frac{\partial}{\partial q_i} V(q) \frac{\partial}{\partial q_j} V(q) - \beta M_{i,j}^{-1} \frac{\partial}{\partial q_i} V(q) \frac{\partial}{\partial q_j} V(q) \right] e^{-\beta V(q)} dq.$$

Hence,

$$\int_{\mathcal{D}} T_{ij}(q, p) dq = (\beta^2 \tilde{p}_i \tilde{p}_j - \beta M_{i,j}^{-1}) \int_{\mathcal{D}} \frac{\partial}{\partial q_i} V(q) \frac{\partial}{\partial q_j} V(q) e^{-\beta V(q)} dq,$$

so that

$$\int_{\mathcal{D}} (A + B)g(q, p)\nu(q) dq = \sum_{i,j} (\beta^2 \tilde{p}_i \tilde{p}_j - \beta M_{i,j}^{-1}) \int_{\mathcal{D}} \frac{\partial}{\partial q_i} V(q) \frac{\partial}{\partial q_j} V(q) e^{-\beta V(q)} dq,$$

which we rewrite

$$(3.29) \quad \left((\beta M^{-1} p)^{\otimes 2} - \beta M^{-1} \right) : \int_{\mathcal{D}} (\nabla V \otimes \nabla V)(q) \nu(q) dq = \text{Tr} \left(\left((\beta M^{-1} p)^{\otimes 2} - \beta M^{-1} \right)^T \text{Cov}_{\nu}(\nabla V) \right),$$

using the fact that ∇V is a centered observable with respect to ν , and concluding the proof. \square

Remark 11. This expression for the discrepancy term is not particularly wieldy, however it does explain the behavior observed in [7]. In the case $d = N = \beta = M = 1$, it becomes,

$$\kappa_{\Delta t, P}(p) - \kappa_{\Delta t, Q}(p) = \frac{\Delta t^2}{8}(p^2 - 1)\text{Var}_\nu(V')\kappa(p) + O(\Delta t^3),$$

which is, up to a constant, the same correction term for any potential V . We plot this correction profile in figure 3.1. The shape of this profile explains the higher peak observed in $\kappa_{\Delta t, Q}$.

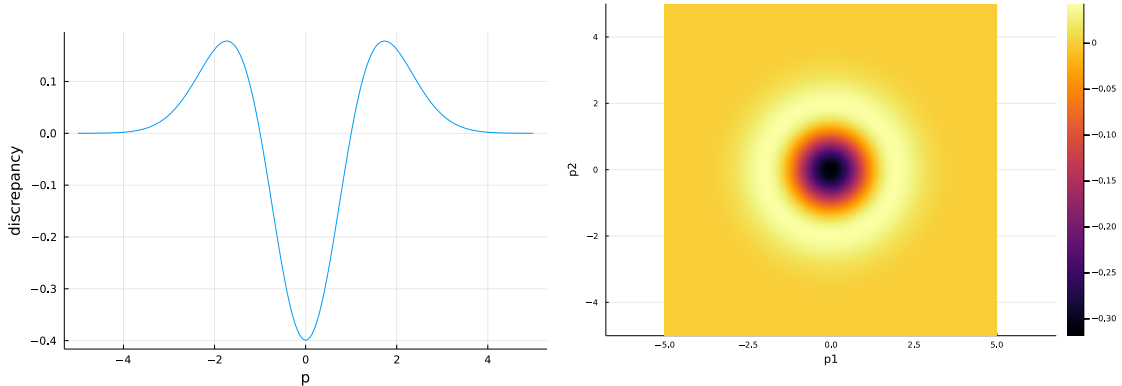


Figure 3.1: Profile of the discrepancy term in one and two dimension, in the case of identity covariances for ∇V .

3.1 Numerical results

We propose illustrating our computations with numerical examples, on toy one dimensional systems.

- (i) In section 3.1.1, we define the potentials used for all the following experiments, and describe the sampling method used.
- (ii) In section 3.1.2, we verify numerically the relation (3.8).
- (iii) In section 3.1.3, we show that there is a significant discrepancy between the two kinetic marginal distributions. We also pinpoint the main, and possibly only source of this error, namely the γ -independent term (3.26).
- (iv) In section 3.1.4, we numerically verify that the first order behavior (3.13) is correct.
- (v) In section 3.1.5, we give an explicit example of an observable for which the BAOA scheme yields a bias of order Δt .
- (vi) Finally, in section 3.1.6, we show that the effect of the parameter γ is undetectable at the level of the kinetic marginals, motivating Conjecture 1.

3.1.1 Models

We take $\beta = 1$, $M = \text{Id}$, and consider four potentials:

- Periodic potential

$$\mathcal{D} = L(\mathbb{R}/\mathbb{Z}), \quad L = 1, \quad V(q) = \sin(2\pi q/L),$$

- Quadratic potential

$$\mathcal{D} = \mathbb{R}, V(q) = \alpha \frac{q^2}{2}, \alpha = 1,$$

- Double well potential

$$\mathcal{D} = \mathbb{R}, V(q) = \alpha \frac{q^2}{2} + \beta e^{-\frac{q^2}{2\sigma^2}}, \alpha = 1, \beta = 4, \sigma = 0.5,$$

- Tilted double well potential

$$\mathcal{D} = \mathbb{R}, V(q) = \alpha \frac{q^2}{2} + \gamma q + \beta e^{-\frac{q^2}{2\sigma^2}}, \alpha = 1, \beta = 4, \gamma = 1, \sigma = 0.5.$$

Analytically unknown normalizing constants and reference quantities were obtained through numerical integration of μ , using trapezoid rules with a mesh size of 10^{-6} . For unbounded coordinates, we truncated the domain to the interval $[-5, 5]$. Approximations of $\mu_{\Delta t, P}, \mu_{\Delta t, Q}$ were computed by recording the states of 10,000 independently evolving trajectories over 2×10^6 timesteps in a 1000×1000 two-dimensional histogram on the truncated domain. The rare sample points outside of the truncated domain were discarded.

3.1.2 Equality of marginal configurational distributions

On Figures 3.2 and 3.3, we verify numerically the equality (3.8) between the configurational marginal distributions $\nu_{\Delta t, Q}$ and $\nu_{\Delta t, P}$, which holds for any Δt . This point was demonstrated in [7].

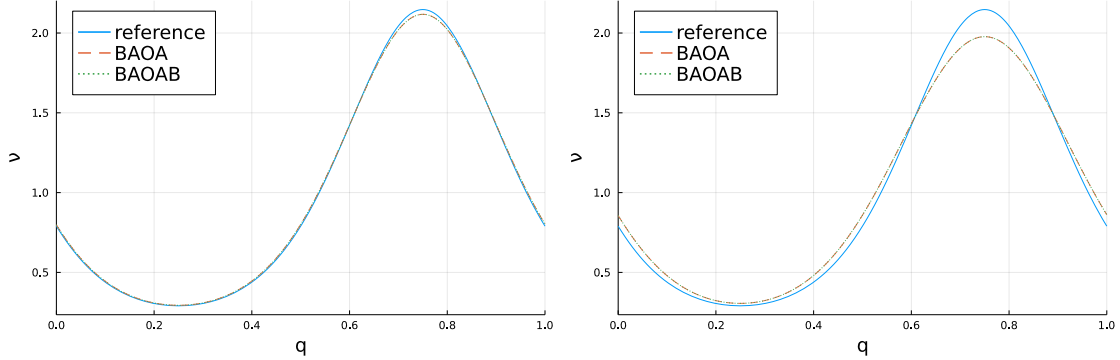


Figure 3.2: Marginal configurational distributions for the periodic potential. Left: $\Delta t = 0.1$. Right: $\Delta t = 0.2$. Even for large timesteps, the distributions coincide perfectly.

3.1.3 Comparison of marginal kinetic distributions

We observe, as in [7], that the kinetic marginal distribution $\kappa_{\Delta t, Q}$ departs from the reference at a faster rate than $\kappa_{\Delta t, P}$, and more precisely appears to underestimate the variance, leading to a sharper distribution. Additionally we observe that removing the part of the bias on BAOAB due to the discrepancy term (3.26) leads to a significant improvement. These corrected marginals are plotted under the label "correction". See Figures 3.4 and 3.5.

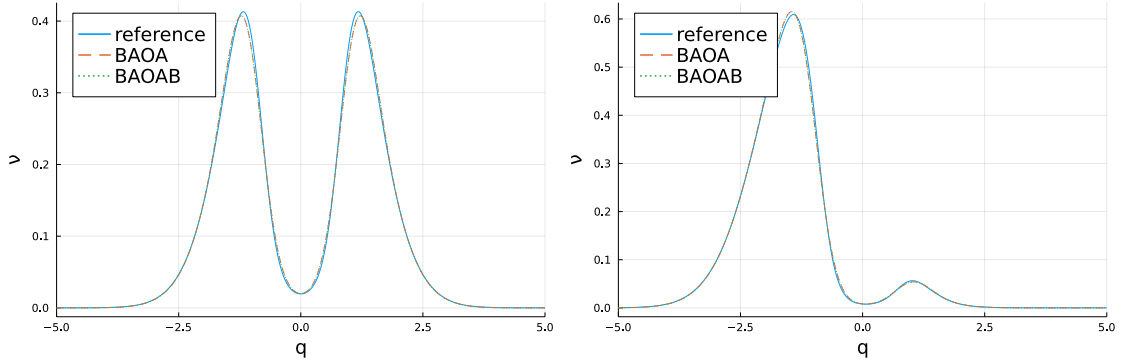


Figure 3.3: Marginal configurational distributions for $\Delta t = 0.4$. Left: double well potential. Right: tilted double well potential.

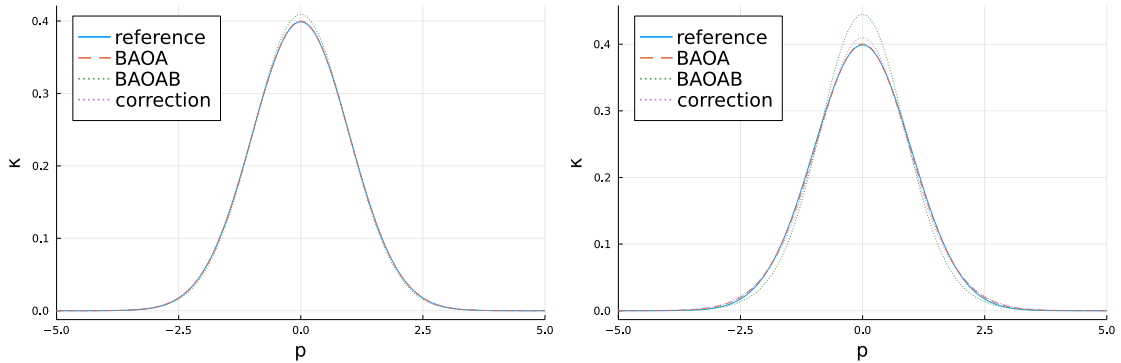


Figure 3.4: Marginal kinetic distributions for the periodic potential. Left: $\Delta t = 0.1$. Right: $\Delta t = 0.2$.

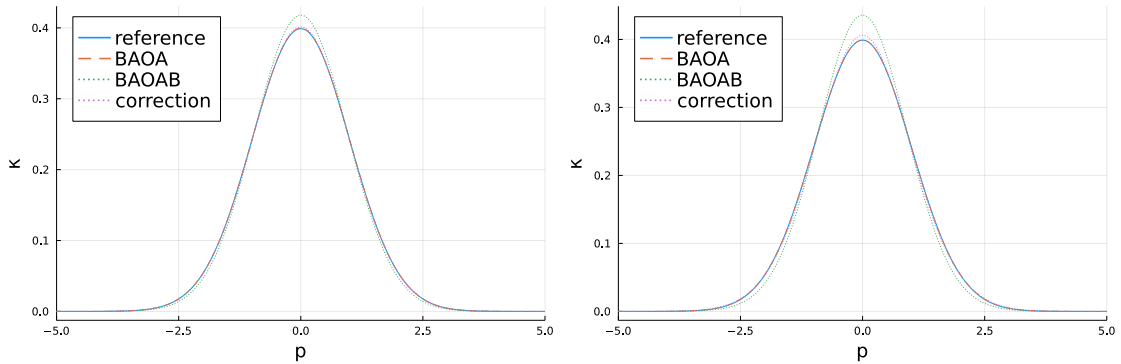


Figure 3.5: Marginal kinetic distributions for the double well potential. Left: $\Delta t = 0.3$. Right: $\Delta t = 0.4$.

3.1.4 Verification of the first-order expansion

We verify the correctness first-order expansion of $\mu_{\Delta,P}$ obtained in (3.13), by comparing the joint distributions obtained from Monte-Carlo simulations with a reference calculation of the first-order expansion for $\mu_{\Delta t,P}$. Additionally, we plot the empirical estimate of $\mu_{\Delta t,Q}$ and μ . The plots show joint likelihoods as a function of the state, using a color mapping. Empirical joint distributions for BAOA and BAOAB trajectories are plotted on the top row of each figure. On the bottom row, a reference computation of μ is plotted on the right, as well as a reference computation of

$$\left(1 + \frac{\Delta t}{2} g\right) \mu$$

on the left. The results visually confirm our result, while suggesting that, as a whole, $\mu_{\Delta t,Q}$ is the superior approximation of μ . See Figures 3.6, 3.7 and 3.8.

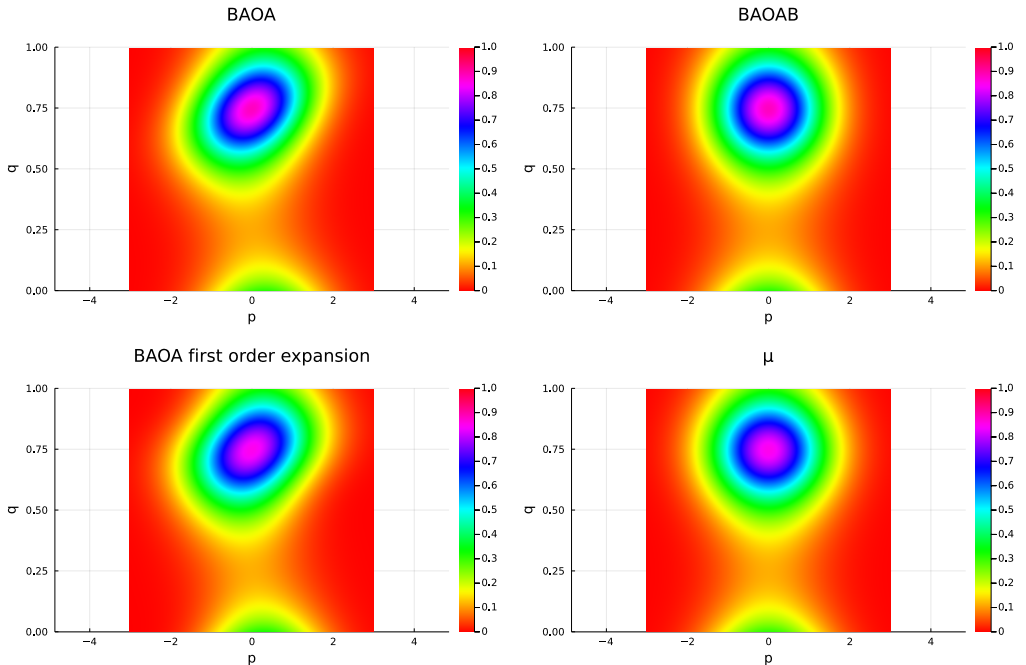


Figure 3.6: Joint distributions for the periodic potential, $\Delta t = 0.1$.

3.1.5 Example of first-order bias in a BAOA average

We demonstrate that for certain observables, BAOA is drastically outperformed by BAOAB, by calculating the average of g for increasing timesteps. Note by (3.15), the true average is 0. Figures 3.9 and 3.10 show the estimated averages as a function of the timestep on the left, and the same data on a log-log plot on the right. The order of the error on the BAOAB averages suggest that the second order error term

$$\int_{\mathcal{E}} g f_2 \, d\mu$$

given in (3.9) cancels out, yielding a fourth-order bias in Δt for BAOAB averages of g .

3.1.6 Effect of the friction parameter

All experiments shown above used a value of $\gamma = 1$ for the friction parameter. In this final experiment, we examine the effect of changing γ . We show the marginal kinetic distributions for

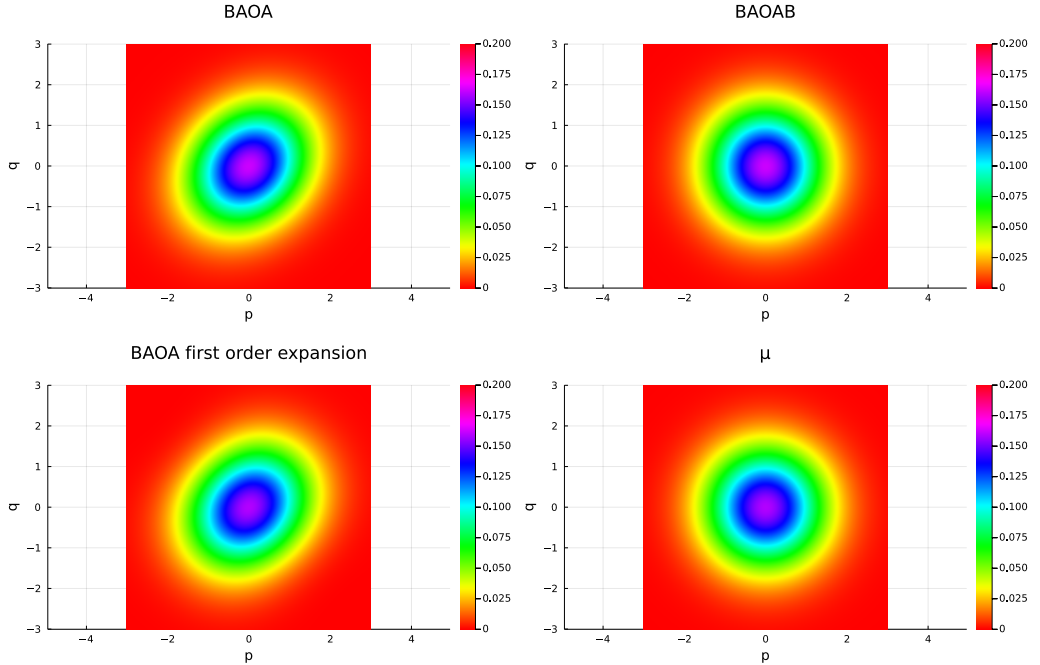


Figure 3.7: Joint distributions for the quadratic potential, $\Delta t = 0.4$.

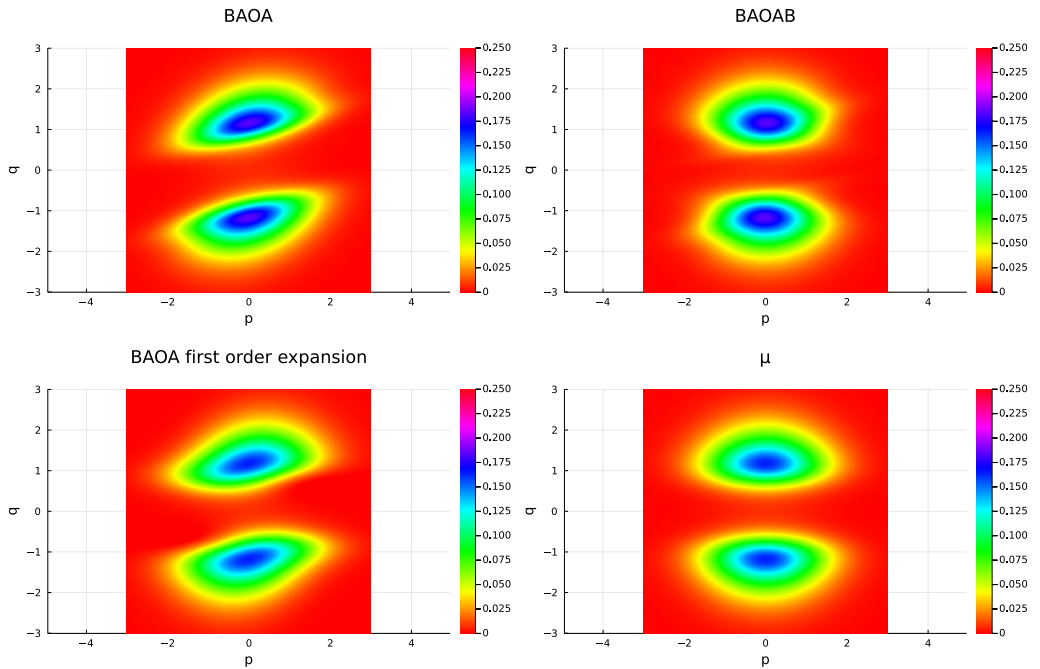


Figure 3.8: Joint distributions for the double well potential, $\Delta t = 0.4$.

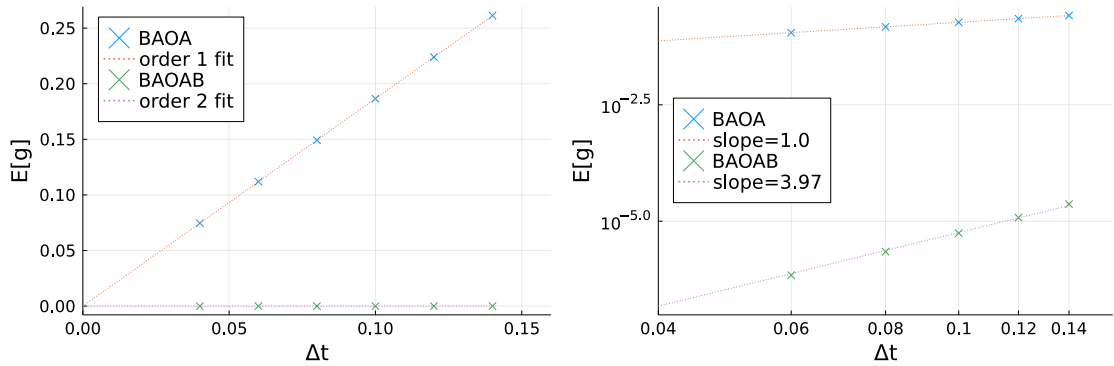


Figure 3.9: Averages of g for the double well potential.

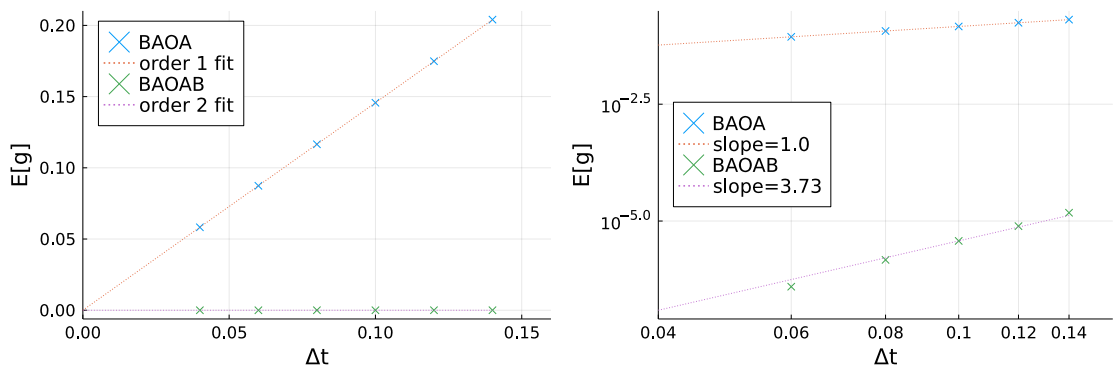


Figure 3.10: Averages of g for the tilted double well potential.

three values of $\gamma \in \{0.1, 1, 10\}$. The results show that there is no visually discernable effect of the parameter γ : all $\kappa_{\Delta t, P}$ s are superposed close to the reference curve, and all $\kappa_{\Delta t, Q}$ s are superposed above. This suggest that most of the error on $\kappa_{\Delta t, Q}$ arises from the additional term

$$-\frac{\Delta t^2}{8} \int_{\mathcal{E}} \varphi(A + B) g d\mu,$$

which is the dominant discrepancy term in (3.26), and which is independent of γ . This is the fact we observed numerically on figures 3.5 and 3.4. See figure 3.11.

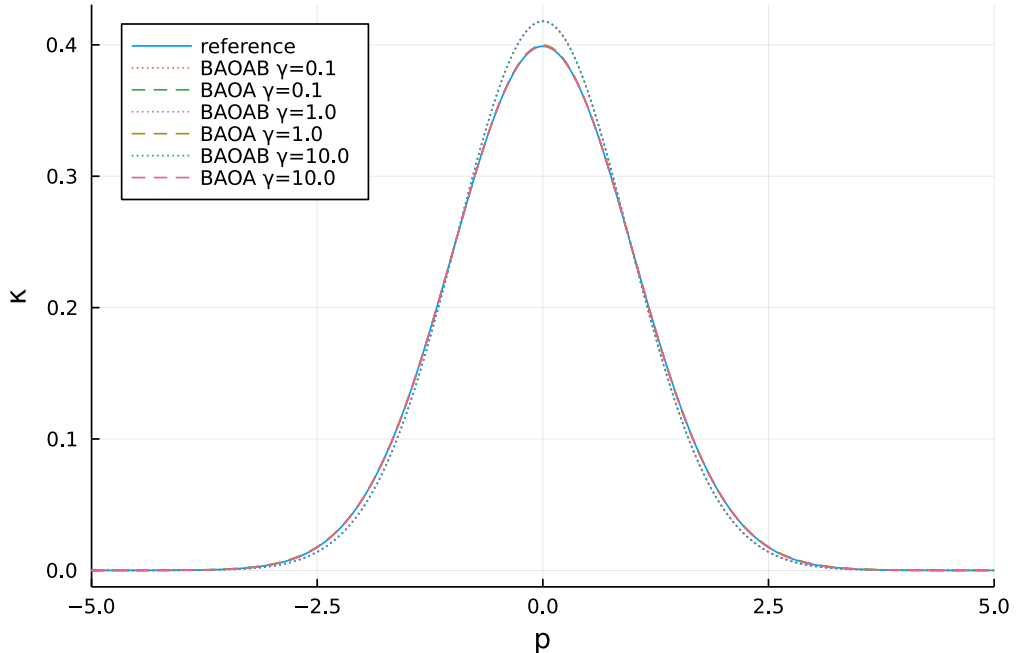


Figure 3.11: Kinetic marginal distributions for $\Delta t = 0.3$ on the double well potential.

Chapter 4

Non-equilibrium Molecular Dynamics

So far, we have only considered methods to sample static averages, which concern quantities at thermodynamic equilibrium. Such techniques yield information about the bulk macroscopic properties of the system, for which there is no discernable macroscopic evolution. We now turn to the next natural question, which is to consider systems in which there is such an evolution, which typically arises from a perturbation of the equilibrium dynamics, either by the introduction of a non-gradient forcing term, or a modification of the fluctuation-dissipation part for which the fluctuation-dissipation relation (2.25) is not verified. We will not consider the latter case, which is relevant for instance to the modelling of heat transport within an atomic system, to concentrate on the first case. In general, systems undergoing such a perturbation of the dynamics will reach a new steady state in which there is a net flux in some observable. Mathematically, this translates into the existence of a response observable R which has zero average with respect to the canonical measure μ , but which has a positive average with respect to the perturbation steady-state. A natural question is that of the sensitivity of the system to the perturbation: one way to quantify this is to modulate the strength of the perturbation by a positive real parameter $\eta > 0$, and, assuming that the average response is asymptotically linear as $\eta \rightarrow 0$, to compute the linear coefficient linking η and the average response. This quantity is called a *transport coefficient*, and we will dedicate the next two chapters to different methods of computing them using molecular simulation.

4.1 Non-equilibrium molecular dynamics

4.1.1 General framework

We first consider the most natural method, which is to directly apply a forcing term which is not the gradient of a periodic function. The general framework is that of a classical Langevin dynamics

$$(4.1) \quad \begin{cases} dq_t = M^{-1} p_t dt, \\ dp_t = -\nabla V(q_t) dt - \gamma M^{-1} p_t dt + \sqrt{\frac{2\gamma}{\beta}} dW_t + \eta F(q_t) dt, \end{cases}$$

perturbed by the configuration-dependent forcing term F , and where the strength of the perturbation is modulated by the parameter $\eta > 0$. Its generator is given by the operator

$$(4.2) \quad \mathcal{L}_{\gamma,F} = \mathcal{L}_\gamma + \eta F \cdot \nabla_p = \mathcal{L}_\gamma + \eta \tilde{\mathcal{L}}.$$

It is also possible to consider non-equilibrium generalized Langevin equations, which are analogous perturbations of (2.15). Given a response of interest R , the transport coefficient is given by the following definition:

$$(4.3) \quad \rho_{R,F} = \lim_{\eta \rightarrow 0} \frac{\mathbb{E}[R]}{\eta},$$

where \mathbb{E}_η denotes the expectation with respect to the steady-state probability distribution. If the context makes R clear from the knowledge of F , we will drop it from the notation and simply write ρ_F for the transport coefficient. For this definition to make sense, one has to show that the steady-state with respect to which we take the expectation is well-defined. Since the steady-state is defined by the fact that it is invariant with respect to the dynamics (4.1), this translates into the fact that it is the solution to a stationary Fokker-Planck equation, in the sense of distributions:

$$(4.4) \quad (\mathcal{L}_\gamma + \eta \tilde{\mathcal{L}})^\dagger \psi_\eta = 0,$$

where ψ_η is the steady state measure. Using analytic properties of $\mathcal{L}_{\gamma,F}$ (such as hypoellipticity), one can hope to infer regularity results of its solutions, such as the existence of a smooth density. Existence and unicity can in principle be inferred following Klieman's method [8]. The steady-state measure \mathbb{E}_η is a high-dimensional measure on phase space for which a closed form is generally unavailable. Thus, as usual, one has to resort to ergodic averages under the dynamics (4.1) to compute ensemble averages. This poses another theoretical difficulty, that of showing that the steady-state measure is ergodic.

In fact, for our purposes, F will always be $L\mathbb{T}^{dN}$ -periodic, and so we can invoke a special case of Proposition 1 in [6] with time-constant forcings, provided V and F are smooth.

Theorem 3 (Existence of a unique ergodic measure with smooth density). *Let $\eta_* > 0$. For all $\eta \in [-\eta_*, \eta_*]$, the Fokker-Planck equation (4.4) admits a unique solution with a C^∞ density ψ_η . Additionally, the evolution semigroup decays exponentially in a Lyapunov sense: for all $n \geq 1$, there exist $C_n, \lambda_n > 0$ such that*

$$(4.5) \quad \|e^{t\mathcal{L}_{\gamma,F}} \varphi - \mathbb{E}_\eta[\varphi]\|_{L^\infty(\mathcal{E})} \leq C_n e^{-\lambda_n t} \|\varphi\|_{L^\infty_{\mathcal{K}_n}},$$

where we define the Lyapunov weight functions

$$\mathcal{K}_n(q, p) = 1 + |p|^{2n},$$

and the corresponding weighted L^∞ spaces by the norm

$$\|f\|_{L^\infty_{\mathcal{K}_n}} = \left\| \frac{f}{\mathcal{K}_n} \right\|_{L^\infty(\mathcal{E})}.$$

Because of the continuous injections $L^\infty \subset L^\infty_{\mathcal{K}_n}$, this result implies in particular that the operator $(-\mathcal{L}_{\gamma,F})^{-1}$ is well-defined on

$$L^\infty_{\mathcal{K}_n,0} = \{f \in L^\infty_{\mathcal{K}_n} \mid \mathbb{E}_\eta[f] = 0\},$$

with an inverse given by the formula (2.36). Proposition 2 from the same papers also gives the almost-sure convergence of ergodic averages.

Remark 12 (Size of the linear regime). *As $\eta \rightarrow 0$, it is reasonable to expect that the statistical error in ergodic averages for $\mathbb{E}_\eta[R]$ arise at dominant order in η from the asymptotic variance at equilibrium σ_R^2 (2.37). In particular the finite difference estimator for $\rho_{R,F}$*

$$(4.6) \quad \frac{\mathbb{E}_\eta[R]}{\eta}$$

has, for a fixed simulation time, a variance which scales like $\frac{1}{\eta^2}$ as $\eta \rightarrow 0$. To achieve an acceptable statistical error at minimal cost, one should thus aim to take η as large as possible. On the other hand, if the perturbation is too large, then non-linear effects on R will be observed and (4.6) will give a poor estimation of the transport coefficient. Thus, if one manages to devise another forcing F which does not change the steady-state, but which extends the range of linearity of the response, it may be very beneficial to do so from a computational standpoint. These kinds of methods, sometimes called synthetic forcings, are an area of ongoing research. (ref...)

4.1.2 Numerical implementation

To integrate the perturbed dynamics, we again rely on a splitting strategy. We split the dynamics into elementary evolutions, whose respective evolution semigroups are given analogously to (2.39). The only difference is in the additional ηF term, which we incorporate into the B step, yielding a $B_{\eta F}$ step, which corresponds to the evolution semigroup

$$(4.7) \quad e^{tB_{\eta F}} \varphi(q, p) = \varphi(q, p - t(\nabla V(q) - \eta F(q))).$$

Note it would also have been possible to incorporate the forcing term into the Ornstein-Uhlenbeck part of the dynamics, which then corresponds to an Ornstein-Uhlenbeck process with constant drift. However, we will always choose the method described above. We will use the same terminology for these methods, referring to the scheme with evolution operator

$$(4.8) \quad e^{\frac{\Delta t}{2}B_{\eta F}} e^{\frac{\Delta t}{A}} e^{\Delta t \gamma C} e^{\frac{\Delta t}{2}A} e^{\frac{\Delta t}{2}B_{\eta F}}$$

as the BAOAB scheme, for example. Numerical estimates for $\mathbb{E}_\eta[R]$ are then obtained through

$$(4.9) \quad \widehat{R}_{\eta, N_{\text{iter}}} = \frac{1}{N_{\text{iter}}} \sum_{n=0}^{N_{\text{iter}}-1} R(q^n, p^n),$$

where $(q^n, p^n)_{n \geq 0}$ denote the numerical trajectory under the Markov chain obtained for a chosen splitting of the non-equilibrium dynamics (4.1). To estimate the transport coefficient, we fix different forcing intensities

$$0 < \eta_1 < \dots < \eta_k, \quad \eta := (\eta_i)_{1 \leq i \leq k}$$

all in the linear response regime, and given corresponding estimators

$$\widehat{R} := (\widehat{R}_i)_{1 \leq i \leq k}$$

of the form (4.9), we estimate ρ_F by a least squares linear fit

$$(4.10) \quad \widehat{\rho}_F = |\eta|^{-2} \eta \cdot \widehat{R} = \underset{\rho \in \mathbb{R}}{\operatorname{argmin}} \left| \rho \eta - \widehat{R} \right|^2.$$

Note the case $k = 1$ recuperates the finite difference estimator (4.6). Note that the variance of this estimator is likely to be much smaller than for the latter estimator. In fact, provided $|\eta|^2 \geq 1$, the pitfall of the NEMD technique mentioned in Remark 12 is completely avoided. Indeed, assume that each \widehat{R}_i is an ergodic estimator simulated with $N_{i,\text{iter}}$ timesteps, say

$$\widehat{R}_i = \frac{S_i}{\eta_i N_{i,\text{iter}}}.$$

We assume that the asymptotic regime is reached, thus we may assume that \widehat{R}_i is Gaussian with variance

$$\frac{\sigma_i^2}{\eta_i^2 N_{i,\text{iter}}},$$

where σ_i^2 is the asymptotic variance associated with the ergodic mean $S_i/N_{i,\text{iter}}$. Thus,

$$(4.11) \quad \text{Var}(\hat{\rho}_F) = |\eta|^{-4} \sum_{i=1}^k \frac{\sigma_i^2}{\eta_i^2 N_{i,\text{iter}}}.$$

If we make the approximation $\sigma_i^2 \approx \sigma_R^2$, which is good at first order in η , and assume $N_{i,\text{iter}} \geq N_{\text{iter}}$, we can estimate an upper bound on the variance,

$$\text{Var}(\hat{\rho}_F) \lesssim \frac{\sigma_R^2}{|\eta|^2 N_{\text{iter}}}.$$

4.1.3 Mobility

As a first and simplest example, we introduce a method for computing the mobility. In this case the forcing is simply a constant vector, and the response is velocity in the direction F , which we may think of as the particle flux through F 's orthogonal hyperplane. The transport coefficient corresponding to the forcing

$$(4.12) \quad F \in \mathbb{R}^{dN} \quad R(q, p) = F \cdot M^{-1}p$$

is called the mobility. Let us assume once and for all that $|F|^2 = 1$. For practical computations, we will be considering two cases:

- (i) **Single drift:** this corresponds to a perturbation where the force acts on a single component of the momentum, which we can assume by indistinguishability of the particles to be the x component of the first particle,

$$F_S = (1, 0, \dots)^T \in \mathbb{R}^{dN}.$$

- (ii) **Color drift:** this corresponds to a perturbation in which we the force acts on half of the particles in one direction, and on half of the particles in the opposite direction. By isotropy, we may assume this direction is the x direction,

$$F_C = \frac{1}{\sqrt{N}} \underbrace{(1, 0, \dots,}_{d \text{ components}} -1, 0, \dots, 1, 0 \dots)^T \in \mathbb{R}^{dN}.$$

The color drift method derive its name from the fact that it divides the particles into two categories: the particles with a positive color charge (corresponding to those whose x-component of momentum see a positive force contribution from F), and those with a negative color charge. The equations of motion are analogous to a system of charged particles under a constant electric field, but where the charges do not interact between themselves. The idea is taken from [2], Chapter 6. Intuitively, we expect the color drift method to be more economical than the single drift method, since the latter should give essentially equilibrium dynamics for the majority of particles outside of the first particle's sphere of influence. On the other hand, the normalization condition implies that the forcing is more dilute in the color drift case, which may make the response more difficult to measure. In fact, numerical evidence presented below shows that the two effects roughly compensate one another.

In order for the two methods to be useful, we need to be able to relate them to a shared dynamical property of the considered system. Doing is more conveniently done upon reformulating the linear response in terms of integrated autocorrelation functions, a point we postpone to the next section. For now, let us show a few numerical results. In order to compare different methods, we fix a thermodynamical condition, which we give in reduced units below.

$$(4.13) \quad T = 1.25, \quad \rho = 0.6, \quad \gamma = 1.0, \quad N = 1000.$$

Let us also mention here that all simulations for mobility were performed using a BAOAB splitting, a timestep $\Delta t = 10^{-3}$ and a linearly corrected cutoff at distance $r_c = 2.5$. In Figure 4.1, we plot the response profile as a function of the forcing intensity. It appears that the linear response regime is longer for the color drift method. Estimates of ρ_F seem to roughly agree, although it is dubious that the small discrepancy observed is due to a systematic effect rather than statistical fluctuations persisting after very long integration times (all simulations for $\eta \leq 1$ ran for reduced physical times of over 2.5×10^5).

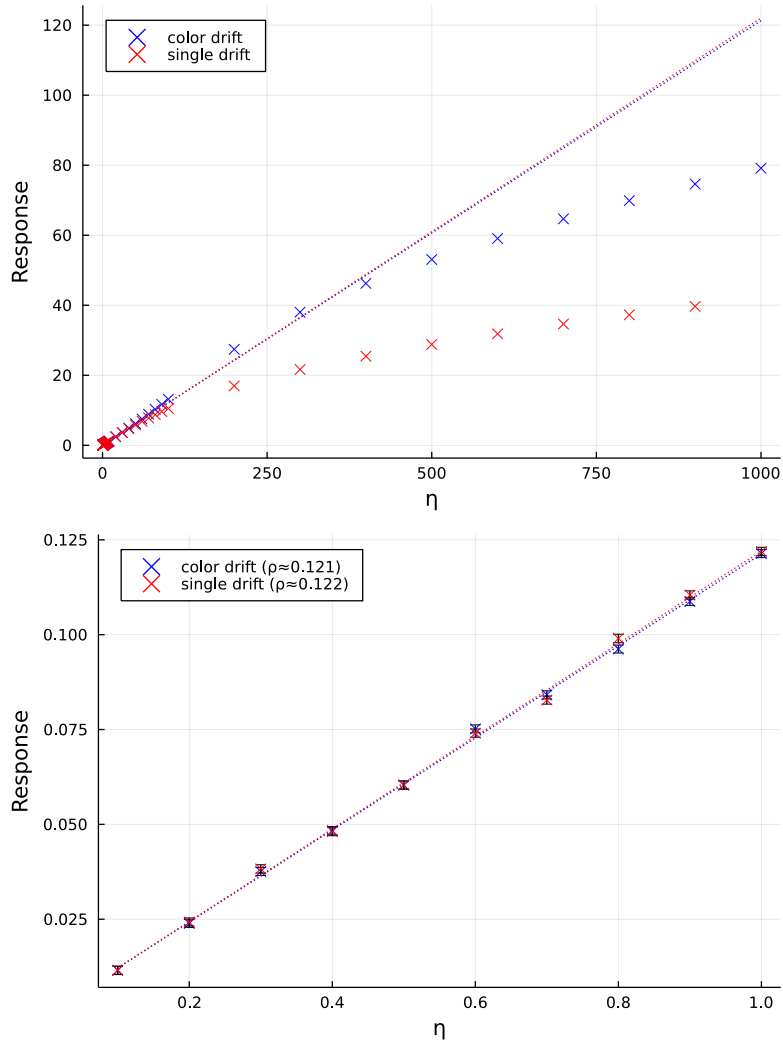


Figure 4.1: Average mobility response against forcing intensity for the Lennard-Jones system (4.13). Extrapolations of the linear response are plotted in dotted lines.

Estimating the transport coefficients using (4.9) and the variance through (4.11), we obtain

$$(4.14) \quad \rho_{F_S} = 0.12204 \pm 0.0009, \quad \rho_{F_C} = 0.12128 \pm 0.0009,$$

where \pm denotes one standard deviation.

4.1.4 Shear viscosity

As a second example, we discuss the methods of [9] for computing shear-viscosity. We refer to this paper for thorough statements and proofs. Let us assume for notational simplicity that $M = m\text{Id}$. We consider a case of the dynamics (4.1) with a forcing which acts on the longitudinal (x) momenta, and is dependent on the transverse (y) positions. More precisely, we fix a reference periodic function $F_y : L\mathbb{T} \rightarrow \mathbb{R}$, and index the state as

$$(q_{i\alpha})_{\substack{1 \leq i \leq N \\ 1 \leq \alpha \leq d}}, \quad (p_{i\alpha})_{\substack{1 \leq i \leq N \\ 1 \leq \alpha \leq d}}.$$

The non-equilibrium dynamics is defined by the following expression for F :

$$(4.15) \quad \forall 1 \leq i \leq N, \forall 2 \leq \alpha \leq d, \quad F(q)_{i1} = F_y(q_{i2}), \quad F(q)_{i\alpha} = 0.$$

The idea is that by imposing a forcing *profile* in the x -direction, we observe a velocity profile in response, which depends on the y -coordinate.

Remark 13 (Anisotropic friction). *In fact the precise model considered in [9] also imposes a separate friction coefficient γ_x for the longitudinal fluctuation-dissipation part of the dynamics. This can be interpreted as a simple case of a generalized Langevin dynamics where the friction coefficient γ is an anisotropic diagonal matrix, which does not pose any difficulties from the theoretical point of view. We therefore restrict our attention to the case where γ is scalar.*

More precisely, we define

$$(4.16) \quad u_x(Y) := \lim_{\epsilon \rightarrow 0} \lim_{\eta \rightarrow 0} \frac{L_y \mathbb{E}_\eta \left[\sum_{i=1}^N p_{i1} \chi_\epsilon(q_{i2} - Y) \right]}{\eta m N}$$

to be the linear response profile in the longitudinal velocity, where $(\chi_\epsilon)_{\epsilon > 0}$ is an approximation to the identity (that is a sequence of smooth compactly supported test functions which converge to the Dirac delta function in the sense of distributions). In practice, u_x can be estimated from numerical trajectories by decomposing the domain \mathcal{D} in a finite number of transverse slices, and measuring the average longitudinal velocity in each of these slices. The shear viscosity σ is then defined by the differential equation

$$(4.17) \quad \sigma u''_x(Y) + \gamma \rho u_x(Y) = \rho F_y(Y),$$

where $\rho = N/L^3$ is the particle density. In fact, the solutions to (4.17) are periodic, thus the magnitude of the linear response can be estimated through Fourier-like coefficients. This has the advantage of giving an estimation of the linear response in the general framework defined above, and avoiding the discretization error arising from the finite number of transverse slices. To this effect, we define the response observables as empirical Fourier coefficients:

$$(4.18) \quad R_k(q, p) = \frac{1}{N} \sum_{i=1}^N \frac{p_{i1}}{m} \exp \left(\frac{2ik\pi q_{i2}}{L} \right),$$

and the corresponding transport coefficients

$$(4.19) \quad \rho_{F,k} = \lim_{\eta \rightarrow 0} \frac{\mathbb{E}_\eta[R_k(q, p)]}{\eta}.$$

It is easy to show that for the sinusoidal forcing, the response velocity profile, solution to (4.17), is still sinusoidal, so that the Fourier response is a meaningful measure of the magnitude of the response in the velocity profile. In practice, it is sufficient to consider $k = 1$.

Remark 14. *To obtain better statistics, one may for the purpose of numerical simulations want to consider a periodic domain whose unit cell is still a cuboid, but with a side length in the longitudinal direction that is longer than in the transverse direction. In this case we simply replace L by L_y in the response observables, where L_y is the length of the unit cell in the transverse direction.*

Forcing	Sinusoidal	Piecewise constant	Piecewise linear
F_1	$i/2$	$2i/\pi$	$-4/\pi^2$

Figure 4.2: First Fourier coefficients for transverse forcing profiles.

The shear viscosity can then be computed from equation (4.17), through

$$(4.20) \quad \sigma = \rho \left(\frac{F_k}{\rho_{F,k}} - \gamma \right) \left(\frac{L}{2k\pi} \right)^2,$$

by taking Fourier coefficients in equation (4.17), where F_k is the counterpart Fourier coefficient for the forcing,

$$F_k = \frac{1}{L} \int_0^L F_y(s) \exp \left(\frac{2ik\pi s}{L} \right) ds,$$

and again only considering $k = 1$ in practice. Numerically, $\rho_{F,k}$ can be approximated by an estimator of the form (4.10). In our numerical experiments, we consider the same three forcing profiles as in [9], namely:

(i) A sinusoidal forcing profile

$$F_y(u) = \sin \left(\frac{2\pi u}{L} \right),$$

(ii) a piecewise constant forcing profile

$$F_y(u) = \mathbb{1}_{u < \frac{L}{2}} - \mathbb{1}_{u \geq \frac{L}{2}},$$

(iii) and a piecewise linear forcing profile

$$F_y(u) = \frac{4}{L} \left(u - \frac{L}{4} \right) \mathbb{1}_{u < \frac{L}{2}} - \frac{4}{L} \left(\frac{3L}{4} - u \right) \mathbb{1}_{u \geq \frac{L}{2}}.$$

These forcings have the advantage that the Fourier coefficients can be analytically computed. We record in Figure 4.2 the value of the first Fourier coefficient F_1 for each of these forcings. As in the case of mobility, we fix a reference thermodynamic condition,

$$(4.21) \quad T = 0.8, \quad \rho = 0.7, \quad \gamma = 1.0, \quad N = 1000.$$

4.2 The Green-Kubo method

An alternative route to the perturbation method described above leverages a famous expression for the transport coefficient in terms of an integrated correlation function, or, in less prosaic language, in terms of the fluctuations at equilibrium of the response observable. This is the Green-Kubo method, which we describe in this section. We consider the invariant measure for the non-equilibrium dynamics (4.1). By Theorem 3, there exists a unique invariant measure with density ψ_η . For notational consistency, let us write ψ_0 for the density of the equilibrium measure μ . Then the following result holds

Theorem 4 (Series expansion for the non-equilibrium steady state). *There exists $r > 0$ such that for all $0 < \eta < r$,*

$$(4.22) \quad \frac{\psi_\eta}{\psi_0} = \left(1 + \eta (\tilde{\mathcal{L}} \Pi \mathcal{L}_\gamma^{-1} \Pi)^* \right)^{-1} \mathbb{1}_{\mathcal{E}} = \left(1 + \sum_{k=1}^{\infty} (-\eta)^k \left[(\tilde{\mathcal{L}} \Pi \mathcal{L}_\gamma^{-1} \Pi)^* \right]^k \right) \mathbb{1}_{\mathcal{E}},$$

where $\tilde{\mathcal{L}}$ is defined by (4.2), Π is the equilibrium centering projector defined in (2.33), and the adjoint is taken in $L^2(\mu)$.

Sketch of proof. The second equality identifies the Neumann series on the right as the resolvent of $-(\tilde{\mathcal{L}}\Pi\mathcal{L}_\gamma^{-1}\Pi)^*$, provided η is taken small enough. In fact, from the spectral theory of bounded operators, r can be determined as the spectral radius of $(\tilde{\mathcal{L}}\Pi\mathcal{L}_\gamma^{-1}\Pi)^*$ in the space of bounded operators $\mathcal{B}(L_0^2(\mu))$. The core of the argument lies in making the ansatz

$$(4.23) \quad \psi_\eta = \psi_0(1 + \eta f_1 + \eta^2 f_2 + \dots).$$

The stationary Fokker-Planck equation (4.4) writes

$$(\mathcal{L}_\gamma + \eta \tilde{\mathcal{L}})^\dagger \psi_0(1 + \eta f_1 + \eta^2 f_2 + \dots) = (\mathcal{L}_\gamma + \eta \tilde{\mathcal{L}})^*(1 + \eta f_1 + \eta^2 f_2 + \dots) = 0.$$

By formally separating terms by degree in η , we obtain

$$\begin{aligned} \mathcal{L}_\gamma^* \mathbb{1}_{\mathcal{E}} &= 0, \\ \tilde{\mathcal{L}}^* \mathbb{1}_{\mathcal{E}} + \mathcal{L}_\gamma^* f_1 &= 0, \\ \tilde{\mathcal{L}}^* f_1 + \mathcal{L}_\gamma^* f_2 &= 0, \end{aligned}$$

and so on. Note that the first equality is the equilibrium Fokker-Planck equation. Thus, by induction, again formally, we obtain.

$$\begin{aligned} f_1 &= (-\mathcal{L}_\gamma^*)^{-1} \tilde{\mathcal{L}}^* \mathbb{1}_{\mathcal{E}}, \\ f_2 &= (-\mathcal{L}_\gamma^*)^{-1} \tilde{\mathcal{L}}^* f_1, \\ &\dots \\ f_n &= \left[(-\mathcal{L}_\gamma^*)^{-1} \tilde{\mathcal{L}}^* \right]^n \mathbb{1}_{\mathcal{E}}, \end{aligned}$$

whence the formal proof follows, by observing that we can write

$$(-\mathcal{L}_\gamma^*)^{-1} \tilde{\mathcal{L}}^* = -(\tilde{\mathcal{L}}\Pi\mathcal{L}_\gamma^{-1}\Pi)^*.$$

For a rigorous proof, several points should be made precise:

- (i) The convergence of the series (4.22) for sufficiently small η , which can be obtained by showing the boundedness of the operator

$$(\tilde{\mathcal{L}}\Pi\mathcal{L}_\gamma^{-1}\Pi)^*$$

on $L_0(\mu)$.

- (ii) The fact that

$$\psi_0 \left(1 + \eta (\tilde{\mathcal{L}}\Pi\mathcal{L}_\gamma^{-1}\Pi)^* \right)^{-1} \mathbb{1}_{\mathcal{E}}$$

is indeed a solution to the stationary Fokker-Planck equation.

- (iii) The fact that it is indeed a probability density.

One can then conclude by unicity of the steady-state measure. \square

Strikingly, we can read the linear response directly from the first term of the series expansion.

Corollary 4 (Green-Kubo formula). *Let R be any response observable such that $\mathbb{E}_\mu[R] = 0$, and $R \in L_{\mathcal{K}_n}^\infty$ for some n . Then we have the following formula for the linear response*

$$(4.24) \quad \lim_{\eta \rightarrow 0} \frac{\mathbb{E}_\eta[R]}{\eta} = \int_0^\infty \mathbb{E}_\mu[R(q_t, p_t) S(q_0, p_0)] dt,$$

where the expectation on the right hand side is with respect to all equilibrium dynamics trajectories with canonical initial distribution, and S is defined by

$$(4.25) \quad S = \tilde{\mathcal{L}}^* \mathbb{1}_{\mathcal{E}} = \beta F(q) \cdot M^{-1} p,$$

and is called the conjugate response function. The latter expression follows from a simple integration by parts.

Proof. By Theorem 4, we can write

$$\begin{aligned}\lim_{\eta \rightarrow 0} \frac{\mathbb{E}_\eta[R]}{\eta} &= \int_{\mathcal{E}} R(q, p) (-\mathcal{L}_\gamma^*)^{-1} \tilde{\mathcal{L}}^* \mathbb{1}_{\mathcal{E}} \psi_0(q, p) dq dp \\ &= \int_{\mathcal{E}} (-\mathcal{L}_\gamma)^{-1} R(q, p) S(q, p) \psi_0(q, p) dq dp \\ &= \int_{\mathcal{E}} \int_0^\infty \mathbb{E}^{(q,p)}[R(q_t, p_t) S(q_0, p_0)] \psi_0(q, p) dt dq dp \\ &= \int_0^\infty \mathbb{E}_\mu[R(q_t, p_t) S(q_0, p_0)] dt,\end{aligned}$$

where we rely on an expression like (2.36) for $(-\mathcal{L}_\gamma)^{-1}$. \square

The Green-Kubo formula has a great advantage, in that it allows us to estimate the transport coefficients for as many different perturbations and response observables as we want **from a single equilibrium trajectory**. Indeed, one only needs to compute the corresponding integrated correlation functions (4.24).

4.2.1 Numerical implementation

We now describe a method to compute correlation functions necessary to the Green-Kubo method from a single long numerical trajectory. This method is described by Tuckerman in [12], section 13.4.2 for Hamiltonian trajectories. In fact we consider a slight extension in which we let R and S to be vector-valued observables. For notational simplicity, we assume that R and S are component-wise centered. The quantities we want to estimate are

$$(4.26) \quad C(t) = \mathbb{E}_\mu[R(q_t, p_t)^\top S(q_0, p_0)]$$

we let $(q^n, p^n)_{n \geq 0}$ be a numerical trajectory, which we see as the random iterates of the Markov chain associated with a numerical scheme, with a regular timestep $\Delta t > 0$. We further assume that the trajectory is stationary for this Markov chain, which is a realistic assumption if we take care of equilibrating the system using our numerical scheme before recording states. By stationarity, the equality in law

$$(q^n, p^n, q^0, p^0) \xrightarrow{\text{law}} (q^{n+k}, p^{n+k}, q^k, p^k)$$

for all k . Hence we define the following estimator for $C(n\Delta t)$, for $0 \leq n \leq N_{\text{iter}}$:

$$(4.27) \quad \widehat{C}_{N_{\text{iter}}}(n\Delta t) = \frac{1}{N_{\text{iter}} - n + 1} \sum_{k=0}^{N_{\text{iter}}-n} R(q^{n+k}, p^{n+k})^\top S(q^k, p^k).$$

Note the quality of these estimators degrades with n . Thus in practice, we fix $N_{\text{corr}} \ll N_{\text{iter}}$, and compute these estimators for $0 \leq n \leq N_{\text{corr}}$. For implementation details, we refer to the Appendix and links therein to relevant Julia code.

Using these estimators, we can estimate the transport coefficient through the Green-Kubo formula (4.24). The simplest way is to use a naive Riemann sum, or rectangle rule:

$$\rho_F \approx \Delta t \sum_{k=0}^{N_{\text{corr}}} \widehat{C}_{N_{\text{iter}}}(k\Delta t).$$

In fact, analysis shows that using a trapezoidal rule reduces the error. However, these procedures introduce a truncation in time of the integral in (4.24). Another approach consists of extrapolating the behavior of $\widehat{C}_{N_{\text{iter}}}$ by fitting a parametric model

$$(4.28) \quad C_\theta(t) = \left(\sum_{k=1}^m a_k e^{-\lambda_k t} \cos(f_k t) \right),$$

where

$$\theta = (\lambda_k, a_k, f_k) \in (\mathbb{R}_{>0} \times \mathbb{R} \times \mathbb{R})^m$$

is the parameter. The form of this model is justified empirically, although a formal argument based on a diagonalisation of the evolution semigroup can be made, and using the conjugate symmetry property $\mathcal{L}_\gamma \bar{\psi} = \overline{\mathcal{L}_\gamma \psi}$ for ψ a complex-valued observable. Rigorously justifying and quantifying the accuracy of this model requires fine knowledge of the spectrum of \mathcal{L}_γ . At any rate, we can then fit the model in a least-squares sense,

$$(4.29) \quad \theta^* = \underset{\theta \in (\mathbb{R}_{>0} \times \mathbb{R} \times \mathbb{R})^m}{\operatorname{argmin}} \sum_{n=0}^{N_{\text{corr}}} \left| C_\theta(n\Delta t) - \hat{C}_{N_{\text{iter}}}(n\Delta t) \right|^2,$$

using gradient descent, or the Gauss-Newton method, and deduce an estimator for the transport coefficient,

$$(4.30) \quad \hat{\rho}_{F,N_{\text{iter}}}^{\text{GK}} = \int_0^\infty C_{\theta^*}(t) dt,$$

leveraging the simple identity

$$(4.31) \quad \int_0^\infty e^{-\lambda t} a \cos(ft) dt = \frac{a\lambda}{\lambda^2 + f^2},$$

we get a closed form for the estimator,

$$\hat{\rho}_{F,N_{\text{iter}}}^{\text{GK}} = \sum_{k=1}^m \frac{a_k \lambda_k}{\lambda_k^2 + f_k^2}.$$

4.2.2 Mobility

The Green-Kubo formula asserts that

$$(4.32) \quad \lim_{\eta \rightarrow 0} \frac{\mathbb{E}_\eta[F \cdot M^{-1} p]}{\eta} = \beta \int_0^\infty \mathbb{E}_\mu[(F \cdot M^{-1} p_t) (F \cdot M^{-1} p_0)] dt.$$

Using this expression, in the case of a mass-homogeneous system where the potential V is of pair interaction form (1.3), we can relate the transport coefficients for different forcings. As a useful example, we compute an equation relating the transport coefficients for the single drift and color drift forcings. The argument is taken from unpublished notes by Julien Roussel.

Example 6 (Relating linear responses). *We assume $M = m\text{Id}$. Let us define, for $1 \leq i, j \leq N$,*

$$c_{ij} = \frac{\beta}{m^2} \int_0^\infty \mathbb{E}_\mu[p_{i1,t} p_{j1,0}] dt.$$

By the form of the potential (Newton's third law), for all q ,

$$\sum_{i=1}^N \frac{\partial}{\partial q_{i1}} V(q) = 0.$$

This implies upon summing over i the longitudinal p -components of the SDE (2.14) and integrating

$$\sum_{i=1}^N p_{i1,t} = \sum_{i=1}^N \left[p_{i1,0} + \int_0^t \left(-\frac{\partial}{\partial q_{i1}} V(q_s) - \frac{\gamma}{m} p_{i1,s} ds + \sqrt{\frac{2\gamma}{\beta}} dW_{i1,s} \right) \right] = \sum_{i=1}^N \left[p_{i1,0} - \frac{\gamma}{m} \int_0^t p_{i1,s} ds + \sqrt{\frac{2\gamma}{\beta}} W_{i1,t} \right].$$

Multiply by $p_{11,0}$ and take the expectation with respect with the canonical initial distribution, the Brownian terms vanish, and we get

$$(4.33) \quad \mathbb{E}_\mu \left[\left(\sum_{i=1}^N p_{i1,t} \right) p_{11,0} \right] = \sum_{i=1}^N \left[\mathbb{E}_\mu [p_{i1,0} p_{11,0}] - \frac{\gamma}{m} \int_0^t \mathbb{E}_\mu [p_{i1,s} p_{11,0}] ds \right].$$

By the decay properties of the evolution semigroup, the left hand side converges to 0 as $t \rightarrow \infty$, while the integral is well-defined. Since p_0 has diagonal covariance with respect to μ , we get

$$(4.34) \quad \sum_{i=1}^N \frac{\gamma}{m} \int_0^\infty \mathbb{E}_\mu [p_{i1,s} p_{11,0}] ds = \mathbb{E}_\mu [p_{11,0}^2] = \frac{m}{\beta}.$$

Equivalently,

$$\sum_{i=1}^N c_{i1} = \frac{1}{\gamma}.$$

Using the indistinguishability property

$$c_{ii} = c_{11}, \quad c_{ij} = c_{12}$$

for all $i \neq j$, we can rewrite this identity as

$$c_{12} = \frac{1}{N-1} \left(\frac{1}{\gamma} - c_{11} \right).$$

Using this computation, we can relate the linear responses of the single drift and the color drift. By the Green-Kubo formula, the transport coefficient for the single drift is given by c_{11} ,

$$\rho_{F_S} = c_{11}.$$

For the color drift, we expand, by the Green-Kubo formula,

$$\rho_{F_C} = \frac{\beta}{m^2} \int_0^\infty \mathbb{E}_\mu [(F_C \cdot p_t) (F_C \cdot p_0)] dt = \frac{1}{N} \left(\sum_{i=1}^n c_{ii} + \sum_{i \neq j} (-1)^{i+j} c_{ij} \right)$$

By indistinguishability, and using

$$\sum_{1 \leq i \neq j \leq N} (-1)^{i+j} = -2 \left\lfloor \frac{N}{2} \right\rfloor,$$

we get

$$(4.35) \quad \rho_{F_C} = c_{11} - \frac{2 \lfloor N/2 \rfloor}{N(N-1)} \left(\frac{1}{\gamma} - c_{11} \right).$$

Note that in our numerical example, we expect $\rho_{F_C} \approx \rho_{F_S} - \frac{0.88}{N}$, which is consistent with what we observe numerically, although because of persisting statistical uncertainty, much longer trajectories (or smaller systems) have to be considered to confirm this relation numerically. Let us also, the discrepancy vanishes in the thermodynamic limit, at rate $O(N^{-1})$. Since the system we consider is isotropic, we also have

$$c_{11} = \frac{\beta}{m^2} \int_0^\infty \mathbb{E}_\mu [p_{i\alpha,s} p_{i\alpha,0}] ds$$

for any $1 \leq i \leq N$ and $1 \leq \alpha \leq d$. Thus, the mobility can be computed through an expression of the form (4.26):

$$(4.36) \quad \rho_{F_S} = c_{11} = \frac{\beta}{m^2 d N} \int_0^\infty \mathbb{E}_\mu [p_s^\top p_0] ds,$$

which is the Green-Kubo relation we use in our numerical experiments. In Figure 4.3, we plot the velocity autocorrelation function used in the estimator (4.36), and its integral. We used the same thermodynamics conditions as for the NEMD method (4.13). In Figure 4.4, we show the fitted

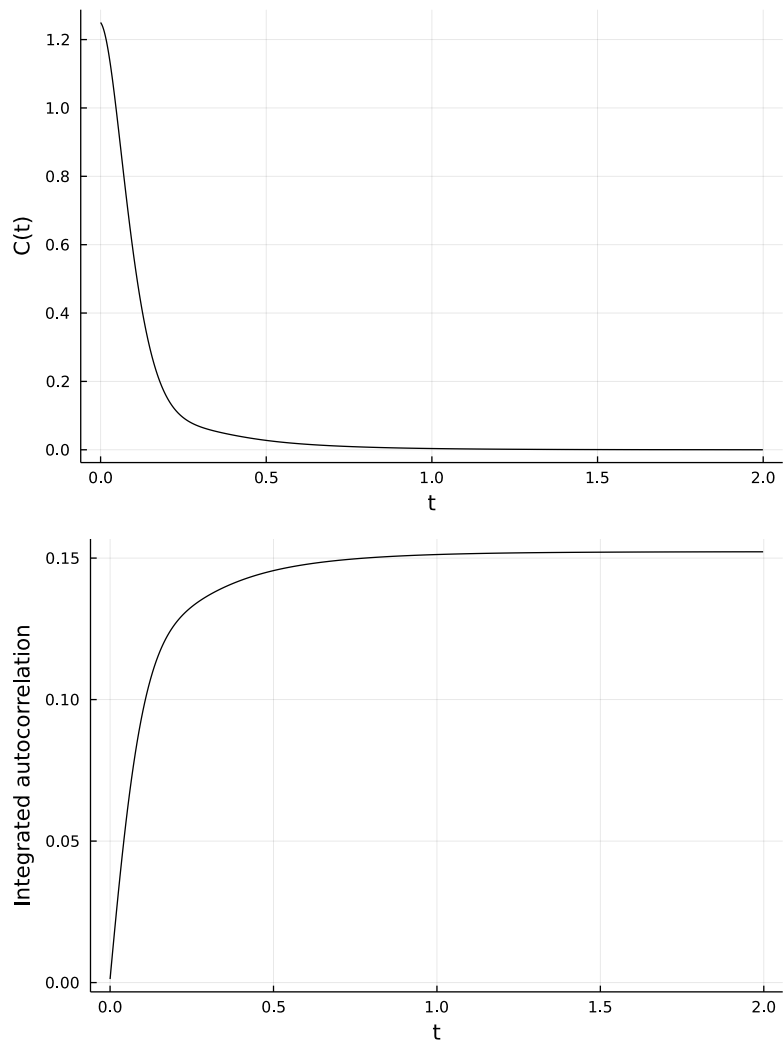


Figure 4.3: Velocity autocorrelation function (top) and its integral (bottom) for the Lennard-Jones system (4.13).

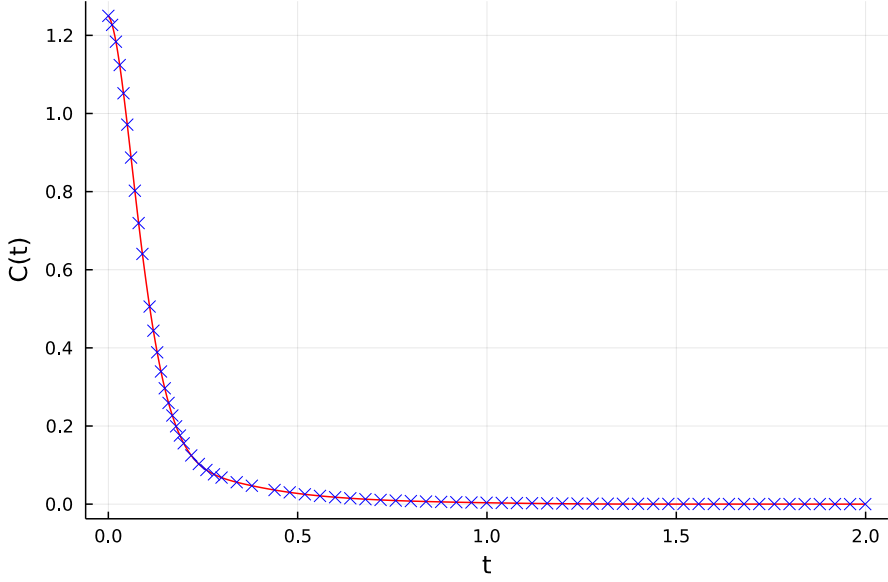


Figure 4.4: Fitted autocorrelation function (in red) with a few data points from the numerically estimated autocorrelation function (in blue) for the Lennard-Jones system (4.13).

non-linear least squares model (4.28) for the autocorrelation function, using $m = 4$ modes, trained using the Gauss-Newton algorithm. The estimated correlation function was obtained from a single numerical trajectory with a physical reduced time of $t_{\text{fin}} = 1.628 \times 10^5$. The corresponding estimated values for the mobility are 0.1218 based on a trapezoid quadrature of the truncated autocorrelation function, and 0.1215 for the analytic integral of the parametric model.

We conclude this section on mobility computations by the discussion of a final method, which yields a nice physical interpretation for the mobility.

Remark 15 (Einstein relation for mobility). *Recalling the computations in Section 2.2.5, we can write, for R a centered response observable,*

$$(4.37) \quad \mathbb{E}_\mu \left[\left(\frac{1}{\sqrt{T}} \int_0^T R(q_t, p_t) dt \right)^2 \right] = 2 \int_0^T \mathbb{E}_\mu [R(q_t, p_t) R(q_0, p_0)] \left(1 - \frac{t}{T} \right) dt.$$

Assuming an exponential decay of the evolution semigroup, we get

$$(4.38) \quad \int_0^\infty \mathbb{E}_\mu [R(q_t, p_t) R(q_0, p_0)] dt = \lim_{T \rightarrow \infty} \frac{1}{2T} \mathbb{E}_\mu \left[\left(\int_0^T R(q_t, p_t) dt \right)^2 \right].$$

This is the Einstein formula. In the case of mobility $R(q, p) = F \cdot M^{-1}p$, the right-hand side rewrites

$$(4.39) \quad \lim_{T \rightarrow \infty} \frac{1}{2T} \mathbb{E}_\mu \left[(F \cdot (Q_T - Q_0))^2 \right],$$

where

$$(4.40) \quad Q_t = Q_0 + \int_0^t M^{-1} p_s ds = \int_0^t dq_s$$

is the so called **self-diffusion** process, which formally satisfies the same SDE as q , but in the unperiodic domain \mathbb{R}^{dN} . Its trajectories corresponds to the unwrapped or unperiodicized trajectories of the coordinates, which makes them particularly easy to keep compute throughout a numerical simulation. This terminology is justified by a result (see Theorem 1 in [11]) asserting that the diffusively rescaled self-diffusion process

$$\sqrt{\varepsilon}(Q_{\varepsilon^{-1}t} - Q_0)$$

converges in law to a Brownian motion with diffusion matrix \mathfrak{D} characterized by

$$(4.41) \quad F \cdot \mathfrak{D} F = \lim_{T \rightarrow \infty} \frac{1}{T} \mathbb{E}_\mu \left[(F \cdot (Q_T - Q_0))^2 \right].$$

In the case of an isotropic system, the diffusion matrix is characterized by a single number, the diffusion coefficient, which is given by the half normalized trace of the diffusion matrix.

$$(4.42) \quad D = \frac{1}{2dN} \text{Tr}(\mathfrak{D}) = \lim_{T \rightarrow \infty} \frac{1}{2dNT} \mathbb{E}_\mu \left[|Q_T - Q_0|^2 \right]$$

In view of the Einstein relation (4.39) and of the Green-Kubo relation (4.32), the mobility is linked to the diffusion coefficient through

$$(4.43) \quad \rho_{F_S} = \beta D.$$

This yields a new family of estimators for the mobility, based on a computation of the self-diffusion coordinates expression (4.42). In Figure 4.5 we illustrate the strategy we used to compute the mobility using the Einstein formula, which we proceed to explain. We define the mean-squared deviation as the process

$$(4.44) \quad M_t = \frac{|Q_t - Q_0|^2}{dN}.$$

Fixing a number of independent realizations N_{run} and a number of simulation iterations N_{iter} , we consider, for each $i = 1, \dots, N_{\text{run}}$, a numerical trajectory of regularly sampled points from the mean-squared deviation, $M^i = (M_i^k)_{0 \leq k \leq N_{\text{iter}}}$. These correspond to points sampled at regular time intervals $T_{\text{samp}} = N_{\text{samp}} \Delta t$, where Δt is the simulation timestep, and computed from the numerical trajectory of the self-diffusion coordinates. We then obtain N_{run} estimators for D by a linear regression on the mean-squared deviation trajectories,

$$(4.45) \quad \hat{D}_{N_{\text{iter}}}^i = \frac{1}{2|\tau|^2} \tau \cdot M^i,$$

where

$$\tau = (kT_{\text{samp}})_{0 \leq k \leq N_{\text{iter}}}$$

is the vector of sampling times. An estimator for D , and thus for ρ_{F_S} , is obtained by averaging over the number of independent runs:

$$(4.46) \quad \hat{D}_{N_{\text{iter}}} = \frac{1}{N_{\text{run}}} \sum_{i=1}^{N_{\text{run}}} \hat{D}_{N_{\text{iter}}}^i.$$

Independent runs can be computed over a single trajectory, using the Markov property,

$$(Q_T - Q_0)_{T \geq 0} \sim (Q(T + t) - Q_t)_{T \geq 0} \perp\!\!\!\perp (Q_s)_{0 \leq s \leq t} \forall T, t \geq 0.$$

This can be very simply exploited in a simulation, by resetting the self-diffusion coordinates to zero following each sample run. In practice, one has to take care to take N_{samp} large enough so that the mean-squared deviation behaves approximately linearly over the sample time range $[0, T_{\text{samp}}]$. In Figure 4.5, we illustrate the principle underlying this method. For our final computation, we used $N_{\text{run}} = 256$, $N_{\text{iter}} = 10^6$, $\Delta t = 10^{-3}$, $N_{\text{samp}} = 1$. The estimated mobility is

$$(4.47) \quad \rho_{F_S} = 0.1214 \pm 0.003.$$

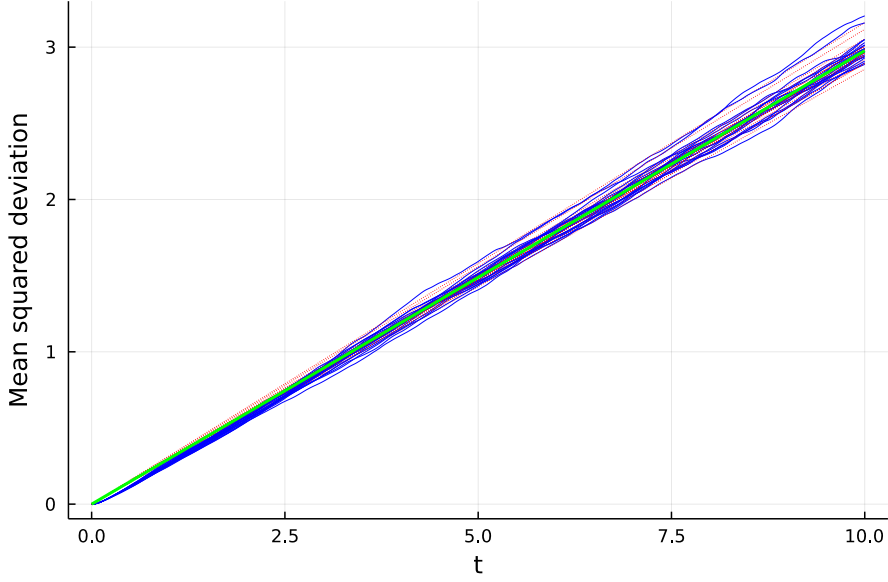


Figure 4.5: Twenty independent realizations of the mean squared-deviation (in blue) superimposed with their corresponding linear regression lines (in red dotted lines). The regression line corresponding to the final estimator (4.46) is plotted in bright green.

4.2.3 Shear viscosity

We conclude by applying the Green-Kubo formula to shear viscosity computations. It asserts, with $\rho_{F,k}$ given by (4.19),

$$(4.48) \quad \rho_{F,k} = \beta \int_0^\infty \mathbb{E}_\mu [R_k(q_t, p_t) (F(q_0) \cdot M^{-1} p_0)],$$

where R_k is given by (4.18). At this point, let us remark that we can, similar to the mobility case in (4.36), exploit the isotropy of the equilibrium measure to our statistical advantage. To do this let us define versions of the transverse forcing method for any pair of orthogonal canonical directions in \mathbb{R}^d . More precisely, we define, for any $1 \leq \alpha \neq \beta \leq d$,

$$R_{k,\alpha\beta}(q, p) = \frac{1}{N} \sum_{i=1}^N \frac{p_{i\alpha}}{m} \exp\left(\frac{2ik\pi q_{i\beta}}{L}\right),$$

$$F_{\alpha\beta}(q)_{i\beta} = F_y(q_{i\alpha}), \quad F_{\alpha\beta}(q)_{i\delta} = 0, \forall 1 \leq i \leq N, \forall \delta \neq \beta.$$

Then, by isotropy, we have

$$(4.49) \quad \rho_{F,k} = \frac{2\beta}{d(d-1)} \sum_{1 \leq \alpha \neq \beta \leq d} \int_0^\infty \mathbb{E}_\mu [R_{k,\alpha\beta}(q_t, p_t) (F_{\alpha\beta}(q_0) \cdot M^{-1} p_0)].$$

This can be rewritten as an expression of the form (4.26), with $d(d-1)/2$ -dimensional observables. This is slightly theoretical since in practice d is always 2 or 3. If $d = 2$, there is nothing to gain from this method. However, when $d = 3$, the speedup in convergence is appreciable. We also take advantage of this opportunity to showcase the power of the Green-Kubo method by computing transport coefficients for all three forcing profiles using a single numerical trajectory. In Figure (4.6), we plot the correlation functions and corresponding integral for the three different forcing

profiles. We note that the results are roughly consistent with the analytic computations of Figure 4.2, in the sense that the normalized transport coefficient

$$\frac{\rho_{F,k}}{F_k}$$

should be real and positive. The persistence of an imaginary component in the estimation of this normalized transport coefficient can be attributed to statistical error, and is useful as a direct empirical (albeit unrigorous) monitor for the convergence of the Green-Kubo estimator. Computations were run under the reference thermodynamic condition (4.21), for a physical simulation time of $t_{\text{fin}} = 1.26 \times 10^4$, with a timestep $\Delta t = 10^{-3}$ and a number of decorrelation steps $N_{\text{corr}} = 10^4$. The corresponding estimates for the shear viscosity, based on equation (4.20), are respectively 1.26, 1.24 and 1.15 for the sinusoidal, piecewise constant and piecewise linear forcing profiles. Error bars are estimated from the

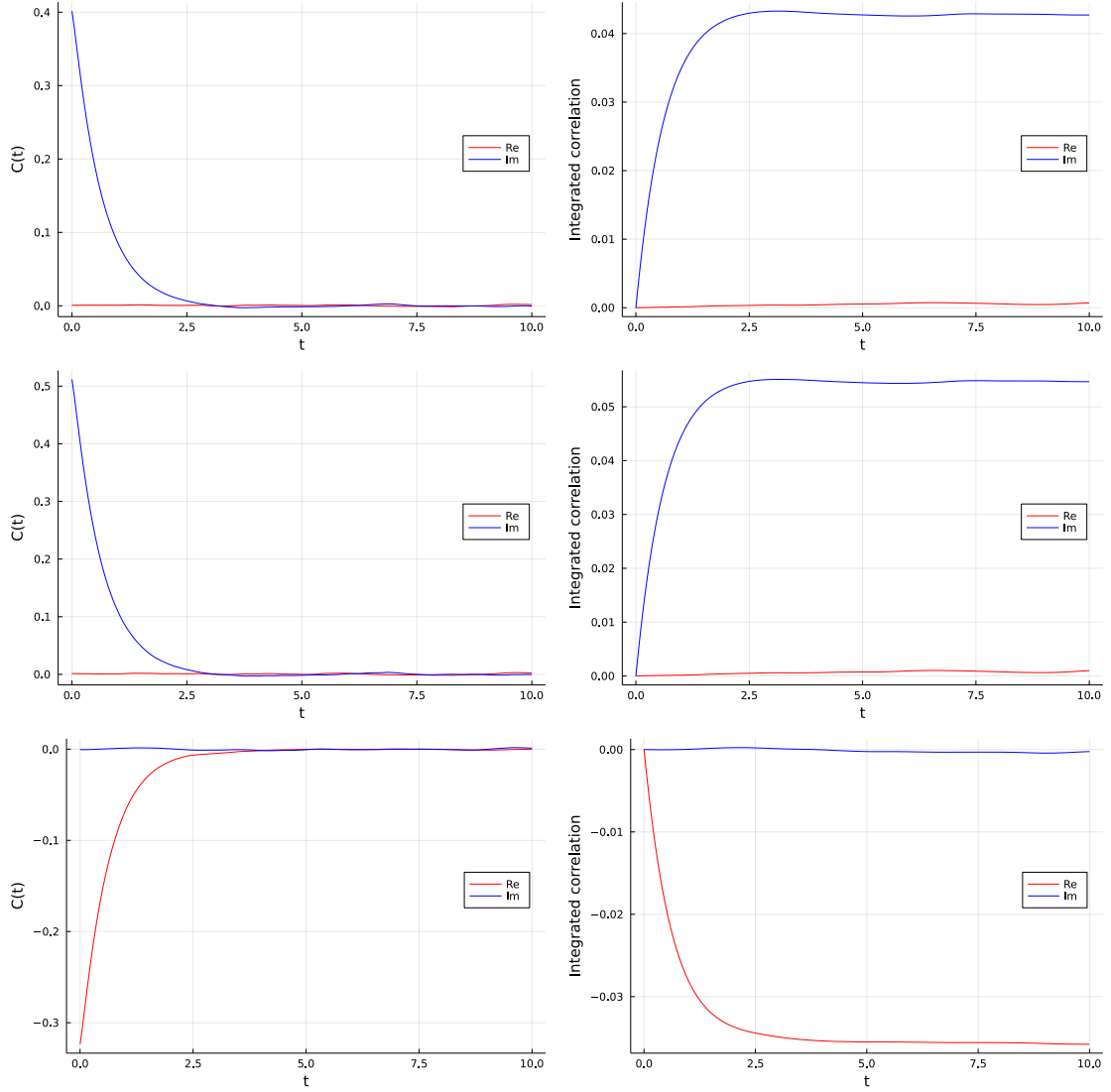


Figure 4.6: Correlation functions (left) and corresponding integrated correlation functions (right) for the shear viscosity dynamics. Top row: sinusoidal forcing, middle row: piecewise constant forcing, bottom row: piecewise linear forcing. Real parts are plotted in red and imaginary parts are plotted in blue. Integrals were obtained with a trapezoid rule.

Chapter 5

Norton dynamics

5.1 Introduction

We have presented so far two methods for computing transport coefficients. The Green-Kubo method, which relies on analysis of autocorrelations in the fluctuation of zero-average equilibrium quantities, and the linear response method, which relies in measuring the linear dependence between an equilibrium-centered observables's average under a steady-state corresponding to a perturbed dynamics and the magnitude of this perturbation, or forcing. In the case of mobility, we apply a small constant force, and measure the resulting particle flux in the direction of the perturbation. We can thus think of the mobility ρ_F as measuring the mass conductance of a substrate. A natural question to ask is whether it is possible to measure the resistance instead. One possible strategy, in very loose terms, would be to *constrain* the response to be constant, and measure the average magnitude of the forcing needed to maintain it. In the limit of a small response, the linear dependency between these quantities can be hoped to provide an equivalent measure of resistance. By analogy with the Thevenin and Norton circuit theorems, we will refer to the standard non-equilibrium perturbation method as the Thevenin method, and the dual method as the Norton method. We will again be using the mobility and the shear viscosity as our examples, both to clarify the general strategy in designing a Norton method, and to leverage reference calculations with which to evaluate its usefulness.

5.2 Mobility

Again, we fix a direction $F \in \mathbb{R}^{dN}$ and consider as a response the velocity in the direction F ,

$$F \cdot (M^{-1}p).$$

As before, we study a perturbed Langevin dynamics, but in which this time the constant magnitude of the non-gradient perturbation η is replaced by a fluctuating magnitude Λ_t , which is determined in order to ensure that the response

$$v = F \cdot (M^{-1}p) = p \cdot (M^{-1}F)$$

is a constant.

5.2.1 The dynamics

The system is the following:

$$(5.1) \quad \begin{cases} dq_t = (M^{-1}p_t) dt \\ dp_t = -\nabla V(q_t)dt - \gamma (M^{-1}p_t) dt + \sqrt{\frac{2\gamma}{\beta}} dW_t + F d\Lambda_t, \end{cases}$$

where Λ_t is a real-valued stochastic process. We can derive an expression for $d\Lambda_t$ by enforcing the constant response constraint. Using Itô's formula on the response, we get

$$(5.2) \quad d((M^{-1}F) \cdot p)_t = (M^{-1}F) \cdot \left(-\nabla V(q_t)dt - \gamma M^{-1}p_t dt + \sqrt{\frac{2\gamma}{\beta}}dW_t \right) + ((M^{-1}F) \cdot F) d\Lambda_t = 0,$$

which gives Λ_t as an Itô process,

$$(5.3) \quad d\Lambda_t = ((M^{-1}F) \cdot F)^{-1} (M^{-1}F) \cdot \left(\nabla V(q_t)dt + \gamma M^{-1}p_t dt - \sqrt{\frac{2\gamma}{\beta}}dW_t \right).$$

At this point, let us introduce the linear maps

$$(5.4) \quad \begin{aligned} P_{M,F} u &= \frac{(M^{-1}F) \cdot u}{(M^{-1}F) \cdot F} F \quad \forall u \in \mathbb{R}^{dN} \\ P_{M,F}^\perp &= \text{Id} - P_{M,F} \end{aligned}$$

which are simply the orthogonal projectors onto the subspace spanned by F and its orthogonal complement, with respect to the weighted scalar product

$$(5.5) \quad \langle x, y \rangle_M = \langle M^{-1}x, y \rangle.$$

Using this projector and substituting $d\Lambda_t$ for its value, we get the equation for the augmented dynamics $(q_t, p_t, \Lambda_t) \in \mathcal{E} \times \mathbb{R}$.

$$(5.6) \quad \begin{cases} dq_t = M^{-1}p_t dt \\ dp_t = P_{M,F}^\perp \left(-\nabla V(q_t)dt - \gamma M^{-1}p_t dt + \sqrt{\frac{2\gamma}{\beta}}dW_t \right) \\ d\Lambda_t = \frac{M^{-1}F}{(M^{-1}F) \cdot F} \cdot \left(\nabla V(q_t)dt + \gamma M^{-1}p_t dt - \sqrt{\frac{2\gamma}{\beta}}dW_t \right) \end{cases}$$

Notice this equation is almost the same as for the Langevin dynamics. The kinetic part is projected onto the F -subspace with respect to $\langle \cdot, \cdot \rangle_M$, and $d\Lambda_t$ is minus the coordinate in the F direction of the standard Langevin equation for dp_t , again with respect to $\langle \cdot, \cdot \rangle_M$. The Brownian motions W_t are the same in the last two equations, hence p_t and Λ_t are coupled processes.

5.2.2 Analytic calculations for the kinetic dynamics

The kinetic part of the dynamics splits into two analytically integrable dynamics: a ballistic Hamiltonian evolution

$$(5.7) \quad \begin{cases} dq_t = 0 \\ dp_t = -P_{M,F}^\perp \nabla V(q_t) \end{cases} \implies \begin{cases} q_t = q_0 \\ p_t = p_0 - tP_{M,F}^\perp \nabla V(q_0) \end{cases}$$

and a diffusion process describing the fluctuation-dissipation part of the dynamics,

$$(5.8) \quad dp_t = -\gamma P_{M,F}^\perp M^{-1}p_t dt - \sqrt{\frac{2\gamma}{\beta}} P_{M,F}^\perp dW_t,$$

which can also be analytically solved. Indeed, applying Itô's formula to the rescaled process $e^{\gamma P_{M,F}^\perp M^{-1}t} p_t$ yields

$$e^{\gamma P_{M,F}^\perp M^{-1}t} \left(\gamma P_{M,F}^\perp M^{-1}p_t dt - \gamma P_{M,F}^\perp M^{-1}p_t dt - \sqrt{\frac{2\gamma}{\beta}} P_{M,F}^\perp dW_t \right),$$

hence we get

$$(5.9) \quad \begin{aligned} p_t &= e^{-\gamma P_{M,F}^\perp M^{-1} t} p_0 - \sqrt{\frac{2\gamma}{\beta}} \int_0^t e^{\gamma P_{M,F}^\perp M^{-1}(s-t)} P_{M,F}^\perp dW_s \\ &= e^{-\gamma P_{M,F}^\perp M^{-1} t} p_0 - \sqrt{\frac{2\gamma}{\beta}} \left(\int_0^t e^{-\gamma P_{M,F}^\perp M^{-1}s} P_{M,F}^\perp e^{-\gamma P_{M,F}^\perp M^{-1}s} ds \right)^{\frac{1}{2}} G, \end{aligned}$$

where the last equality holds in law if G is a standard dN -dimensional Gaussian, using Itô's isometry and the symmetry of $e^{\gamma P_{M,F}^\perp M^{-1} t}$ for all t . The matrix exponentials and integrals can be computed, however there is no concise expression like (2.39) because $P_{M,F}^\perp M^{-1}$ is not invertible.

In the case of a homogeneous system with $M = \alpha \text{Id}$ (in which case we can assume by a judicious choice of mass unit that $M = \text{Id}$), a more concise expression can be found, using the identity

$$(5.10) \quad e^{r\Pi} = \sum_{k=0}^{\infty} \frac{r^k}{k!} \Pi^k = \text{Id} + \left(\sum_{k=1}^{\infty} \frac{r^k}{k!} \right) \Pi = \text{Id} + (e^r - 1) \Pi.$$

This identity follows, for Π a linear projector, from applying the projector identity

$$\Pi = \Pi^2 = \Pi^3 = \dots$$

We write the following derivation in the case of a general projector Π , and conclude by taking the case $\Pi = P_{M,F}^\perp$. We also note $\Pi^\perp = \text{Id} - \Pi$.

$$(5.11) \quad \begin{aligned} e^{-\gamma \Pi t} p_0 - \sqrt{\frac{2\gamma}{\beta}} \Pi \left(\int_0^t e^{2\gamma s \Pi} ds \right)^{\frac{1}{2}} G &= (\text{Id} + (e^{-\gamma t} - 1) \Pi) p_0 - \sqrt{\frac{2\gamma}{\beta}} \Pi \left(\int_0^t (\text{Id} + (e^{-2\gamma s} - 1) \Pi) ds \right)^{\frac{1}{2}} G \\ &= (\Pi^\perp + e^{-\gamma t} \Pi) p_0 - \sqrt{\frac{2\gamma}{\beta}} \Pi \left(t \Pi^\perp + \frac{1 - e^{-2\gamma t}}{2\gamma} \Pi \right)^{\frac{1}{2}} G. \end{aligned}$$

Now, observe that \mathbb{R}^{dN} writes as the sum of two orthogonal spaces, each of which is an eigenspace for both Π and Π^\perp , and correspond respectively to the eigenvalues 0 and 1 (this correspondence being flipped upon passing from Π to Π^\perp). By an easy spectral calculation, we also have $\Pi^\alpha = \Pi$ for any $\alpha > 0$, which allows to conclude that

$$(a\Pi^\perp + b\Pi)^\alpha = a^\alpha \Pi^\perp + b^\alpha \Pi \quad \forall a, b, \alpha > 0,$$

and finally

$$(5.12) \quad \begin{aligned} e^{-\gamma \Pi t} p_0 - \sqrt{\frac{2\gamma}{\beta}} \Pi \left(\int_0^t e^{2\gamma s \Pi} ds \right)^{\frac{1}{2}} G &= \Pi^\perp p_0 + e^{-\gamma t} \Pi p_0 - \sqrt{\frac{2\gamma t}{\beta}} \Pi \Pi^\perp G - \sqrt{\frac{1 - e^{-2\gamma t}}{\beta}} \Pi G \\ &= \Pi^\perp p_0 + e^{-\gamma t} \Pi p_0 - \sqrt{\frac{1 - e^{-2\gamma t}}{\beta}} \Pi G, \end{aligned}$$

where we use $\Pi \Pi^\perp = 0$ for the last equality. Comparing equation (5.12) and equation (2.39) yields a clear interpretation of the action of the fluctuation-dissipation term on the dynamics: there is no effect in the direction tangent to F , and a standard Ornstein-Uhlenbeck process applies to the dynamics projected onto the subspace orthogonal to F (note ΠG can then be viewed as a $(dN - 1)$ -dimensional standard Gaussian by isotropy). We also note that a similar computation may be performed in the case where both M and $P_{M,F}$ are simultaneously diagonalizable, for instance if M is a diagonal matrix and F has a single non-zero component.

5.2.3 Splitting schemes

Consider the Norton dynamics on the state variable (q_t, p_t) . Its generator is given by the operator

$$(5.13) \quad \mathcal{L}_F \varphi(q, p) = (M^{-1}p) \cdot \nabla_q \varphi(q, p) - (P_{M,F}^\perp \nabla V(q) - \gamma P_{M,F}^\perp M^{-1}p) \cdot \nabla_p \varphi(q, p) - \frac{\gamma}{\beta} \text{Tr}(P_{M,F}^\perp \nabla_p^2 \varphi(q, p)),$$

which we rewrite as

$$(5.14) \quad \mathcal{L}_F = A + B_F + \gamma C_F, \quad \text{with} \quad \begin{cases} B_F \varphi(q, p) = (P_{M,F}^\perp \nabla V(q)) \cdot \nabla_p \varphi(q, p) \\ C_F \varphi(q, p) = -(P_{M,F}^\perp M^{-1}p) \cdot \nabla_p \varphi(q, p) + \frac{1}{\beta} \text{Tr}(P_{M,F}^\perp \nabla_p^2 \varphi(q, p)). \end{cases}$$

The A and B_F operators are the generators of exactly integrable dynamics (namely ballistic Hamiltonian dynamics), and C_F generates an analytically solvable diffusion process given in (5.9). Hence we can use a splitting scheme exactly as we did in the case of the Langevin dynamics, as discussed in section 2.2.6. We will use the exact same terminology in this context, referring to a scheme by the order in which the elementary dynamics are integrated. We give as a reference one of the simplest splitting schemes for the Norton dynamics.

Algorithm 2 (BAO-like scheme for (5.6)). *For a fixed timestep $\Delta t > 0$, iterate the following update rule.*

$$(5.15) \quad \begin{cases} p^{n+\frac{1}{2}} = p^n - \Delta t P_{M,F}^\perp \nabla V(q^n) \\ q^{n+1} = q^n + \Delta t M^{-1} p^{n+\frac{1}{2}} \\ p^{n+1} = e^{-\gamma P_{M,F}^\perp M^{-1} \Delta t} p^{n+\frac{1}{2}} - \sqrt{\frac{2\gamma}{\beta}} \left(\int_0^{\Delta t} e^{-\gamma P_{M,F}^\perp M^{-1} s} P_{M,F}^\perp e^{-\gamma P_{M,F}^\perp M^{-1} s} ds \right)^{\frac{1}{2}} G^n \end{cases}$$

The γC_F -step is cumbersome to write in full, but it is always of the form

$$p^{n+1} = R_{\Delta t} p^n + S_{\Delta t} G^n$$

for fixed matrices $R_{\Delta t}$ and $S_{\Delta t}$ which only have to be computed once.

5.2.4 Estimation of ρ_F

To estimate the mobility, we need to estimate the average forcing. For this we rely on two crucial assumptions. Firstly, that for v small enough, the dynamics (5.6) admits and reaches a unique steady-state on \mathcal{E} , whose expectation we denote by \mathbb{E}_v . Secondly, we assume that ergodicity holds, allowing us to compute the average forcing under \mathbb{E}_v from trajectory averages. We refrain from giving precise conjectures, simply noting that a potential source of added technical difficulty relative to the Thevenin setting is the fact that such a steady-state is not absolutely continuous with respect to the equilibrium measure μ , since \mathbb{E}_v is necessarily supported on the constant response manifold which is μ -negligible. It is likely that rigorously establishing existence and ergodicity results for Norton steady-states will require working in a reduced set of coordinates. Nevertheless, under these assumptions, and recalling the SDE (5.6) for $d\Lambda$, the martingale term involving the Brownian motion disappears under steady-state averaging. Hence we can estimate the average forcing using the following ergodic average:

$$(5.16) \quad \lim_{T \rightarrow \infty} \frac{1}{T} \int_0^T \frac{M^{-1} F}{(M^{-1} F) \cdot F} \cdot (\nabla V(q_t) + \gamma M^{-1} p_t) dt.$$

In practice, we can estimate the average forcing through numerical trajectory averages, which yields the following estimator.

$$(5.17) \quad \widehat{d\Lambda}_{N_{\text{iter}}, v} = \frac{1}{N_{\text{iter}}} \sum_{n=1}^{N_{\text{iter}}} \frac{M^{-1}F}{(M^{-1}F) \cdot F} \cdot (\nabla V(q^n) + \gamma M^{-1}p^n).$$

We can then estimate ρ_F by directly computing the following ratio for a fixed small v ,

$$(5.18) \quad \rho_F \approx v \left(\widehat{d\Lambda}_{N_{\text{iter}}, v} \right)^{-1},$$

or by a least-squares fit

$$\left(\widehat{d\Lambda}_{N_{\text{iter}}, v_i} \right)_{i=1 \dots K} \approx \frac{1}{\rho_F} (v_i)_{i=1 \dots K}.$$

Statistical errors estimates can be established using the block averaging method on

$$\left(\frac{M^{-1}F}{(M^{-1}F) \cdot F} \cdot (\nabla V(q^n) + \gamma M^{-1}p^n) \right)_{n \geq 0},$$

which can then be transposed to the estimator for ρ_F by applying the appropriate delta-method. ref Billingsley

5.3 Shear viscosity

5.3.1 A Norton method

The corresponding Norton method consists of fixing the longitudinal velocity profile to be of a prescribed shape, say proportional to a smooth periodic function G , and applying a fluctuating transverse force profile dF_x to enforce this constraint. We hope that the shear viscosity can be computed from the resulting linear response in the forcing profile, which we will denote $f_x(Y)$, through a Norton analog of equation (??),

$$(5.19) \quad \eta G''(Y) + \gamma_1 \rho G(Y) = \rho f_x(Y).$$

Formally, we write

$$(5.20) \quad \begin{cases} dq_{ij,t} = \frac{p_{ij,t}}{m} dt, & 1 \leq j \leq d, \\ dp_{i1,t} = -\nabla_{q_{i1}} V(q_t) dt - \gamma_1 \frac{p_{i1,t}}{m} dt + \sqrt{\frac{2\gamma_1}{\beta}} dW_t^{i1} + dF_x(t, q_{i2,t}), \\ dp_{ij,t} = -\nabla_{q_{ij}} V(q_t) dt - \gamma \frac{p_{ij,t}}{m} dt + \sqrt{\frac{2\gamma}{\beta}} dW_t^{ij}, & 2 \leq j \leq d. \end{cases}$$

where F_x is now a process indexed by both the time and the transverse coordinate in $L_y \mathbb{T}$. As in the case of the mobility, we can restate the dynamics with no reference to F_x , by enforcing the constraint

$$(5.21) \quad \frac{p_{i1,t}}{m} = vG(q_{i2,t}) \quad \forall 1 \leq i \leq N,$$

where $v > 0$ is the magnitude of the velocity perturbation. By Ito's lemma, since q is a bounded variation process, we get

$$dp_{i1,t} = mvG'(q_{i2,t}) dq_{i2,t} = vG'(q_{i2,t}) p_{i2,t} dt.$$

This allows for a formal rewriting

$$(5.22) \quad \begin{aligned} dF_x(t, q_{i2,t}) &= vG'(q_{i2,t}) p_{i2,t} dt + \nabla_{q_{i1}} V(q_t) dt + \gamma_1 \frac{p_{i1,t}}{m} dt - \sqrt{\frac{2\gamma_1}{\beta}} dW_t^{i1} \\ &= vG'(q_{i2,t}) p_{i2,t} dt + \nabla_{q_{i1}} V(q_t) dt + \gamma_1 vG(q_{i2,t}) dt - \sqrt{\frac{2\gamma_1}{\beta}} dW_t^{i1} \end{aligned}$$

of the forcing term. We finally can enforce the constraint to obtain a simple expression for the Norton dynamics.

$$(5.23) \quad \begin{cases} dq_{ij,t} = \frac{p_{ij,t}}{m} dt, & 1 \leq j \leq d, \\ dp_{i1,t} = vG'(q_{i2,t}) p_{i2,t} dt, \\ dp_{ij,t} = -\nabla_{q_{ij}} V(q_t) dt - \gamma \frac{p_{ij,t}}{m} dt + \sqrt{\frac{2\gamma}{\beta}} dW_t^{ij}, & 2 \leq j \leq d. \end{cases}$$

At this point, let us remark that unlike the mobility case where we had an explicit SDE for the forcing intensity, (5.22) does not give an expression for the full process F_x , but rather N coupled SDEs for the real-valued processes $F_x(t, q_{i2,t})$. Note that a strictly equivalent way to define the Norton dynamics is through the processes $(F_{x,t}^i := F_x(t, q_{i2,t}))_{i=1\dots N}$, so that there is no theoretical need for the full F_x , but it is useful in highlighting the idea of a fluctuating force profile enforcing the constant velocity constraint. Based on these expressions, we can define a candidate average forcing profile, as the following limit, provided it is well-defined:

$$(5.24) \quad f_x(Y) := \lim_{\epsilon \rightarrow 0} \lim_{v \rightarrow 0} \frac{L_y}{vN} \mathbb{E}_v \left[\sum_{i=1}^N (vG'(q_{i2}) p_{i2} + \nabla_{q_{i1}} V(q) + \gamma_1 vG(q_{i2})) \chi_\epsilon(q_{i2} - Y) \right].$$

Where \mathbb{E}_v denotes again the expectation with respect to a hypothesized steady-state for the Norton dynamics, χ_ϵ denotes an approximation of unity, and where we dropped the centered Brownian term of the force, similar to the mobility case. We estimate the expectation with respect to the steady state through the use of trajectory averages, assuming an ergodicity property. For instance, the average of f_x over an interval $I \subset [0, L_y]$ can be estimated by the following

$$(5.25) \quad \frac{L_y}{|I|vNN_{\text{iter}}} \sum_{i=1}^N \sum_{k=1}^{N_{\text{iter}}} \mathbb{1}_{q_{i2}^k \in I} (vG'(q_{i2}^k) p_{i2}^k + \nabla_{q_{i1}} V(q^k) + \gamma_1 vG(q_{i2}^k)),$$

for a small v , where the (q^k, p^k) are iterates of a discretization of the continuous dynamics. We can recover an estimation of the full forcing profile by subdividing the transverse domain into regularly sized bins. Similar to the Thevenin case, we estimate Fourier coefficients

$$(5.26) \quad \bar{F}_k := \frac{1}{L_y} \int_0^{L_y} f_x(y) \exp\left(\frac{2ik\pi y}{L_y}\right) dy$$

directly from the numerical trajectory, through

$$(5.27) \quad \frac{1}{vNN_{\text{iter}}} \sum_{k=1}^{N_{\text{iter}}} \sum_{i=1}^N (vG'(q_{i2}^k) p_{i2}^k + \nabla_{q_{i1}} V(q^k) + \gamma_1 vG(q_{i2}^k)) \exp\left(\frac{2ik\pi q_{i2}^k}{L_y}\right),$$

and relate them to the shear viscosity through

$$(5.28) \quad \eta = \rho \left(\frac{\bar{F}_k}{G_k} - \gamma_1 \right) \left(\frac{L_y}{2k\pi} \right)^2,$$

where G_k are the Fourier coefficients of the velocity profile,

$$G_k = \frac{1}{L_y} \int_0^{L_y} G(y) \exp\left(\frac{2ik\pi y}{L_y}\right) dy$$

which can be analytically or numerically computed to arbitrary precision at minimal cost.

5.3.2 Numerical integration

We can view the marginal Norton dynamics in the unconstrained degrees of freedom as non-stationary Langevin dynamics where the potential varies with time through a dependence on the process of constrained variables. This suggests using a standard splitting scheme for the unconstrained degrees of freedom and coordinates, and handling the constrained momenta differently. Since by definition we know for all i and t that $p_{i1,t} = mvG(q_{i2,t})$, a very simple solution consists in setting $p_{i1}^{n+\alpha} = mvG(q_{i2}^{n+\alpha})$ after any intermediate coordinate update. We now give for reference the BABO-like scheme we used in our numerical results.

Algorithm 3 (BABO scheme for (5.23)). *For a fixed timestep Δt and for all $1 \leq i \leq N$, iterate the following update rule.*

$$(5.29) \quad \begin{cases} p_{ij}^{n+\frac{1}{3}} = p_{ij}^n - \frac{\Delta t}{2} \nabla_{q_{ij}} V(q^n), & 2 \leq j \leq d \\ q_{ij}^{n+1} = q_{ij}^n + \Delta t \frac{p_{ij}^{n+\frac{1}{3}}}{m}, & 1 \leq j \leq d \\ p_{i1}^{n+1} = mvG(q_{i2}^{n+1}) \\ p_{ij}^{n+\frac{2}{3}} = p_{ij}^{n+\frac{1}{3}} - \frac{\Delta t}{2} \nabla_{q_{ij}} V(q^{n+1}), & 2 \leq j \leq d \\ p_{ij}^{n+1} = \alpha_{\Delta t} p_{ij}^{n+\frac{2}{3}} + \sigma_{\Delta t} G_{ij}^n, & 2 \leq j \leq d \end{cases}$$

with (G_{ij}^n) i.i.d. standard Gaussian variables, and $\alpha_{\Delta t}$, $\sigma_{\Delta t}$ defined as usual.

5.3.3 Numerical results

5.4 Norton method- fixed

5.5 The dynamics

We consider the following general form of the Norton dynamics, where we perturb the standard Langevin dynamics in the same direction as the Thevenin method, but with a variable amplitude chosen to induce a constant flux constraint. It writes

$$(5.30) \quad \begin{cases} dq_t = m^{-1} p_t dt, \\ dp_t = -\nabla V(q_t) dt - \gamma m^{-1} p_t dt + \sqrt{\frac{2\gamma}{\beta}} dW_t + d\Lambda_t F(q_t), \\ U(q_t, p_t) = U(q_0, p_0), \end{cases}$$

where Λ_t is the magnitude of the perturbation, which is a real-valued Itô process defined by the constraint $U(q_t, p_t) = U(q_0, p_0)$. We may assume γ is a positive semi-definite diagonal matrix, as in the Thevenin case. U is the response flux observable, which we take of the form

$$U(q, p) = R(q) \cdot p,$$

with R a smooth vector field. Note in particular that $\nabla_p U(q, p) = R(q)$. A SDE for Λ_t can be obtained by a simple application of Itô's formula to the constraint.

$$\begin{aligned} 0 &= dU(q_t, p_t) \\ &= \nabla_q U(q_t, p_t) \cdot dq_t + \nabla_p U(q_t, p_t) \cdot dp_t \\ &= m^{-1} \nabla_q U(q_t, p_t) \cdot p_t dt + R(q_t) \cdot \left(-\nabla V(q_t) dt - \gamma m^{-1} p_t dt + \sqrt{\frac{2\gamma}{\beta}} dW_t + d\Lambda_t F(q_t) \right) \end{aligned}$$

Note since q_t is a bounded-variation process and $\nabla_p^2 U = 0$, the quadratic covariation terms vanish in the second equality. Rearranging gives

$$(5.31) \quad d\Lambda_t = \frac{-m^{-1}\nabla_q U(q_t, p_t) \cdot p_t dt + R(q_t) \cdot (\nabla V(q_t)dt + \gamma m^{-1}p_t dt - \sqrt{\frac{2\gamma}{\beta}}dW_t)}{R(q_t) \cdot F(q_t)}.$$

This expression allows us to identify the bounded variation and martingale parts of the forcing,

$$(5.32) \quad d\Lambda_t = d\bar{\Lambda}_t + d\tilde{\Lambda}_t,$$

with

$$(5.33) \quad d\bar{\Lambda}_t := \frac{-m^{-1}\nabla_q U(q_t, p_t) \cdot p_t dt + R(q_t) \cdot (\nabla V(q_t)dt + \gamma m^{-1}p_t dt)}{R(q_t) \cdot F(q_t)}$$

being the bounded variation part, which will serve as the basis for statistical estimators of the average forcing, the quantity of main interest.

Remark 16. Note that the $R(q_t) \cdot F(q_t)$ term in the denominator may pose a question of well-posedness of the dynamics. Let us always suppose in our computations that $R(q_t) \cdot F(q_t) > 0$, but this is by no means automatic. Indeed, thinking of the extreme case when F and R are orthogonal everywhere and $V = 0$ highlights the fact that this is an issue of controllability: in that case, by isotropy, the component of the momentum in the direction R will diffuse according to an Ornstein-Uhlenbeck process independent from any forcing applied in the direction F . In this case there is no way to control the response, and thus the dynamics is ill-defined.

As before, we can insert this SDE into the definition of the Norton dynamics to obtain an alternative expression decoupled from the process $d\Lambda_t$. We obtain

$$(5.34) \quad \begin{cases} dq_t = m^{-1}p_t dt, \\ dp_t = -\nabla V(q_t)dt + \frac{R(q_t) \cdot \nabla V(q_t)}{R(q_t) \cdot F(q_t)}F(q_t)dt - m^{-1}\frac{\nabla_q U(q_t, p_t) \cdot p_t}{R(q_t) \cdot F(q_t)}F(q_t)dt \\ \quad - m^{-1}\gamma p_t dt + m^{-1}\frac{R(q_t) \cdot \gamma p_t}{R(q_t) \cdot F(q_t)}F(q_t)dt + \sqrt{\frac{2\gamma}{\beta}}dW_t - \frac{R(q_t) \cdot \sqrt{\frac{2\gamma}{\beta}}dW_t}{R(q_t) \cdot F(q_t)}F(q_t) \end{cases}$$

To lighten the notation, we introduce the matrix

$$(5.35) \quad P_{R,F}(q) = \text{Id} - \frac{R(q) \otimes F(q)}{R(q) \cdot F(q)}.$$

Note this is a non-orthogonal projector, owing to the identities

$$\left(\frac{A \otimes B}{A \cdot B}\right)^2 = \frac{(A \otimes B)(A \cdot B)}{(A \cdot B)^2} = \frac{A \otimes B}{A \cdot B}, \quad (\text{Id} - P)^2 = \text{Id} - 2P + P^2$$

This naturally suggests a splitting of the dynamics into two parts: a fluctuation-dissipation part,

$$(5.36) \quad \begin{cases} dq_t = 0 \\ dp_t = -m^{-1}P_{R,F}(q_t)\gamma p_t dt + P_{R,F}(q_t)\sqrt{\frac{2\gamma}{\beta}}dW_t \end{cases}$$

and a remaining deterministic evolution,

$$(5.37) \quad \begin{cases} dq_t = m^{-1}p_t dt, \\ dp_t = -P_{R,F}(q_t)\nabla V(q_t)dt - m^{-1}\frac{\nabla_q U(q_t, p_t) \cdot p_t}{R(q_t) \cdot F(q_t)}F(q_t)dt. \end{cases}$$

We will again be relying on this splitting, and the fact that the Ornstein-Uhlenbeck part can be analytically solved, to devise an integration strategy.

5.5.1 Fluctuation-dissipation part

The dynamics (5.36) is in Ornstein-Uhlenbeck form. Note as a sanity check that in the case F is constant with respect to q , and $U(q, p)$ is the mobility flux, we recover equation (5.8). By the standard strategy of applying Itô's formula to the rescaled process

$$e^{m^{-1}P_{R,F}(q_0)\gamma t}p_t,$$

we obtain the analytic solution

$$\begin{aligned} (5.38) \quad p_t &= e^{-m^{-1}P_{R,F}(q_0)\gamma t}p_0 + \int_0^t e^{m^{-1}P_{R,F}(q_0)\gamma(s-t)}P_{R,F}(q_0)\sqrt{\frac{2\gamma}{\beta}}dW_s \\ &= e^{-m^{-1}\gamma P_{R,F}(q_0)t}p_0 + \left(\int_0^t \sqrt{\frac{2\gamma}{\beta}}P_{R,F}(q_0)^T e^{-m^{-1}s\gamma P_{R,F}(q_0)^T}e^{-m^{-1}sP_{R,F}(q_0)}P_{R,F}(q_0)\sqrt{\frac{2\gamma}{\beta}}\right)^{\frac{1}{2}}G, \end{aligned}$$

where the equality holds in law for G a dN -dimensional standard Gaussian. We used Itô's isometry with the fact that γ is symmetric. Of course the expression for the covariance matrix may greatly simplify in particular cases, for instance if γ is a constant and $P(q_0)$ is invertible, or if these two matrices commute. We will come back to this point when applying this method to shear viscosity estimation.

5.5.2 Deterministic part

A simple application of the chain rule to (5.37) shows that the dynamics preserves the constant flux manifold:

$$\frac{dU(q_t, p_t)}{dt} = m^{-1}\nabla_q U(q_t, p_t) \cdot p_t + R(q_t) \cdot \left(-\nabla V(q_t) + \frac{R(q_t) \cdot \nabla V(q_t) F(q_t) - m^{-1}(\nabla_q U(q_t, p_t) \cdot p_t) F(q_t)}{R(q_t) \cdot F(q_t)}\right) = 0.$$

It is natural to wonder whether this dynamics corresponds to some physical trajectory. To try to answer this question, we introduce Gauss's principle of least constraint, which is an equivalent statement of the Lagrange-d'Alembert principle. Crucially, it also describes systems undergoing *non-holonomic* constraints, which depend on the momenta as well as the position. We give it in the case (of interest to us here) of a homogeneous system under a single constraint.

Definition 4 (Gauss's principle of least constraint). *Consider a classical constrained homogeneous system defined by a potential V and a non-holonomic constraint $U(q, p) = U(q_0, p_0)$, where U is a smooth function on phase space. The principle states that the equations of motion are given by*

$$(5.39) \quad \begin{cases} \frac{d}{dt}q_t = m^{-1}p_t, \\ \frac{d}{dt}p_t = \underset{f \in \mathcal{A}(q_t, p_t)}{\operatorname{argmin}} |f + \nabla V(q_t)|^2, \end{cases}$$

where

$$\mathcal{A}(q, p) = \{f \in \mathbb{R}^{dN} \mid (m^{-1}p, f) \cdot \nabla U(q, p) = 0\}$$

is the set of admissible forces, which is determined by differentiating the constraint in time, giving a hidden constraint on the acceleration. The principle says in short that the additional force applied to the constrained system relative to the unconstrained system in the same state is minimized in the Euclidean sense at each point along the trajectory.

Example 7. As a useful example, we can compute the evolution equation for the Hamiltonian system constrained to a level set of $U(q, p) = R(q) \cdot p$. Assuming $R(q_t) \neq 0$, the minimization problem is obviously well-posed. Solving it amounts to finding the critical point of the Lagrangian

$$L(f, \lambda) = |f + \nabla V(q_t)|^2 - \lambda(m^{-1}\nabla_q U(q_t, p_t) \cdot p_t + R(q_t) \cdot f).$$

this yields

$$(5.40) \quad \begin{cases} \nabla_f L(f, \lambda) = 2f + 2\nabla V(q_t) - \lambda R(q_t) &= 0, \\ -\frac{\partial}{\partial \lambda} L(f, \lambda) = m^{-1} \nabla_q U(q_t, p_t) \cdot p_t + R(q_t) \cdot f &= 0. \end{cases}$$

Solving, we get

$$(5.41) \quad \begin{cases} f = -\nabla V(q_t) + \frac{\lambda}{2} R(q_t), \\ \frac{\lambda}{2} = \frac{\nabla V(q_t) \cdot R(q_t) - m^{-1} \nabla_q U(q_t, p_t) \cdot p_t}{|R(q_t)|^2}, \\ f = -\nabla V(q_t) - \frac{m^{-1} \nabla_q U(q_t, p_t) \cdot p_t}{|R(q_t)|^2} R(q_t) + \frac{\nabla V(q_t) \cdot R(q_t)}{|R(q_t)|^2} R(q_t), \end{cases}$$

which gives the dynamics

$$(5.42) \quad \begin{cases} \frac{d}{dt} q_t = m^{-1} p_t, \\ \frac{d}{dt} p_t = -\nabla V(q_t) - \frac{m^{-1} \nabla_q U(q_t, p_t) \cdot p_t}{|R(q_t)|^2} R(q_t) + \frac{\nabla V(q_t) \cdot R(q_t)}{|R(q_t)|^2} R(q_t). \end{cases}$$

We note that the constraining force is always in the direction $R(q_t)$, and that its magnitude is given by half the Lagrange multiplier enforcing the constraint. We also note, again as a sanity check, that in the case where F is constant, the $\nabla_q U$ term vanishes, and we recover the Hamiltonian part of the Norton dynamics for mobility, (5.6).

5.5.3 Application to shear viscosity

Comparing equation (5.37) and equation (5.42) strongly suggests considering $R \propto F$, along with Remark 16. While this is restrictive in regards to shear viscosity computations for general forcings, in the case of a transverse sinusoidal forcing, we can interpret the constraint $p_t \cdot R(q_t) = v$ as expressing the fact that the response in the velocity profile is constant. This corresponds to the case, for $1 \leq i \leq N$,

$$(F(q))_{i1} = \left(\sin \left(\frac{2\pi q_{i2}}{L_y} \right) \right)_{i1}, \quad (F(q))_{i\alpha} = 0 \quad \forall 2 \leq \alpha \leq d.$$

Indeed, since the solutions to equation (4.17) are themselves sinusoids, we can quantify the magnitude of the response in the velocity profile by the ratio of the empirical Fourier coefficient, or rather its imaginary component,

$$(5.43) \quad U(q, p) = \frac{1}{Nm} \sum_{i=1}^N p_{i1} \sin \left(\frac{2\pi q_{i2}}{L_y} \right) = \frac{1}{Nm} p \cdot F(q),$$

to that of the forcing,

$$\frac{1}{L_y} \int_0^{L_y} \sin^2 \left(\frac{2\pi y}{L_y} \right) dy = \frac{1}{2}.$$

This particular case allows for nice simplifications of the fluctuation-dissipation part. Indeed, we have $R(q) \cdot F(q) = \frac{1}{Nm} |F(q)|^2$. Thus, (5.35) becomes

$$P(q) = \text{Id} - \frac{F(q) \otimes F(q)}{|F(q)|^2},$$

which is the projector onto the orthogonal complement of the one-dimensional space spanned by $F(q)$, which is easily computed in practice. Furthermore, since F only acts on longitudinal components, the restriction of γ to either one of $P(q)$'s eigenspaces is proportional to an identity, hence γ and $P(q)$ commute. Therefore the analytic solution to the fluctuation-dissipation part of the dynamics writes, as an equality in law,

$$(5.44) \quad p_t \stackrel{\text{law}}{=} P(q_0)^\perp + P(q_0) \left(e^{-m^{-1}\gamma t} p_0 + \sqrt{\frac{1 - e^{-2m^{-1}\gamma t}}{\beta}} G \right)$$

where we denote

$$P(q_0)^\perp = \text{Id} - P(q_0) = \frac{F(q_0) \otimes F(q_0)}{|F(q_0)|^2}$$

the orthogonal projector onto the subspace spanned by $F(q_0)$. This follows verbatim from the same derivation as the one leading up to (5.12). Again, the interpretation is clear.

In addition, the deterministic part of the dynamics can now be interpreted as a constrained Hamiltonian evolution, in view of the discussion in Example 7. Looking back at the bounded variation part of the average forcing (5.33), we can see that it further splits into two parts corresponding to the fluctuation-dissipation part and the constrained Hamiltonian part of the dynamics,

$$d\bar{\Lambda}_t = d\bar{\Lambda}_t^{\text{ham}} + d\bar{\Lambda}_t^{\text{ou}},$$

with

$$(5.45) \quad \begin{cases} d\bar{\Lambda}_t^{\text{ham}} = \frac{-m^{-1}\nabla_q U(q_t, p_t) \cdot p_t + R(q_t) \cdot \nabla V(q_t)}{R(q_t) \cdot F(q_t)} dt, \\ d\bar{\Lambda}_t^{\text{ou}} = \frac{R(q_t) \cdot \gamma m^{-1} p_t}{R(q_t) \cdot F(q_t)} dt = \gamma_1 m^{-1} \frac{R(q_0) \cdot p_0}{R(q_t) \cdot F(q_t)} dt. \end{cases}$$

5.6 Numerical implementation

We initialize the system on the constant response manifold by setting

$$p^0 = P(q^0)\tilde{p}^0 + vF(q_0),$$

where \tilde{p}^0 are canonically sampled momenta. Again, we can consider splitting schemes, in which we integrate the Ornstein-Uhlenbeck part analytically. We fix a timestep $\Delta t > 0$ and define $\alpha_{\Delta t}$ and $\sigma_{\Delta t}$ as usual. The corresponding O -step is given by

$$(5.46) \quad p^{n+1} = P(q^n)p^n + P(q^n)^\perp (\alpha_{\Delta t}p^{n+1} + \sigma_{\Delta t}G^n).$$

Integrating the Hamiltonian part requires more care. We suggest (à voir) the following scheme, which is a modification of the RATTLE scheme (see, for example, the discussion in [LM15], section 4.3.5) for non-holonomic constraints, exploiting the fact that the momenta and the position are jointly constrained, thus eliminating the need for the enforcement of a co-tangency condition.

We first write the scheme in the following form to highlight the similarity with the RATTLE method.

$$(5.47) \quad \begin{cases} p^{n+\frac{1}{2}} = p^n - \frac{\Delta t}{2} \nabla V(q^n) + \lambda^{n+\frac{1}{2}} F(q^n) \\ q^{n+1} = q^n + \Delta t m^{-1} p^{n+\frac{1}{2}} \\ v = F(q^{n+1}) \cdot p^{n+\frac{1}{2}} \\ p^{n+1} = p^{n+\frac{1}{2}} - \frac{\Delta t}{2} \nabla V(q^{n+1}) + \lambda^{n+1} F(q^{n+1}) \\ v = F(q^{n+1}) \cdot p^{n+1} \end{cases}$$

right normalization?

The algorithm is resolved as follows. By substituting the expressions of $p^{n+\frac{1}{2}}$ and q^{n+1} in terms of $(q^n, p^n, \lambda^{n+\frac{1}{2}})$ in the third line, one arrives at a non-linear equation for $\lambda^{n+\frac{1}{2}}$, which can be solved numerically, by Newton's method, or by a fixed-point iteration. Solving this equation yields an intermediary state point $(q^{n+1}, p^{n+\frac{1}{2}})$ on the constant response manifold. Now we can proceed similarly for the last line, except that since q^{n+1} is already resolved, the equation can be solved analytically, giving

$$(5.48) \quad \lambda^{n+1} = \frac{v - \left(p^{n+\frac{1}{2}} - \frac{\Delta t}{2} \nabla V(q^{n+1}) \right) \cdot F(q^{n+1})}{|F(q^{n+1})|^2}.$$

Hence the full scheme rewrites

Algorithm 4 (Non-holonomic RATTLE scheme). *We first write the scheme in the following form to highlight the similarity with the RATTLE method.*

$$(5.49) \quad \begin{cases} v = F \left(q^n + \Delta t m^{-1} \left(p^n - \frac{\Delta t}{2} \nabla V(q^n) + \lambda^{n+\frac{1}{2}} F(q^n) \right) \right) \cdot \left(p^n - \frac{\Delta t}{2} \nabla V(q^n) + \lambda^{n+\frac{1}{2}} F(q^n) \right) \\ p^{n+\frac{1}{2}} = p^n - \frac{\Delta t}{2} \nabla V(q^n) + \lambda^{n+\frac{1}{2}} F(q^n) \\ q^{n+1} = q^n + \Delta t m^{-1} p^{n+\frac{1}{2}} \\ p^{n+1} = P(q^{n+1}) \left(p^{n+\frac{1}{2}} - \frac{\Delta t}{2} \nabla V(q^{n+1}) \right) + \frac{v}{|F(q^{n+1})|^2} F(q^{n+1}). \end{cases}$$

An advantage of this method is that it allows us to estimate the Hamiltonian component of the forcing (5.33) directly from the Lagrange multipliers $\lambda^{n+\frac{1}{2}}$ and λ^{n+1} . (equation 3.06)

Appendix A

Implementation details

Appendix B

Notational conventions

Notational conventions

We convene that the gradient of a function $\varphi : \mathbb{R}^n \mapsto \mathbb{R}$ is a column vector-valued function

$$\nabla \varphi : \mathbb{R}^n \mapsto \mathbb{R}^n := \mathbb{R}^{n \times 1}$$

Notationally,

$$\nabla = \begin{pmatrix} \partial x_1 \\ \vdots \\ \partial x_n \end{pmatrix}$$

So that the Hessian operator writes

$$\nabla^2 := \nabla \nabla^\top = \begin{pmatrix} \partial x_1 \partial_{x_1} & \cdots & \partial x_1 \partial x_n \\ \vdots & \ddots & \vdots \\ \partial x_n \partial x_1 & \cdots & \partial x_n \partial x_1 \end{pmatrix}$$

And for $f = (f_1, \dots, f_n)^\top : \mathbb{R}^n \mapsto \mathbb{R}^n$

$$(B.1) \quad \nabla f = \begin{pmatrix} \nabla^\top f_1 \\ \vdots \\ \nabla^\top f_n \end{pmatrix} = (\nabla \otimes f)^\top, \quad \operatorname{div} f = \partial_{x_1} f_1 + \cdots + \partial_{x_n} f_n = \nabla^\top f$$

are respectively the Jacobian matrix and divergence of f .

Bibliography

- [1] R.N. Bhattacharya. “On the Functional Central Limit Theorem and the Law of the Iterated Logarithm for Markov Processes”. In: *Zeitschrift für Wahrscheinlichkeitstheorie und verwandte Gebiete* 60 (2 1982), pp. 185–201.
- [2] D.J. Evans and G. Morriss. *Statistical Mechanics of Nonequilibrium Liquids*. Cambridge University Press, 2008.
- [3] M. Fathi, A.A. Homman, and G. Stoltz. “Error Analysis of the Transport Properties of Metropolized Schemes”. In: *ESAIM Proc.* 48 (2015), pp. 341–363.
- [4] M. Fathi and G. Stoltz. “Improving dynamical properties of metropolized discretizations of overdamped Langevin dynamics”. In: *Numerische Mathematik* 136 (2 2016), pp. 545–602.
- [5] E. Hairer, C. Lubich, and G. Wanner. “Geometric numerical integration illustrated by the Störmer-Verlet method”. In: *Acta Numerica* 12 (2003), pp. 399–450.
- [6] R. Joubaud, G.A. Pavliotis, and G. Stoltz. “Langevin dynamics with Space-Time Periodic Nonequilibrium Forcing”. In: *Journal of Statistical Physics* 158 (2015), pp. 1–36.
- [7] B.G. Keller and S. Kieninger. “GROMACS Stochastic Dynamics and BAOAB are equivalent configurational sampling algorithms”. URL: <https://arxiv.org/abs/2204.02105v1>.
- [8] W. Kliemann. “Recurrence and Invariant Measures for Degenerate Diffusions”. In: *The Annals of Probability* 15 (2 1987), pp. 690–707.
- [9] B. Leimkuhler and C. Matthews. *Molecular Dynamics With Stochastic and Deterministic Methods*. Interdisciplinary Applied Mathematics. Springer, 2015.
- [10] B. Leimkuhler, C. Matthews, and G. Stoltz. “The computation of averages from equilibrium and nonequilibrium Langevin molecular dynamics”. In: *IMA Journal of Numerical Analysis* 36 (1 2016).
- [11] H. Rodenhausen. “Einstein’s relation between diffusion constant and mobility for a diffusion model”. In: *Journal of Statistical Physics* 55 (1989), pp. 1065–1088.
- [12] M. Tuckerman. *Statistical Mechanics: Theory and Molecular Simulation*. Oxford University Press, 2010.